



It is shown that charged surfactant vesicles have a high efficiency for encapsulating oppositely charged probe molecules with extremely slow release rates. Several probe molecules, both anionic and cationic, were studied including the cancer chemotherapeutic drug doxorubicin (Dox). All probe molecules were captured at high efficiency (ca. 20-70%) when the vesicle bilayer was of opposite charge from the probe molecule; when the charge of vesicle and probe molecule was the same, encapsulation was diminished (ca. 0-8%). Strong electrostatic interaction between surfactant vesicles and charged molecules are responsible for the extremely high encapsulation efficiency. The vesicle/probe formulations are stable for weeks to months due to the inherent stability of these vesicles which form spontaneously and are believed to be equilibrium structures. These properties allow surfactant vesicles to be used to selectively separate oppositely charged dye molecules, and this is demonstrated.

Fluorescence correlation spectroscopy (FCS) was used to gain deeper understanding into the role of electrostatics in the capture of charged probe molecules by charged surfactant vesicles. FCS measures the diffusion of fluorescent probe molecules in aqueous solutions at very low concentrations ( $10^{-9}$ - $10^{-8}$  M) and distinguishes between rapidly diffusing single molecules and slowly diffusing molecules that are adsorbed on a vesicle bilayer. This method is sensitive enough to rapidly determine the fraction of probe molecules bound to the bilayer interface in a given sample. Binding isotherms were constructed from FCS measurements in which a series of solutions were measured by holding the dye concentration constant while increasing the vesicle concentrations. The resulting isotherm yields a measure of binding energy. Comparisons of binding

energies show that probe/bilayer interactions are mainly governed by charge-charge interactions but may also depend on the size and structure of the surfactant counter ions.

Our findings provide useful guidelines for implementing surfactant vesicles in biotechnological applications and also serve as an intriguing example of charge-mediated bilayer interactions.

STUDY OF ELECTROSTATIC INTERACTION BETWEEN CHARGED  
SURFACTANT VESICLES AND IONIC MOLECULES BY BULK AND  
FLUORESCENCE CORRELATION SPECTROSCOPY MEASUREMENTS

By

Xiang Wang

Dissertation submitted to the Faculty and the Graduate School of the  
University of Maryland, College Park in partial fulfillment  
of the requirements for the degree of  
Doctor of Philosophy  
2007

Advisory Committee:  
Professor Douglas English Chair/Advisor  
Professor Robert Walker  
Professor Michael Coplan  
Professor Srinivasa Raghavan  
Professor Philip DeShong

© Copyright by  
Xiang Wang  
2007

## **DEDICATION**

To my family

## ACKNOWLEDGEMENTS

I am extremely grateful to my advisor, Dr. Douglas English for his assistance and guidance throughout this process. His knowledge, discussions, direction and ideas were crucial for my academic performance and this thesis. I would like to thank him for helping develop my research and trouble shooting abilities for my future career.

I sincerely thank Dr. Srinivasa Raghavan and his student Jae-ho Lee for their initiation for my research. I would like to thank Dr. Robert Walker for his advice, encouragement and support. I also want to thank Dr. Philip Deshong and Dr. Sang Bok Lee for being my committee member. Many thanks go to my collaborators. I have a wonderful time together with Dr. Thomas Pons and Dr. Igor Medintz. Dr. Victor Muñoz and his group members, Jianwei Liu and Dr. Luis A. Campos share their knowledge in their specialties with me. Dr. Liqun Wu and Dr. Chao Zhu from Dr. Greg Payne group give me unselfish help and valuable advises for my research.

My warmest thanks go to all the members of the English lab for their help and support: Nikolai Sinkov, Amy Grimes, Emily Danoff, Charles Lockett, Sara Lioi, and Kathy Goodson. I have an enjoyable experience with them. They offer me so many helps in the lab and also, in my life. I would like to thank my best friends, Jin Yiqiang, Shenqin couple, Ling Li, Xuefeng Hua, Li Mingdong, Cui Bingqin couple and Zhang Xin, Zheng Lei couple. With their encouragement and support, I can overcome all the

difficulties in this process. The rest thanks go to all my friends in Chemical Physics Program.

I sincerely thank my family. I never forget the advice from my father, a successful physicist, who led my interest to science, that if you want be a respectable person, you should own your ideas and have a good reputation. My mother told me how to be a reasonable person when I was young. I really appreciate their love and guidance. Also I thank them for taking care of my daughter and so I can focus on my study. Thank you, my sister for your love and help. Finally, many thanks go to my lovely daughter, Kaixin (Lunea) Wang, who bring so much happiness for my life!

# Table of Contents

<b>Dedication</b> .....	ii
<b>Acknowledgements</b> .....	iii
<b>Table of Contents</b> .....	v
<b>List of Tables</b> .....	ix
<b>List of Figures</b> .....	x
<b>List of Abbreviations</b> .....	xiii
<b>Chapter 1 Introduction and Overview</b> .....	1
<b>1.1. Historical Overview and Description of Liposomes</b> .....	1
<b>1.2. Surfactant Vesicles</b> .....	4
1.2.1. Building Blocks and Classification .....	4
1.2.2. Historical Overview.....	6
1.2.3. Spontaneous Vesicle Formation .....	6
1.2.4. Advantages.....	13
<b>1.3. Goals</b> .....	14
<b>Chapter 2 Materials and Experimental Procedures</b> .....	17
<b>2.1. Materials</b> .....	17
<b>2.2. Experimental procedure</b> .....	18
2.2.1. Liposome Preparation.....	18

2.2.2. Surfactant Vesicle Preparation.....	18
2.2.3. Size Exclusion Chromatography (SEC).....	19
2.2.3.1. Determination of Apparent Encapsulation by SEC.....	21
2.2.4. Vesicles Characterization.....	23
2.2.4.1. Dynamic Light Scattering (DLS).....	23
2.2.4.2. Fluorescence quenching.....	27
2.2.5. Fluorescence Correlation Spectroscopy (FCS).....	28
2.2.6. Time Tagged Method.....	32
<b>Chapter 3 Highly Efficient Capture and Long-Term Encapsulation of Dye by Catanionic Surfactant Vesicles.....</b>	<b>38</b>
<b>3.1. Introduction.....</b>	<b>38</b>
<b>3.2. Materials and Methods.....</b>	<b>39</b>
<b>3.3. Results .....</b>	<b>40</b>
3.3.1. Apparent Encapsulation Efficiency.....	40
3.3.2. Long-Term Dye Release.....	44
<b>3.4. Conclusions and discussions.....</b>	<b>49</b>
<b>3.5. Acknowledgments.....</b>	<b>49</b>
<b>Chapter 4 Surfactant Vesicles for High-Efficiency Capture and Separation of Charged Organic Solutes.....</b>	<b>51</b>
<b>4.1. Introduction.....</b>	<b>51</b>
<b>4.2. Experimental and Methods.....</b>	<b>53</b>
4.2.1. Materials.....	53
4.2.2. Vesicle Preparation.....	53

4.2.3. Methods.....	54
4.2.3.1. Evaluation of Apparent Encapsulation Efficiency ( $\epsilon$ ).....	54
4.2.3.2. Long-Term Capture and Dye Release.....	55
4.2.3.3. Dynamic Light Scattering (DLS).....	56
4.2.3.4. Small Angle Neutron Scattering (SANS).....	56
<b>4.3. Results and Discussions.....</b>	<b>57</b>
4.3.1. Capture of Charged Solutes by Vesicles.....	58
4.3.2. Long-Term Solute Release from Vesicles.....	64
4.3.3. Separation of Oppositely Charged Solutes by Vesicles.....	66
4.3.4. Effects of Solutes on Vesicle Stability.....	68
4.3.5. Implications for Applications Involving Surfactant Vesicles.....	72
<b>4.4. Conclusions.....</b>	<b>73</b>
<b>4.5. Acknowledgments.....</b>	<b>74</b>
<b>Chapter 5 Investigation of Excess Charge, Counterion Identity, and Electrostatic Adsorption in Surfactant Vesicles: Bulk and Fluorescence Correlation Spectroscopy Studies.....</b>	<b>79</b>
<b>5.1. Introduction.....</b>	<b>79</b>
<b>5.2. Materials and methods.....</b>	<b>85</b>
5.2.1. Materials.....	85
5.2.2. Measuring encapsulation efficiency.....	85
5.2.3. Fluorescence correlation spectroscopy.....	86
<b>5.3. Results and Discussion.....</b>	<b>91</b>
<b>5.4. Conclusions.....</b>	<b>104</b>

<b>Chapter 6 Conclusions and Future Work</b> .....	108
<b>6.1. Conclusions</b> .....	108
<b>6.2. Future work</b> .....	111
<b>Appendix A</b> .....	115
<b>A.1 Data and Images from SEC Experiments for Evaluation of Apparent Encapsulation Efficiency (<math>\epsilon</math>)</b> .....	115
<b>A.2. Separations Performed on a Mixture of LY and Dox</b> .....	118
<b>Appendix B</b> .....	119
<b>References</b> .....	120

## List of Tables

<b>Table 1.1.</b>	Examples of surfactant molecules.....	5
<b>Table 1.2.</b>	Aggregates of amphiphilic molecules.....	8
<b>Table 2.1.</b>	Reagents Table.....	17
<b>Table 3.1.</b>	Apparent encapsulation efficiency and dye adsorption for CF on both EYPC vesicles and V <sup>+</sup> .....	42
<b>Table 4.1.</b>	Apparent encapsulation efficiencies and vesicle radii.....	63
<b>Table 5.1.</b>	Association constants and encapsulation efficiencies for different vesicle/dye combinations.....	93

## List of Figures

<b>Figure 1.1.</b> Liposomal structure. Liposomes are spherical shells formed from bilayers that occur when lipid molecules such as 1-Palmitoyl-2-oleoyl-sn-glycero-3-phosphocholine (POPC) self-assemble into lamellar structures.....	2
<b>Figure 1.2.</b> Structures of CTAT and SDBS.....	9
<b>Figure 1.3.</b> Water-rich corner of the ternary phase diagram for the CTAT/SDBS/water system. Adapted from ref. 27.....	10
<b>Figure 1.4.</b> a) The formation of ion pairs. b) The asymmetrical curvatures and inhomogeneous compositions of the inner and outer layers of surfactant vesicles.....	12
<b>Figure 2.1.</b> Schematic of size exclusion chromatography (SEC).....	20
<b>Figure 2.2.</b> Quick spin column and Minispin Centrifuge.....	22
<b>Figure 2.3.</b> Schematic of dynamic light scattering.....	24
<b>Figure 2.4.</b> Illustration of wave vectors of incident and scattered light.....	25
<b>Figure 2.5.</b> Cartoon of method for measuring the bound fraction of probe molecules in a vesicle solution.....	30
<b>Figure 2.6.</b> Schematic of scanning confocal fluorescence microscope.....	31
<b>Figure 2.7.</b> Schematic of time tagged method.....	33
<b>Figure 2.8.</b> Schematic of experimental setup of time tagged method.....	34

<b>Figure 2.9.</b> Autocorrelation decays for the samples containing the dye CF in water at room temperature.....	36
<b>Figure 3.1.</b> Phase diagram of CTAT/SDBS showing the dilute (water-rich) corner. Adapted from ref. 15.....	42
<b>Figure 3.2.</b> Denaturation of catanionic vesicles and release of carboxyfluorescein.....	46
<b>Figure 3.3.</b> Comparison of dye released as a function of time, $R(t)$ , between equilibrium vesicles (solid line) and phospholipid vesicles (dotted line).....	47
<b>Figure 4.1.</b> Structures of the five solutes used in these studies.....	60
<b>Figure 4.2.</b> Results from SEC of vesicles with the anionic dye, CF: (a) $V^+$ vesicles; and (b) $V^-$ vesicles.....	62
<b>Figure 4.3.</b> Dye release profiles.....	65
<b>Figure 4.4.</b> Vesicle-mediated separation of mixtures of R6G and CF dyes using (a) $V^+$ vesicles; and (b) $V^-$ vesicles. ....	67
<b>Figure 4.5.</b> SANS data for neat and dye-containing $V^+$ and $V^-$ samples. (a) Scattering data for $V^+$ samples. (b) Scattering data for neat $V^-$ samples (black circles) and for $V^-$ loaded with R6G (red triangles).....	71
<b>Figure 5.1.</b> Structure of surfactnats and illustration of bilayer formation.....	81
<b>Figure 5.2.</b> Structures of the fluorescent probes used for FCS studies.....	84
<b>Figure5.3.</b> Autocorrelation decays for the samples containing the dye CF in water at room temperature.....	88

<b>Figure 5.4.</b> Normalized autocorrelation functions obtained from carboxyfluorescein (10 nM) with varying amounts of CTAT-rich vesicles.....	91
<b>Figure 5.5.</b> Adsorption isotherms obtained from FCS. Each isotherm was fit to equation 4 and the binding constant is given in Table 5.1.....	95
<b>Figure 5.6.</b> Adsorption isotherms illustrating the effects of (A) bilayer charge stoichiometry and (B) excess counter ion identity.....	97
<b>Figure 5.7.</b> Illustration of Debye length.....	100
<b>Figure 5.8.</b> SEC results from studies of dye binding and encapsulation in normal saline. (A) Apparent encapsulation of carboxyfluorescein drops from 24% to 0% under physiological salt concentrations. (B) Conversely, the apparent encapsulation of Rhodamine 6G is unchanged in normal saline.....	102
<b>Figure 5.9.</b> FCS results from studies of dye adsorption as a function of salt concentration. The dots and squares are the fraction of CF bound to the CTAT-rich vesicles and R6G bound to SDBS-rich vesicles as the changes of concentration of sodium chloride, respectively.....	103
<b>Figure A.1.</b> DLS and encapsulation efficiency study through SEC for dye molecules of LY, SR101, R6G and Dox.....	116
<b>Figure A.2.</b> Separation of LY and Dox.....	118
<b>Figure B.1.</b> Square, circle, and cross represents autocorrelation curve of vesicle, SDBS micelle, and free dye, respectively. Corresponding diffusion coefficient ( $\text{cm}^2 \cdot \text{s}^{-1}$ ) is $1.08 \times 10^{-9}$ , $7.9 \times 10^{-8}$ and $2.6 \times 10^{-6}$ , respectively.....	119

## List of Abbreviations

$\Delta C$	Excess charge
$\varepsilon$	Apparent encapsulation efficiency
APD	Avalanche photodiode
CF	5(6)-carboxyfluorescein
CTAB	Cetyltrimethylammonium bromide
CTAT	Cetyltrimethylammonium tosylate
D	Diffusion coefficient
DiIC <sub>18</sub>	1,1'-dioctadecyl-3,3,3',3'- tetramethylindocarbocyanine perchlorate
DLS	Dynamic light scattering
Dox	Doxorubicin hydrochloride
EYPC	Egg yolk phosphatidylcholine
FCS	Fluorescence Correlation Spectroscopy
K	Binding constant
LY	Lucifer yellow
R	Surfactant charge ratio
R6G	Rhodamine 6G
SDBS	Sodium dodecylbenzenesulfonate
SEC	Size exclusion chromatography
SR101	Sulforhodamine 101
UV-vis	Ultra violet-visible
V <sup>-</sup>	Negatively charged (SDBS-rich) vesicle
V <sup>+</sup>	Positively charged (CTAT-rich) vesicle

## Chapter 1. Introduction and Overview

This thesis describes recent work where vesicles formed from single-tailed surfactants are quantitatively evaluated for use in the capture and release of water soluble charged molecules. Before describing this work it is important to have some knowledge of conventional vesicles that form from double-tailed, naturally-occurring phospholipid molecules. Phospholipid vesicles and their weaknesses as drug delivery vehicles will be discussed before turning to surfactant vesicles. For the purpose of this thesis, we will refer to vesicles formed from phospholipids as *liposomes* and vesicles formed from single-tailed surfactants as *catanionic vesicles* or simply surfactant vesicles.

### 1.1. Historical Overview and Description of Liposomes

Liposomes are spherical bilayer shells that enclose an inner water pool, (see Figure 1.1.). Liposomes were first reported by Bangham et al. in the mid-1960s.<sup>1,2</sup> Liposomes have since been investigated extensively as molecular “vessels” due to their hollow structure and ability to hold and release water soluble molecules. Their versatility in terms of size, composition and surface charge make liposomes of particular interest as model systems for cell-membranes and they have been utilized in applications such as drug delivery and cosmetics.

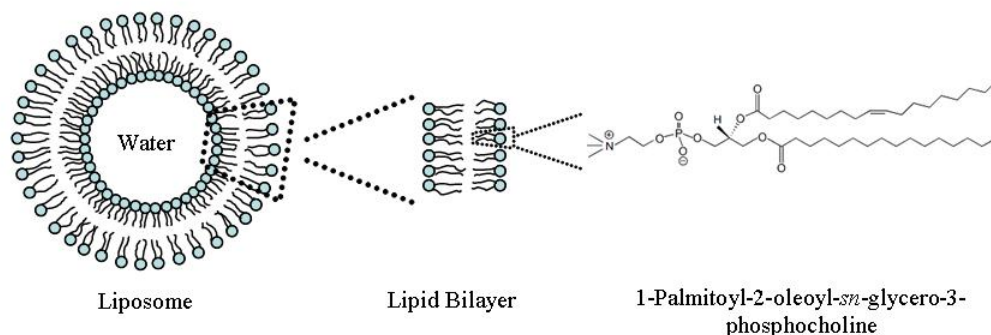


**Figure 2.1.** Liposomal structure. Liposomes are spherical shells formed from bilayers that occur when lipid molecules such as 1-Palmitoyl-2-oleoyl-*sn*-glycero-3-phosphocholine (POPC) self-assemble into lamellar structures.

Liposomes were proposed as a drug delivery system in the 1970s to reduce the toxicity or increase the efficiency of drug molecules.<sup>3</sup> In the 1980s and early 1990s, several liposomal preparations entered the market. Today, the most widely used liposomal formulation from the pharmaceutical industry is DOXIL, and it was also the first liposomal anticancer drug licensed worldwide.<sup>4</sup> DOXIL was used in the treatment of ovarian cancer, AIDS-related Kaposi's sarcoma and multiple myeloma. DOXIL is a reformulated version of the chemotherapeutic agent doxorubicin. DOXIL consists of the active agent doxorubicin contained in a liposome coated with methoxypolyethylene glycol (MPEG). This coating protects liposomes from detection and destruction by the

immune system resulting in an increased blood circulation time. In the cosmetic industry, liposomal formulations have been used to encapsulate functional ingredients, reducing their epidermal permeation rate. This helps to stabilize active ingredients to the outermost skin layers as desired for cosmetic products.

A major drawback that has prevented wider use of liposomes is long term stability. Liposomes are formed by applying external mechanical forces such as sonication or extrusion to phospholipid bilayers. Hence, liposomes are kinetically trapped structures and not in a thermodynamically stable state. Over the time, liposomes tend to fuse or rupture and the molecules encapsulated inside are released during those processes.

Another potential drawback of liposomes is that the encapsulation efficiency for drug delivery purposes is usually very low. Encapsulation efficiency is generally defined as the percentage of the total amount of solute molecules that are held by the liposome when the preparation is first prepared. The unencapsulated solute can be separated from the liposomes by size exclusion chromatography to determine the encapsulation efficiency. Methods to achieve this are described in the next chapter. Efforts to improve the performance of liposomes with respect to stability and drug-loading have been made by changing the compositions of the vesicles bilayer. For instance, by adding cationic lipids to liposomes their ability to deliver DNA and act as transfection vectors was improved substantially.<sup>5-7</sup> Also, pH-sensitive liposomes have been used to enhance the cytoplasmic delivery of drug molecules.<sup>8</sup> However these efforts require very complicated

and expensive preparation processes and do not necessarily improve the stability of liposomes.

Finding a replacement for liposomes with higher encapsulation ability and longer shelf-life has motivated researchers to explore other drug delivery systems such as polymers<sup>9</sup>, dendrimers,<sup>10</sup> or hydrogels<sup>11</sup>. Those systems also suffer drawbacks such as low encapsulation efficiency. A promising alternative is the use of surfactant vesicles formed from aqueous mixtures of single-tailed common surfactants.

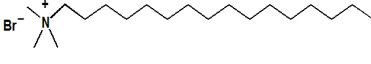
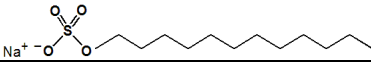
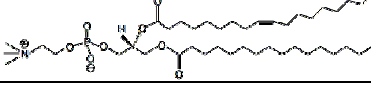
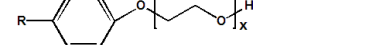
## **1.2. Surfactant Vesicles**

### **1.2.1. Building Blocks and Classification**

The building blocks of surfactant vesicles are amphiphilic molecules or surfactants (“**surface active agents**”). Generally surfactant molecules have a long single or double-tailed alkyl chain, covalently linked to a hydrophilic head group. Based on the charges present in the hydrophilic head group, surfactant can be classified as (See Table1.1):

1. Cationic, with the hydrophilic head group carrying a positive charge such as a tertiary amine.
2. Anionic, with the hydrophilic head group bearing a negative charge, for instance a phosphate or sulfonate group.
3. Zwitterionic, in which the molecule contains both a positive and a negative charge as in many phospholipid molecules (see Figure 1.1).

4. Nonionic, where the hydrophile has no charge, but derives its water solubility for highly polar group such as  $\text{RC}_6\text{H}_4(\text{OC}_2\text{H}_4)_x\text{OH}$  (polyoxyethylenated alkylphenol) and  $\text{R}(\text{OC}_2\text{H}_4)_x\text{OH}$  (polyoxyethylenated alcohol)

	Name	Abbreviation	Structure
<b>Cationic</b>	Cetyltrimethylammonium Bromide	CTAB	
<b>Anionic</b>	Sodium dodecylsulfate	SDS	
<b>Zwitterionic</b>	Palmitoyl oleoyl phosphatidylcholine	POPC	
<b>Nonionic</b>	Octyl phenol ethoxylate	Triton X-100	

**Table 1.1.** Examples of surfactant molecules.

To date, several different types of surfactant vesicles have been discovered and classified. When non-ionic surfactants such as polyglyceryl alkyl ethers are used to make vesicles, they are referred to as “*Niosomes*”.<sup>12,13</sup> “*Catanionic*” vesicles are the topic of this research thesis and are made from simple mixtures of cationic and anionic surfactants in aqueous solution. A feature of catanionic vesicles that is of particular importance to this work is the presence of a net charge on the bilayer due to a molar excess of either the cationic or anionic surfactant. The work described herein focuses exclusively on catanionic systems.

### **1.2.2. Historical Overview**

The initial study of surfactant vesicles started after Gebicki and Hicks reported that vesicles can spontaneously form from deprotonated unsaturated fatty acids (such as oleic acid) in 1973.<sup>14</sup> Partially ionized acids play an important role in the formation and stability of such systems which is different from the formation mechanism of liposomes. Based on this discovery, many surfactant vesicle systems have been explored.<sup>15,16</sup> The mechanism of formation of such vesicles also has been discussed.<sup>17-19</sup> Properties of surfactant vesicles such as composition, vesicle size and phase behaviors have been well-described in these studies.<sup>20</sup> Of particular interest are surfactant vesicles that form spontaneously in mixtures of two single-tailed and oppositely charged surfactants. Spontaneous vesicle formation requires a molar excess of one surfactant and therefore cationic vesicles always have a net charge. Because they form spontaneously, they are commonly referred to as equilibrium vesicles. Whether or not they are a truly equilibrium system is still under debate,<sup>21,22</sup> but it is well-confirmed that cationic vesicles are extremely stable and can exist over months or even years.<sup>23</sup> Kaler and coworkers have studied several vesicle systems that form from common surfactants. The low cost and simple methods for forming these types of vesicles make them extremely attractive for industrial applications.

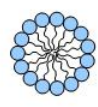
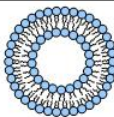
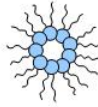
### **1.2.3. Spontaneous Vesicle Formation**

When amphiphilic molecules such as surfactants, fatty acids or lipids dissolve in aqueous solution these molecules tend to aggregate into specific structures in order to shield the hydrophobic regions from water. The dominant driving force governing self

assembly in water is the hydrophobic effect. The “hydrophobic effect” refers to the reduction in the free energy ( $\Delta G_{agg}$ ) that occurs when aggregates form thermodynamic stable states in water. Some aggregates include spherical micelles, cylindrical micelles, and reverse micelles (see Table 1.2.). The type of structure formed is strongly dependent on the geometry of the amphiphile and consequently its packing properties, which can be characterized by the packing parameter,  $P$ . First defined by Israelachvili in 1976, the packing parameter is the ratio of the volume of the hydrophobic tail of the amphiphile,  $v$ , to the product of the chain length of the hydrophobic tail,  $l$ , and the cross-sectional area of the hydrophilic headgroup,  $a_o$ .<sup>24,25</sup>

$$P = \frac{v}{a_o l} \quad (1)$$

The value of  $P$ , and the corresponding geometry of the amphiphile, can be used to predict which aggregate structure is formed by a particular amphiphile.<sup>26</sup> Molecules with a value of  $P$  that is less than 1/3 (cone shaped) tend to form spherical micelles, while molecules with a  $P$  value between 1/3 and 1/2 (truncated cone) tend to form cylindrical, or rod-like, micelles (see Table 1.2 ). If the  $P$  value is between 1/2 and 1 (cylindrical), then the molecules form curved bilayers which can assemble into vesicles (as  $P$  approaches 1, flat bilayers become predominant). Conversely, a  $P$  value greater than 1 means the geometry is that of an inverted cone, and the molecules, if they are in a hydrophobic environment, form reverse micelles (the hydrophobic tails point outward and the polar headgroups are on the inside of the micelle). The relationship between “critical packing parameter” and amphiphilic molecule geometry is listed in Table 1.2.

Packing Parameter $P=v/a_0l$	Amphiphile Shape	Predicted Aggregate	
$< 1/3$		Spherical Micelles	
$1/3 - 1/2$		Cylindrical Micelles	
$1/2 - 1$		Bilayers/ Vesicles	
$> 1$		Reverse Micelles	

**Table 1.2.** Aggregates of amphiphilic molecules. Depending on the packing parameter of the amphiphile, and the corresponding geometry, various aggregate structures can form. In all cases (except reverse micelles) the hydrophobic regions are positioned so as to be shielded from the hydrophilic environment. Vesicles enclose an aqueous compartment separate from the bulk solution. Figure adapted from Ref. 24.

The very first report of spontaneously-formed surfactant vesicles was in 1989 by Kaler.<sup>23</sup> Their system consisted of aqueous mixtures of cetyltrimethylammonium tosylate (CTAT) and sodium dodecylbenzenesulfonate (SDBS). Both CTAT and SDBS are single tailed surfactants. CTAT is a positive charged surfactant, which has a positive head group  $\text{CTA}^+$  associated with a tosylate counter ion. While SDBS is a negative charged surfactant, which has a sulfonate head group coupled with a sodium counter ion.

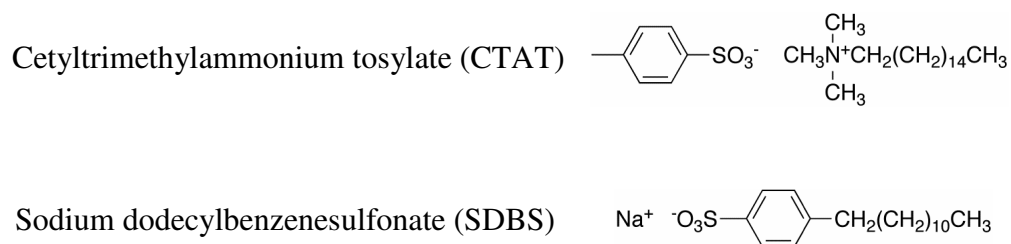


**Figure 1.2.** Structures of CTAT and SDBS.

The ternary phase diagram of the CTAT/SDBS/Water system was constructed by Kaler, *et al.* in 1989.<sup>23</sup> Figure 1.3. shows the water rich corner of this phase diagram.<sup>27</sup> Shown in Figure 1.3. is the water rich corner of this ternary phase diagram<sup>23</sup> at 25 °C and compositions are on a weight percent basis. In this diagram, starting from CTAT-rich region (left hand side) are CTAT-rich rodlike micelles. Next to it is a two phase region that includes liquid crystalline and an unresolved multiphase. Vesicles are observed in compositions corresponding to the two lobes labeled V<sup>+</sup> and V<sup>-</sup>. The two-phase regions labeled III and shaded are V<sup>+</sup> and CTAT-rich lamellar phase (*La*<sup>+</sup>) to the left of the equimolar line and V<sup>-</sup> and SDBS-rich lamellar phase (*La*<sup>-</sup>) on the right of the equimolar line. Region IV contains SDBS-rich micelles. Precipitation occurs along the equimolar line.

Vesicles are observed in compositions corresponding to the two lobes labeled V<sup>+</sup> and V<sup>-</sup>. The vesicles can be easily obtained by preparing solutions at these compositions and allowing them to equilibrate for about 48 h. Under these conditions surfactant

vesicles form spontaneously. The fact that vesicles only form in mixtures where one surfactant is in excess will be important to the work described in this thesis. Also, it should be noted that in equimolar solutions the surfactants actually precipitate. When the CTAT concentration is greater than SDBS the vesicles are denoted as  $V^+$ . For the opposite situation  $V^-$  is used.

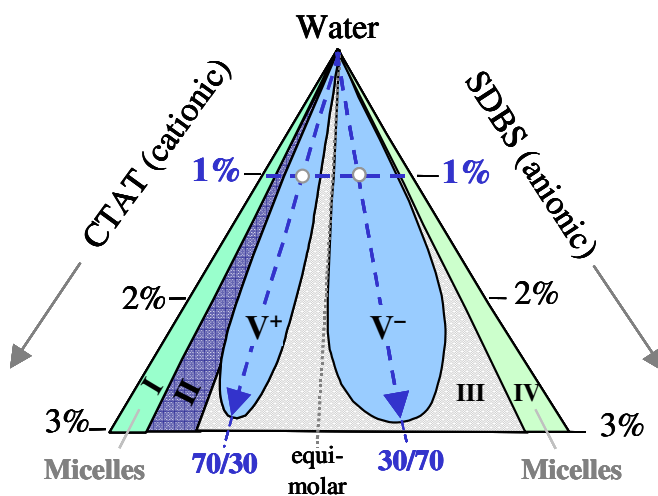


**Figure 1.3.** Water-rich corner of the ternary phase diagram for the CTAT/SDBS system. Two blue lobes indicate the presence of vesicles. The bottom axis of the phase diagram is weight ratio of surfactants and the side axes show total surfactant concentration. Adapted from ref. 27.

In addition to the CTAT/SDBS system a number of other surfactant vesicles have been found that can be formed by simply mixing two oppositely charged single tailed surfactants together with water.<sup>20</sup> The mechanism of formation is believed to be based on the formation of surfactant ion pairs for which the formation is favored by both electrostatic and hydrophobic interactions. The geometry of an ion pair formed from two single tailed surfactants is an analog of a phospholipid molecule with a packing parameter close to 1. This is a necessary condition for the formation of a lamellar

aggregate, i.e. bilayer. But different from liposomes, surfactant vesicles always have an excess of one charged surfactant due to the molar excess of either cationic or anionic surfactant. Equal molar mixture of two oppositely charged surfactants causes phase separation. It is thought that the excess surfactant helps to fluidize the vesicle bilayer.<sup>23</sup>

A single tailed surfactant usually has a larger head group compared with its hydrophobic tail which gives  $P < 1/2$ . Hence, in most cases, surfactants form micelles spontaneously when mixed with water. However, if two oppositely charged single tailed surfactants are mixed together, due to the electrostatic interaction, ion pairs form. The average head group area of an ion pair is decreased by electrostatic attraction. Therefore, it is smaller than the sum of the two single surfactant head groups. Since, the average tail volume of an ion pair is the sum of two single tails, the  $P$  of such an ion pair is close to unity. This allows bilayer structure to form from mixtures of two single tailed oppositely charged surfactants. The formation of ion pairs describes why a bilayer forms spontaneously but does not account for the spontaneous bilayer curvature that is necessary to form an equilibrium vesicle.

To understand how a catanionic vesicle forms spontaneously, a theoretical model used to describe the stability and formation of liposomes, can be utilized for surfactant vesicles.<sup>17</sup> In 1973, Helfrich used curvature elastic energy,  $f_c$ , to help explain vesicle stability. In this model, the simplified bending energy per unit area for liposome is:

$$f_c = 2K[(c + c_o)^2 + (c - c_i)^2] \quad (1)$$

where  $K$  is bending modulus,  $c_o$  and  $c_i$  are the two spontaneous curvatures of outer and inner monolayers given by the inverses of their radii. The quantity  $c$  is the actual vesicle curvature. For a single component system,  $c_o$  and  $c_i$  are equal. In this case, when  $c = 0$  or flat bilayer, the minimum  $f_c$  can be obtained. This explains why the formation of lipid vesicles needs extra energy.

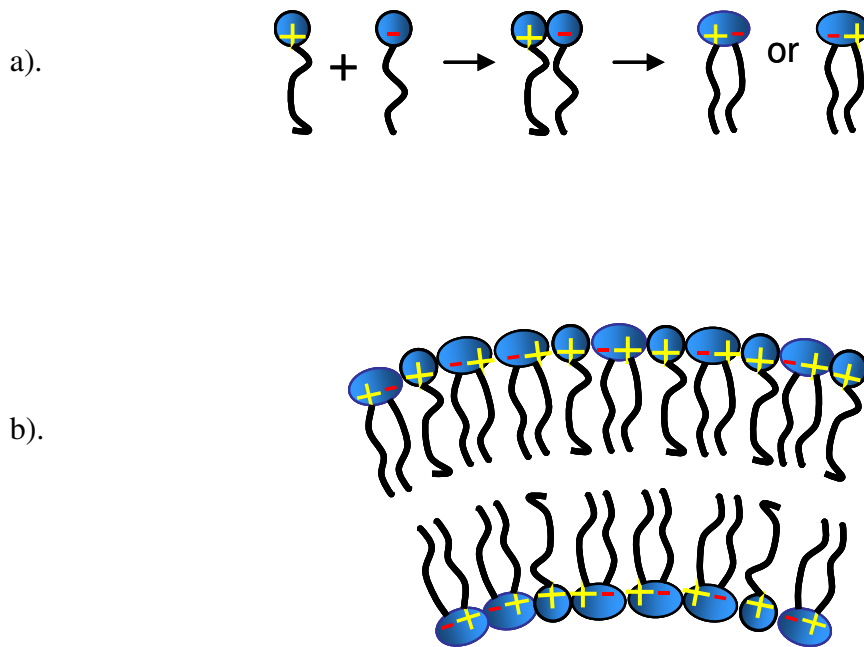


**Figure 1.4.** a) The formation of ion pairs. b) The asymmetrical curvatures and inhomogeneous compositions of the inner and outer layers of surfactant vesicles.

In a mixed system of two surfactants is possible for the two layers of the bilayer to have different composition, i.e. nonideal mixing. This composition asymmetry effect must be considered. Safran *et al.* gave a detailed calculation.<sup>18,28</sup> The total free energy is<sup>18</sup>

$$f = 2K \left( -\frac{1}{2} \varepsilon \phi^2 + \frac{1}{4} A \phi^4 \right) \quad (2)$$

where  $\phi$  is the composition difference between two layers. Both  $\varepsilon$  and  $A$  are parameters determined by the volume fraction of one surfactant, interaction between two different surfactants and the curvature of vesicles. The sign of  $\varepsilon$  is negative for a planar bilayer with zero curvature and positive for vesicles. In mixtures of surfactants where the surfactants tend to form micelles in water (both curvatures are negative), nonideal mixing in which more of the unpaired surfactants are present on the outer layer favors vesicle formation.

Both surfactant geometry and mixing are of critical importance for spontaneous vesicle formation. For these reasons, vesicles only form in the well defined regions of the phase diagram, as shown in Figure 1.3. The asymmetric distribution of surfactants is crucial for determining the functions of surfactant vesicles in stability and encapsulation efficiency. The details of which will be discussed in Chapter 5.

#### **1.2.4. Advantages**

Some areas where surfactant vesicles differ from conventional liposomes are: 1) less expensive components, 2) simple preparation methods 3) vesicles can be readily prepared with either negatively or positively charged bilayers 4) surfactant vesicles are much more stable than phospholipid vesicles.

### 1.3. Goals

The features of surfactant vesicles reveal that they hold some promise as a potential replacement for liposomes in applications such as drug delivery. The goal of the research presented in this thesis is to provide an initial exploration into this possibility by examining the ability of surfactant vesicles to encapsulate and release water soluble molecules. Until now, there have been very few studies reported in this area. In 1989, Kaler mentioned glucose encapsulation in CTAT/SDBS system, but did not give any quantitative results.<sup>23</sup> Caillet *et al.* investigated the encapsulate of the small neutral molecules glucose and riboflavin in surfactant vesicles formed from cetyltrimethylammonium bromide (CTAB) and sodium octyl sulfate (SOS).<sup>29</sup> They achieved an encapsulation efficiency of about ~1%, for glucose and 0.4% for riboflavin. Caillet also attempted to encapsulate the anionic dye carboxyfluorescein (CF) but observed no encapsulation.<sup>29</sup> In their studies it appears that the presence of CF inhibited vesicle formation due to its high concentration (50 mM). Results reported in this thesis show that the original work by Caillet is misleading and that ionic molecules can in fact be encapsulated with high efficiency. The work reported in this thesis is the first to show that cationic vesicles can be used as highly-efficient and long-term storage media for ionic solutes.

## References:

1. Bangham, A. D.; Horne, R. W. *J. Mol. Biol.* 1964, 8, 660-668.
2. Bangham, A. D.; Standish, M. M.; Watkins, J. C. *J. Mol. Biol.* 1965, 13, 238-252.
3. Bangham, A. D. *Liposome Letters*; Academic Press, 1983.
4. Lasic D. D., T. N. S. *Gene therapy: therapeutic mechanisms and strategies*,; Marcel Dekker,; New York, 2000.
5. Xu, Y. H.; Szoka, F. C. *Biochemistry* 1996, 35, 5616-5623.
6. Wu, G. Y.; Wu, C. H. *J. Biol. Chem.* 1987, 262, 4429-4432.
7. Felgner, P. L.; Gadek, T. R.; Holm, M.; Roman, R.; Chan, H. W.; Wenz, M.; Northrop, J. P.; Ringold, G. M.; Danielsen, M. *P. Natl. Acad. Sci. USA* 1987, 84, 7413-7417.
8. Sheff, D. *Adv. Drug. Deliver. Rev.* 2004, 56, 927-930.
9. Langer, R. *Nature* 1998, 392, 5-10.
10. Esfand, R.; Tomalia, D. A. *Drug. Discov. Today* 2001, 6, 427-436.
11. Peppas, N. A.; Bures, P.; Leobandung, W.; Ichikawa, H. *Eur. J. Pharm. Biopharm.* 2000, 50, 27-46.
12. Baillie, A. J.; Florence, A. T.; Hume, L. R.; Muirhead, G. T.; Rogerson, A. J. *Pharm. Pharmacol.* 1985, 37, 863-868.
13. Schreier, H.; Bouwstra, J. *J. Controlled Release* 1994, 30, 1-15.
14. Gebicki, J. M.; Hicks, M. *Nature* 1973, 243, 232-234.
15. Hargreaves, W. R.; Deamer, D. W. *Biochemistry* 1978, 17, 3759-3768.
16. Fendler, J. H. *Accounts Chem Res* 1980, 13, 7-13.
17. Helfrich, W. *Z. Naturforsch., C: Biosci.* 1973, C 28, 693-703.
18. Safran, S. A.; Pincus, P.; Andelman, D. *Science* 1990, 248, 354-356.
19. Lasic, D. D. *Trends Biotechnol.* 1998, 16, 307-321.
20. Tondre, C.; Caillet, C. *Adv. Coll. Inter. Sci* 2001, 93, 115-134.
21. Laughlin, R. G. *Colloids Surf., A* 1997, 128, 27-38.

22. Almgren, M.; Rangelov, S. *Langmuir* 2004, *20*, 6611-6618.
23. Kaler, E. W.; Murthy, A. K.; Rodriguez, B. E.; Zasadzinski, J. A. N. *Science* 1989, *245*, 1371-1374.
24. Israelachvili, J. N.; Mitchell, D. J.; Ninham, B. W. *J. Chem. Soc., Faraday Trans. II* 1976, *72*, 1525-1568.
25. Israelachvili, J. N. *Intermolecular and Surface Forces*; Academic Press: London, 1985.
26. Zana, R., Ed. *Dynamics of Surfactant Self-Assemblies*; CRC Press: Boca Raton, 2005.
27. Koehler, R. D.; Raghavan, S. R.; Kaler, E. W. *J. Phys. Chem. B* 2000, *104*, 11035-11044.
28. Safran, S. A.; Pincus, P. A.; Andelman, D.; Mackintosh, F. C. *Phys. Rev. A* 1991, *43*, 1071-1078.
29. Caillet, C.; Hebrant, M.; Tondre, C. *Langmuir* 2000, *16*, 9099-9102.

## Chapter 2. Materials and Experimental Procedures

### 2.1. Materials

Reagents used in the study are listed in the Table 2.1

Table 2.1

<b>Name</b>	<b>Abbreviation</b>	<b>Source</b>
5-(and-6)-carboxyfluorescein	CF	Invitrogen (USA)
Cetyltrimethylammonium bromide	CTAB	Sigma Aldrich (USA)
Cetyltrimethylammonium tosylate	CTAT	Sigma Aldrich (USA)
Doxorubicin hydrochloride	Dox	Fluka (Germany)
Egg yolk phosphatidylcholine	EYPC	Avanti Polar Lipids, Inc. (USA)
Lucifer yellow	LY	Invitrogen (USA)
Rhodamine 6G	R6G	Invitrogen (USA)
Sephadex G50	Sephadex G50	Amersham Pharmacia Biotech (USA)
Sterile solution of sodium chloride	Saline	CVS (USA)
Sodium dodecylbenzenesulfonate	SDBS	Tokyo Chemical Industry (TCI) (USA)
Sodium chloride	NaCl	J.T. Baker (USA)
Sulforhodamine 101	SR101	Invitrogen(USA)
Triton X-100	Triton X-100	Fisher Scientific

Deionized water was used in bulk experiments that included encapsulation efficiency studies, long term release experiments or dye separations. In FCS experiments, ultrapure water from a Milli-Q water purification system (Millipore, USA) was used throughout. Organic solvents such methanol and acetone were used in either histological or HPLC grade.

## **2.2. Experimental Procedures**

### **2.2.1. Liposome Preparation**

EYPC was purchased from Avanti Polar Lipids, Inc. and used without further purification. The mechanism of liposome formation is described as following. Chloroform was evaporated from solutions of pure EYPC (13.2 mM) using a gentle stream of nitrogen before being placed overnight in a vacuum desiccator to remove all organic solvent. The resulting films were hydrated with 1 mL of highly purified water. Disruption of the multilamellar aggregates was achieved by five freeze-thaw cycles by immersion in liquid nitrogen. Large unilamellar vesicles (LUV) (150 nm in diameter) were formed by extruding 13 times using a polycarbonate membrane with 100 nm pore size (Avanti Polar Lipids). Vesicle samples were purified using gel permeation chromatography (Sephadex G50, medium mesh, Amersham Pharmacia Biotech).

### **2.2.2. Surfactant Vesicle Preparation**

All surfactant vesicles samples were prepared at a total surfactant concentration of 1 wt.%. The surfactants were weighed and mixed with deionized water by gentle stirring,

and then allowed to equilibrate at room temperature for at least 72 h.<sup>1</sup> Following equilibration, the samples were passed through a 25 mm syringe filter (0.45  $\mu\text{m}$  mesh) to remove impurities. Vesicle formation was confirmed by dynamic light scattering measurement to give the average sizes. Vesicle samples were prepared at two different surfactant compositions, 70:30 and 30:70 w/w CTAT to SDBS, which are denoted as  $V^+$  and  $V^-$ , respectively.  $V^+$  refers to the excess positive charge on the vesicle bilayers when there is an excess of CTAT. The average size of bare  $V^+$  or  $V^-$  sample is  $81 \pm 13$  nm and  $98 \pm 6$  nm, respectively. In 70:30  $V^+$  samples, the concentrations of CTAT and SDBS are 15.4 mM and 8.6 mM, respectively. This corresponds to 6.8 mM excess CTAT, or a 1.8 fold molar excess of cations. Likewise,  $V^-$  refers to vesicles with a net negative charge due to a 13.5 mM excess of SDBS (the samples contain 6.6 mM CTAT and 20.1 mM SDBS), or a 3.0 fold molar excess of anions.

### **2.2.3. Size Exclusion Chromatography (SEC)**

Size exclusion chromatography (SEC) is a technique used to separate macromolecules according to their hydrodynamic volumes (sizes). Small particles are entrapped in the porous medium and take a longer path and more time in comparison to large particles which never enter into the pores. The size of surfactant vesicles ( $r > 50$  nm) is much larger than free dyes ( $r < 1$  nm), so when an appropriate porous medium is selected, SEC can be used to separate these two distinguishable species.

The separation is performed in an ordinary glass chromatography column with a frit and is packed with very small porous polymer beads designed to have pores of different sizes. If the packing material is a gel, this technique is called gel-filtration

chromatography (GFC). Samples are loaded together with an elution buffer. Different fractions of the filtered solution can be collected. Subsequently, detection techniques such as UV-vis absorption spectroscopy (UV-vis), fluorescence spectroscopy and dynamic light scattering (DLS) can be applied to those fractions in order to analyze molecular absorption, fluorescence and particle sizes. The apparatus and illustration for this process are shown in Figure 2.1.

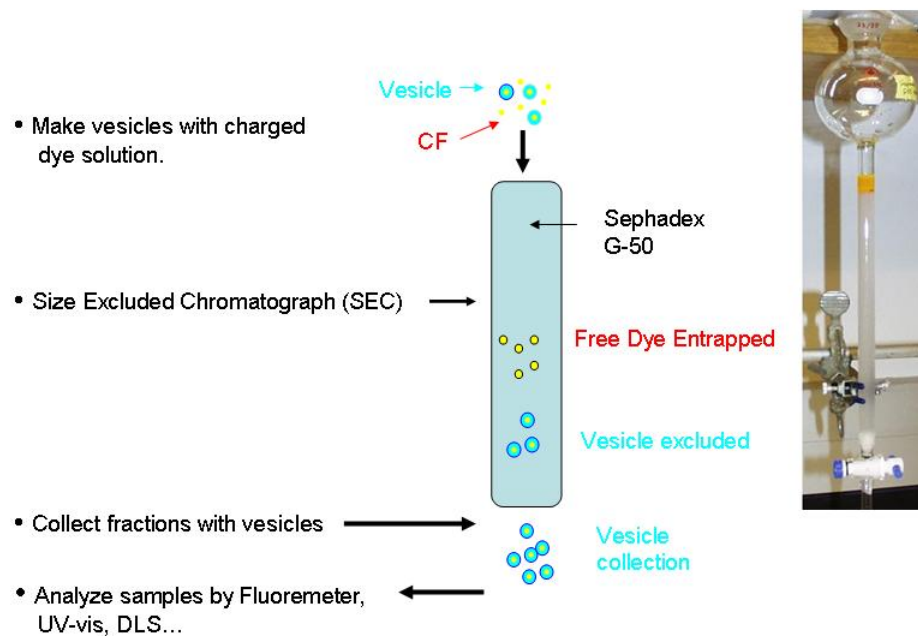


**Figure 2.1.** Schematic of size exclusion chromatography (SEC).

### 2.2.3.1. Determination of Apparent Encapsulation Efficiency by SEC

After vesicles are formed, they should be separated from the probe molecules that are not encapsulated and are free in solution. Therefore, the fraction of probe molecules that have been captured by the vesicles is determined.

In our experiment, a 2 x 25 cm column packed with Sephadex G50 resin (medium mesh, Amersham Biosciences) was used. During elution, vesicle solutions divided into two clear bands, one containing the dye-bearing vesicles and the other consisting of free dye. The apparent encapsulation efficiency ( $\varepsilon$ ) was determined by measuring the amount of encapsulated dye relative to the total initial amount, using UV-vis absorption (Hitachi U-3010 Spectrometer). It is thus defined as:

$$\varepsilon = \frac{V_f C_f}{V_i C_i} \quad (1)$$

where  $V$  and  $C$  are volume and concentration and  $i$  denotes initial values taken from the original preparation and  $f$  denotes values taken from the leading band in the SEC column. To avoid artifacts in UV-vis spectroscopy from light scattering or from dye aggregation inside the vesicles, the absorbance of the encapsulated dye was determined after first disrupting the vesicle membranes by the addition of Triton X-100 surfactant. Since  $\varepsilon$  reflects contributions from a probe dye molecule that is both encapsulated in the water pool of the vesicle and electrostatically adsorbed on the bilayers of the vesicle sample.

In addition to conventional SEC, quick spin columns proved to also be effective tools for rapidly analyzing the encapsulation of a vesicle sample. Quick spin columns are small columns that fit into an ordinary centrifuge and allow centrifugal force to be

used to accelerate elution. The columns and centrifuge for this work is shown in Figure 2.2. Quick Spin columns contain gel filtration media that allow large molecules (*e. g.* vesicles) to pass through quickly while retaining small molecules (*e. g.* free dyes). The quick and clean separation is achieved by using centrifugation. In this work, quick spin columns were used in long term experiments that determined the release rates over the course of weeks in order to determine how long cationic vesicles retain solutes after an initial separation from free dye.



**Figure 2.2.** Quick spin column and Minispin Centrifuge.

To evaluate long term release profiles for dye-bearing vesicles the following procedure was used. First, the initial vesicle-solute mixture was purified using SEC (as

described above) to remove the free, un-encapsulated solute. The sample was then checked for release of solute from the vesicles over the course of several weeks. For this purpose, quick-spin columns pre-packed with Sephadex G50 (fine) were used (Roche Applied Science, USA, additional beads for repacking the columns from Sigma). On a specific day, a 100  $\mu$ L aliquot was run through a quick-spin column by centrifugation (Minispin, Eppendorf, USA) at 3000 rpm for 15 s, and the eluted fraction was evaluated using UV-vis spectroscopy. Any solute that had been released from the vesicles was retained by the quick-spin column. The amount of solute eluted by the column corresponded to the solute still encapsulated by the vesicles. The UV-vis absorption value for the eluted sample was divided by the corresponding value obtained on day zero (immediately after SEC) to yield the fraction of solute that remained encapsulated in the vesicles. The above procedure was repeated at various times to create a release curve (i.e., encapsulated solute vs. time elapsed, as shown in Chapter 4, Figure 4.3.).

#### **2.2.4. Vesicle Characterization**

##### **2.2.4.1. Dynamic Light Scattering (DLS)**

Dynamic light scattering (DLS) is a well established technique for measuring particle size over the size range from a few nanometers to a few microns.<sup>2,3</sup> The principle of dynamic light scattering is described below.

When a laser beam passes through an aqueous solution with suspended particles, the beam scatters from those particles in all directions, resulting in a scattering-angle-dependent intensity pattern. If the particles are undergoing Brownian motion, the intensity pattern also fluctuates randomly. Given that the particle sizes are on the order

of the wavelength of the incident light, the intensity and angular dependence of the scattered light can be used to characterize the particles size of scattering materials. The scattered light is recorded as temporal fluctuations of intensities. Correlation of the fluctuations provides dynamical properties of molecules. Hence, the size distribution and diffusion characteristic of the molecules can be resolved.

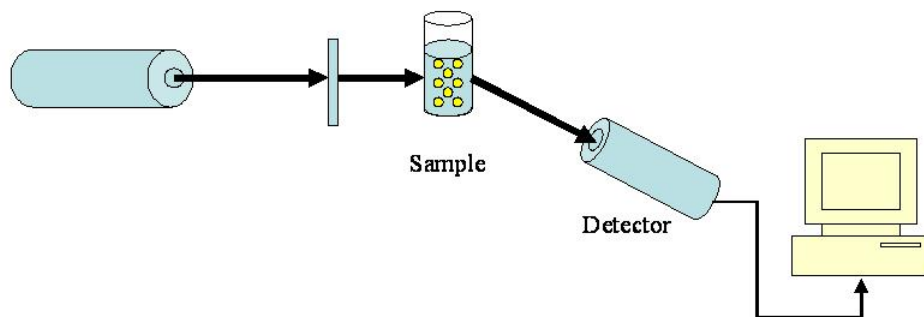


**Figure 2.3.** Schematic of dynamic light scattering.

The setup of dynamic light scattering is shown in the Figure 2.3. When incident light impinges on particles in solution, the scattered light is recorded by the detector which has been set at a certain angle from the direction of the incident light. The

scattering light intensity is  $|I^s(\vec{r}, t)| \propto |\vec{E}^s(\vec{r}, t) * \vec{E}^{s*}(\vec{r}, t)|$ , where  $|\vec{E}^s(\vec{r}, t)|$  is the electric field of the scattering light. Therefore, the light intensity is proportional to the electric field squared. The scattered temporal fluctuation intensities can be autocorrelated as below:

$$G(\tau) = \langle I(t) \bullet I(t + \tau) \rangle \quad (2)$$

Furthermore, the autocorrelation function  $G(\tau)$  can be expressed as  $G(\tau) = b + \beta e^{-2\Gamma\tau}$ , when the solution is sufficiently dilute to satisfy the assumption that there are no interactions between particles. In this form of the autocorrelation function,  $b$  is the baseline of the correlation function at infinite delay,  $\beta$  is the correlation function amplitude at zero decay, and  $\Gamma$  is the decay rate.

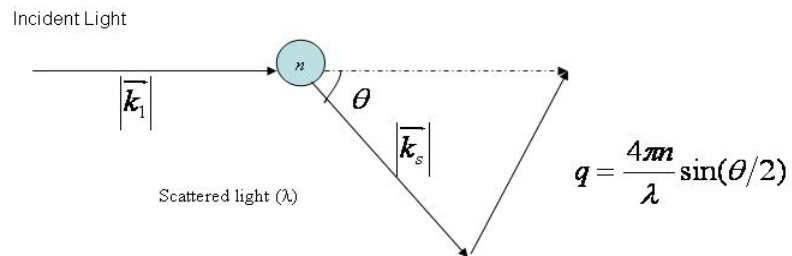


**Figure 2.4.** Illustration of wave vectors of incident and scattered light.

Among the above factors,

$$\Gamma = Dq^2 \quad (3)$$

which links the autocorrelation function with the size, diffusion constant and size distribution of the particles in solution.  $q$ , the wave vector difference between the incident light and scattering light vector, is defined as  $q = \frac{4\pi n}{\lambda} \sin(\theta/2)$ , where  $n$  denotes the refractive index of solvent,  $\lambda$  is the wavelength of incident light and  $\theta$  is the angle between the incident light and detector.  $D$  in equation 3, is the diffusion constant for the particles of interest. Since the random diffusion can be described by Brownian motion, the diffusion constant can be given by the Stokes-Einstein equation  $D = \frac{kT}{6\pi\eta r_h}$ , where  $k$  is Boltzmann's constant,  $T$  is the temperature in K,  $\eta$  is the solvent viscosity and  $r_h$  is the hydrodynamic radius of a diffusing sphere.

In this work a Photocor-FC instrument was utilized to determine the size of surfactant vesicles before and after SEC. The light source was a 5 mW laser at 633 nm and the scattering angle was 90°. A logarithmic correlator was used to obtain the autocorrelation function, which was analyzed by the method of cumulants<sup>4</sup> to yield a diffusion coefficient. The apparent hydrodynamic size of the vesicles was obtained from the diffusion coefficient through the Stokes-Einstein relationship. The intensity (total counts) of the signal was also recorded for each sample.

### 2.2.4.2. Fluorescence Quenching

We exploit the self-quenching behavior of CF to monitor dye release from vesicles. The following experimental protocol was used and is similar to that in an earlier study,<sup>5</sup> except for changes made to allow the calculation of the fraction of dye released over long periods (weeks). Samples were checked on a specific day by placing a fixed aliquot (1.5 mL) into a 1 cm cuvette and monitoring fluorescence at 520 nm while exciting at 490 nm using a Spex Fluorolog-3 spectrometer ( Horiba Jobin Yvon, in USA). The intensity was monitored for several minutes to establish the baseline fluorescence intensity, which contains a contribution from both free and encapsulated dyes. After the baseline was established, 100  $\mu$ L of 10% (w/w) aqueous Triton X-100 was added to disrupt the vesicles. Vesicle disruption results in the release of all dye molecules into solution and a concomitant increase in fluorescence (see Figure 3.1 in Chapter 3). To monitor long-term leakage rates, the fraction of dye released as a function of time,  $R(t)$ , was calculated for a given day. This quantity measures the fraction of encapsulation on *Day t* relative to the initial value on *Day 0*:

$$R(x) = 1 - \left\{ \frac{F_x(\text{final}) - F_x(\text{initial})}{F_0(\text{final}) - F_0(\text{initial})} \bullet \frac{F_o(\text{final})}{F_x(\text{final})} \right\} \quad (4)$$

where  $F(\text{initial})$  and  $F(\text{final})$  are the fluorescence intensities before and after adding the Triton X-100. This approach allows the direct determination of the proportion of the dye released on a daily basis and accounts for deviations due to long-term drift in the spectrophotometer.

### 2.2.5. Fluorescence Correlation Spectroscopy (FCS)

Fluorescence correlation spectroscopy (FCS)<sup>6-8</sup> is a correlation analysis of fluctuations of the fluorescence intensity arising from a dilute solution of fluorophores. An interesting application is the study of molecular interactions in solution. In this application, the random motion of fluorescently labeled molecules inside a defined volume element excited by a focused laser beam is observed. The fluorescence intensities fluctuate because of Brownian motion of the particles. These fluctuations provide information on the diffusion time of a fluorophore through the observation volume and this, in turn, depends directly dependent on the particle size. Any change in the fluorophores diffusion time, e.g. as a result of an interaction with other molecules, is readily detected. Hence, FCS is an ideal technique for the study of thermodynamic and kinetic features of molecular interactions in solution.

The fluctuating fluorescence signal is analyzed by autocorrelation analysis. The autocorrelation function is a mathematical method used to extract information such as amplitude and frequency of correlated fluctuations from data that may appear to consist of random fluctuations. Defining the fluctuation in the measured temporal fluorescence of probe molecules  $F(t)$  from the average value  $\langle F(t) \rangle$

$$\delta F(t) = F(t) - \langle F(t) \rangle \quad (5)$$

The normalized autocorrelation function  $G(\tau)$  of temporal fluctuations in the measured fluorescence  $F(t)$  is given by:<sup>7</sup>

$$G(\tau) = \frac{\langle \delta F(t) \bullet \delta F(t + \tau) \rangle}{\langle F(t) \rangle^2} = \frac{\langle F(t)F(t + \tau) \rangle - \langle F(t) \rangle^2}{\langle F(t) \rangle^2} \quad (6)$$

where  $F(t + \tau)$  is the same temporal fluorescence as  $F(t)$ , but with time lag  $\tau$ .

Further, the autocorrelation function can be related to diffusion of multiple species in solution by below derived equations:<sup>9,10</sup>

$$G_i(\tau) = \sum_{i=1}^M A_i g_i(\tau) \quad (7)$$

$$g_i(\tau) = \left( \frac{1}{1 + 4 * D_i * \tau / \omega^2} \right) \left( \frac{1}{1 + 4 * D_i * \tau / z^2} \right)^{\frac{1}{2}} \quad (8)$$

where  $D_i$  is the diffusion coefficient of the  $i^{th}$  component in the system,  $\omega$  and  $z$  are the beam width in the radial and axial direction at laser focal volume and  $A_i$  denotes the fraction of the  $i^{th}$  species among total species with diffusion coefficient  $D_i$ .  $\sum_i A_i = 1$ .  $g_i$  is the autocorrelation function for each single species with diffusion coefficient of  $D_i$

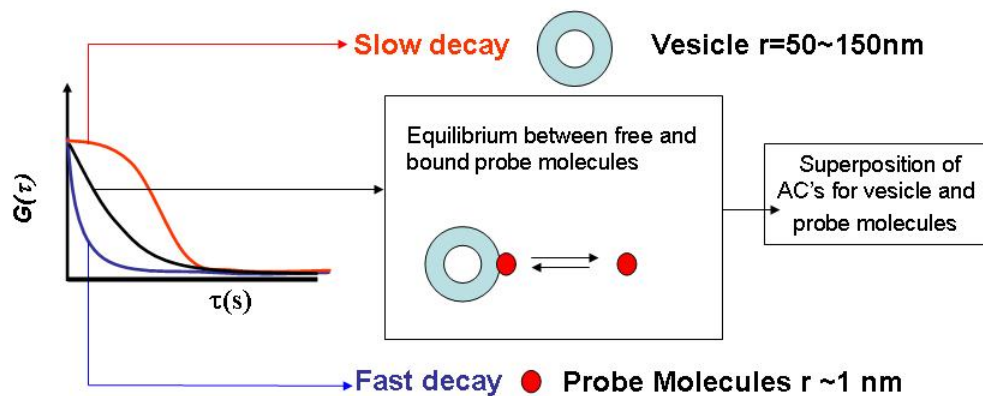


**Figure 2.5.** Cartoon of method for measuring the bound fraction of probe molecules in a vesicle solution. Fast decay corresponds to free probe molecules with small size. Slow decay arises from fluorophores bound to vesicles. In solutions where both free and vesicle-bound dye is present the autocorrelation decay is a superposition of the two pure decays as described by equation 7.

The autocorrelation decay obtained from solutions in which probe molecules are partially bound to vesicles is the superposition of diffusion of free probe molecules and vesicles. Therefore fitting such a curve to equation 7 allows one to determine the fraction of bound molecules.<sup>11</sup> Binding isotherms of probe molecules to vesicle bilayers can be constructed by varying concentrations of vesicles and hence the binding free energy can be obtained from the isotherm curve.

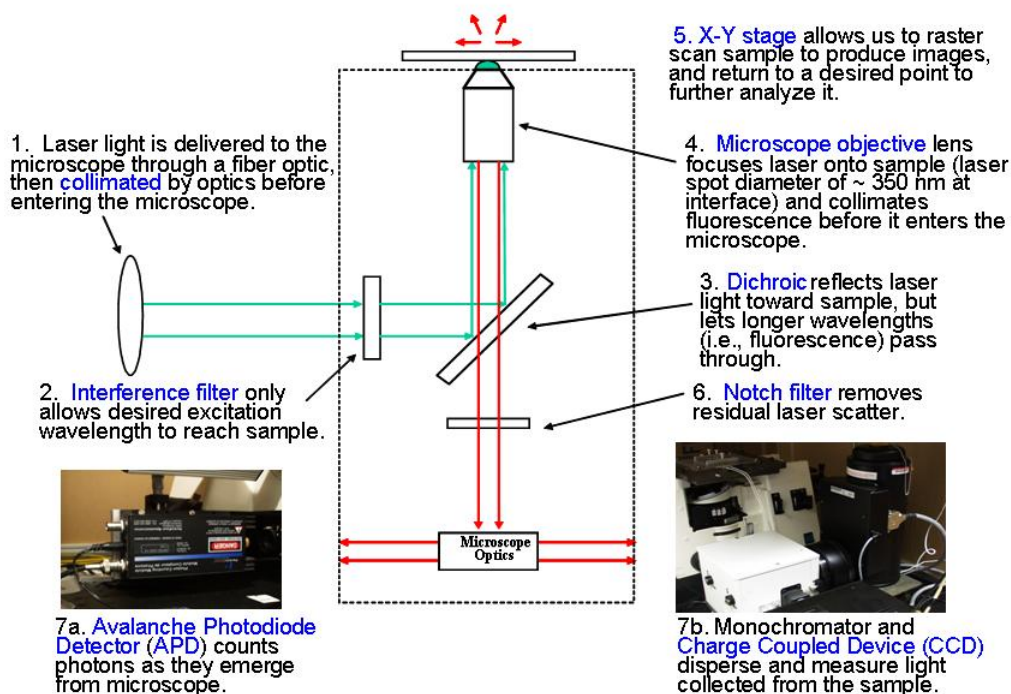


**Figure 2.6.** Schematic of scanning confocal fluorescence microscope.

The FCS experiments were performed with an inverted fluorescence microscope from Carl Zeiss. The sample was excited by an argon ion laser (usually 488 or 514 nm) or a He-Ne laser (543 nm). A Zeiss Neofluar oil immersion objective (100x, N.A.=1.34) was used. Separation of scattered excitation light from the collected emission was achieved by a Raman notch filter and/or long pass filter. The intensity fluctuations were detected by avalanche photodiodes (APDs), and processed with the NI board. The measurement was performed in the solution. The data were collected and analyzed by homemade Labview and Igor program respectively.

### 2.2.6. Time Tagged Method

As described in the previous section, FCS is a powerful technique to measure fluorophores diffusion in dilute solutions ( $\sim$  nM). FCS data are a series of temporal fluorescence intensity fluctuations. Detectors, such as a photomultiplier tubes (PMT) or avalanche photodiode (APD), are used to detect photons, emitted when fluorophores diffuse in and out of a tiny laser focal volume ( $\sim$ 1 fL) producing intensity fluctuations. The conventional method to collect FCS data is to record all temporal fluorescence fluctuations. For example, when acquiring photon intensities with a temporal resolution of 1  $\mu$ s, there are  $10^6$  intensity values recorded in 1 s. While typically the count rate of an FCS measurement is only between  $10^3$  and  $10^5$  due to the low concentration of fluorophores. Therefore, most intensity values for the majority of the time points in this method are zeros. The redundant zeros which are stored in FCS data is the main drawback of this method, leading to a huge file size and making it inconvenient to move, store and analyze. The detector response time limits the sampling time for FCS measurements. For example, the APD (SPCM-AQR-15, Perkin Elmer) used in this study has a dead time 50 ns. Hence, it is desirable to read the detector with a time resolution comparable to 50 ns. In our studies we employ time-tagged analysis with 12.5 ns sampling time. This method allows us to assign a time tag, which corresponds to the arrival time, to every detected photon.

The time-tagged method for FCS overcomes the shortcomings from the conventional method. “Time tagged” concept originates from time-correlated single photon counting (TCSPC) which is used in not only fluorescence intensities but also

fluorescence lifetime measurement by applying a pulsed laser excitation, correlating the photon detection times on a nanosecond timescale and obtaining the time delay between the excitation and detection.<sup>12,13</sup> The time-tagged method is a histogram method and records data only when actual photon events are detected. This method combined with FCS measurement was proposed for improving the signal to noise ratio of FCS measurement<sup>14,15</sup> initially. The time-tagged method for acquiring FCS data was used for studying the binding process of ionic organic molecules on charged surfactant vesicle bilayers due to the electrostatic interaction (Details in Chapter 5).

Time tagged method counts the elapsed time between photons arriving at a detector and stores this elapsed time tagged with 12.5 ns time resolution in time-tagged format. From the lags between the photons, diffusion characters of fluorophores in solution can be obtained by constructed correlation function. This method allows only effective information to be collected and avoids the abundant zeros.

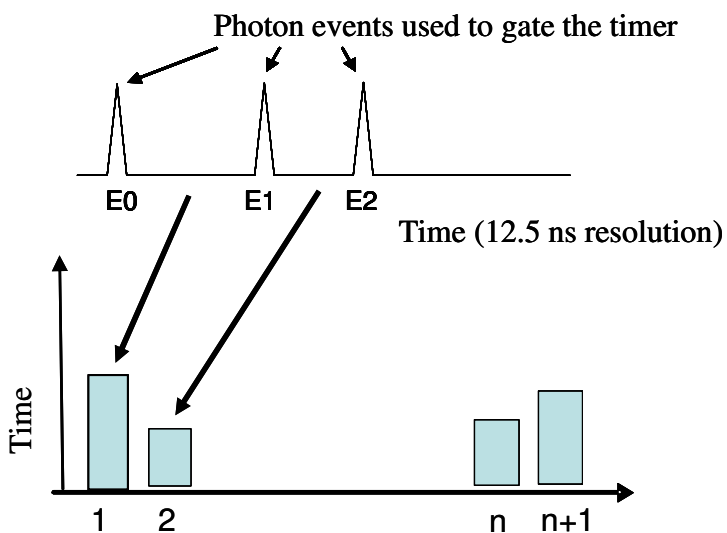


**Figure 2.7.** Schematic of time tagged method.

To collect time tagged data, a very sensitive photon detector, avalanche photon diodes (APD) and a set of timer and counter circuits are required. The schematic of experimental setup is shown in Figure 2.8.

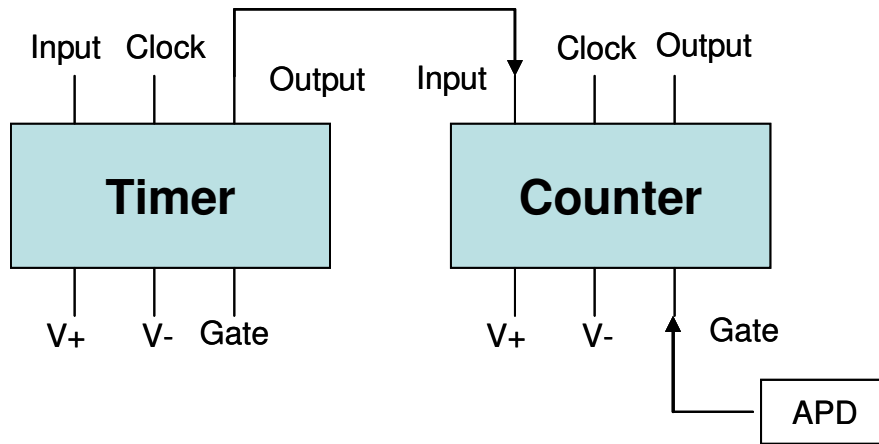


**Figure 2.8.** Schematic of experimental setup of time tagged method.

A timer counter board PCI-6602 (National Instruments) was used to accomplish this acquisition. The timer generates a continuous square wave at a frequency of 80 MHz which corresponds to 12.5 ns between pulses. This timer is connected to an independent counter; the frequency is measured by this counter. The APD is connected to the counter as a gate. Photon events arriving at the APD act as the gating events for the counter. For example, when the first photon hits the APD it sends out a signal to the counter. The counter starts to counter the number of frequencies from the timer. When next photon is detected, the counter records the number of the 80 MHz pulses from the timer that have occurred since it began counting. It converts that value to a total time, stores it and starts to counting pulses for the next photon event. The resulting data file is an array of pulse

counts which can be converted into time. Each value in the file corresponds to the number of 80 MHz pulses that took place since the last value was written, that is, the time between two subsequent photons being detected. Hence, time-tagged data are obtained and an autocorrelation curve can be constructed to conduct further analysis.

The algorithm to convert time-tagged data to a correlation curve is described as follows. As in the traditional FCS technique it is necessary to track the temporal correlation of each photon with all those that follow it. When analyzing the time-tagged data one begins by examining the time difference between the first two photons which corresponds to the first number in the file. Its value is sorted into a histogram as one pair of photons that occurred with a temporal separation of  $x$ . The next photon is then considered relative to the first by adding the time between photon 2 and 3 (value 2 in the file) on to the previous value and sorting that into the histogram. This process is iterated through until the time difference between the very first photon and the final one has been sorted into the histogram. Then the second photon is considered and the time difference between it and all the others are sorted into the histogram. This process continues until the temporal difference between each pair of photons in the data set has been sorted into the histogram. Then the program is terminated and the resulting histogram is the correlation curve which can be fit to obtain values for diffusion.

. Correlation curves constructed by time tagged method of a real measurement of CF diffusion with different concentrations are shown in the Figure 2.9. The first point of correlation curve is reversely proportional to the concentration of sample concentration in

theory. And shown in the Figure 2.9, the first point in the three curves is corresponding to the CF concentration in the solution. Time-tagged method is applicable and accurate in acquiring FCS data in this study.

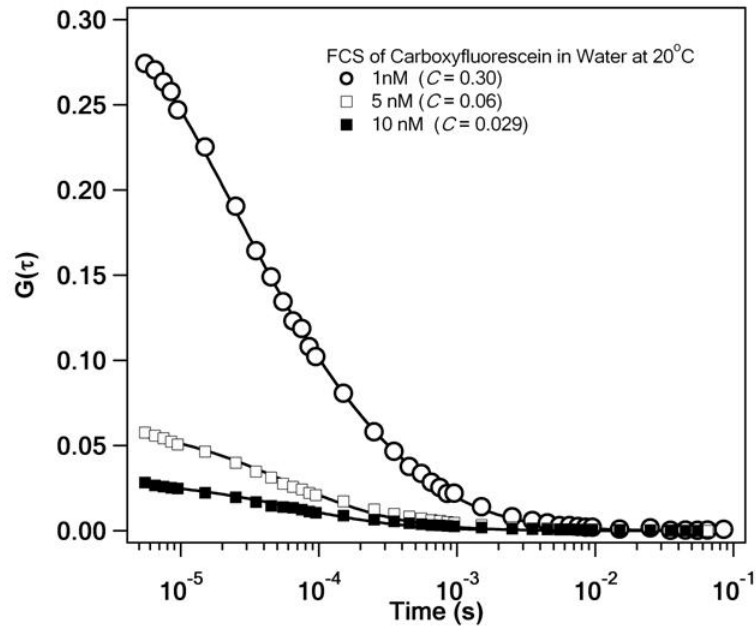


**Figure 2.9.** Autocorrelation decays for the samples containing the dye CF in water at room temperature.

## References:

1. Kaler, E. W.; Murthy, A. K.; Rodriguez, B. E.; Zasadzinski, J. A. N. *Science* 1989, 245, 1371-1374.
2. Berne, B. J.; Pecora, R. *Dynamic Light Scattering: With Applications to Chemistry, Biology, and Physics*; Dover Publications, 2000.
3. Brown, W. *Dynamic Light Scattering: The Method and Some Applications*; Oxford University Press, USA, 1993.
4. Koppel, D. E. *J. Chem. Phys.* 1972, 57, 4814-4820.
5. Jang, H.; Pell, L. E.; Korgel, B. A.; English, D. S. *J. Photoch. Photobio. A* 2003, 158, 111-117.
6. Magde, D.; Webb, W. W.; Elson, E. *Phys. Rev. Lett.* 1972, 29, 705-708.
7. Magde, D.; Elson, E. L.; Webb, W. W. *Biopolymers* 1974, 13, 29-61.
8. Elson, E. L.; Magde, D. *Biopolymers* 1974, 13, 1-27.
9. Rigler, R.; Mets, U.; Widengren, J.; Kask, P. *Eur. Biophys. J. Biophys* 1993, 22, 169-175.
10. Schwille, P.; Haupts, U.; Maiti, S.; Webb, W. W. *Biophys. J.* 1999, 77, 2251-2265.
11. Rusu, L.; Gambhir, A.; McLaughlin, S.; Radler, J. *Biophys. J.* 2004, 87, 1044-1053.
12. O'Connor, D. V.; Philips, D. *Time-Correlated Single Photon Counting*; Academic: London, 1984.
13. Lakowicz, J. R. *Principles of Fluorescence Spectroscopy*; Plenum: New York, 1991.
14. Lamb, D. C.; Schenk, A.; Rocker, C.; Scalfi-Happ, C.; Nienhaus, G. U. *Biophys. J.* 2000, 79, 1129-1138.
15. Eggeling, C.; Berger, S.; Brand, L.; Fries, J. R.; Schaffer, J.; Volkmer, A.; Seidel, C. A. M. *J. Biotechnol.* 2001, 86, 163-180.

## Chapter 3. Highly Efficient Capture and Long-Term Encapsulation of Dye by Catanionic Surfactant Vesicles

*Langmuir*, 22 (15), 6461 -6464, 2006

Xiang Wang, Emily J. Danoff, Nikolai A. Sinkov, Jae-Ho Lee,  
Srinivasa R. Raghavan, and Douglas S. English

### 3.1. Introduction

The development of vesicles and liposomes for controlled release applications (e.g., in drug delivery, agrochemicals, or cosmetics) is a technological objective of great interest. An important challenge in this area is the stability and shelf life of vesicles bearing drugs or other molecules. Conventional phospholipid vesicles formed by sonication or extrusion are kinetically-trapped nonequilibrium structures. Over time, these vesicles tend to fuse or rupture to form lamellar phases, and in the process, their contents are likely to be released. Improvements in vesicle stability and encapsulation properties can be achieved by changing bilayer composition<sup>1-3</sup> or by using micron-sized vesicles.<sup>4</sup>

A simple, attractive alternative to phospholipid vesicles in some applications may be offered by *surfactant* vesicles, formed by mixing single-tailed cationic and anionic surfactants. The existence of such “catanionic” vesicles has been known for over fifteen years.<sup>5</sup> These vesicles are spontaneously generated when the individual surfactants are mixed with water in the right proportion. Vesicle formation is thus quicker and easier

compared to phospholipid vesicles, since extrusion or sonication steps are not required. Furthermore, the required materials are common surfactants that are cheaper than purified or synthetic phospholipids. Catanionic vesicles also tend to be stable for very long periods of time. Whether these vesicles are truly equilibrium structures is still the subject of some debate.<sup>6,7</sup>

For application of catanionic vesicles as storage and delivery agents of small molecules, the critical issue is their ability to *encapsulate* molecules. In particular, a key unanswered question is how do catanionic surfactant vesicles compare to conventional phospholipid vesicles with regard to encapsulation efficiency and membrane permeability? Despite the extensive literature on catanionic vesicles, there is surprisingly little information on their encapsulating abilities or the permeability of their bilayers. The few studies that have explored encapsulation with well-characterized catanionic vesicles focused principally on the entrapment of glucose.<sup>8-10</sup> Another study by Zhao and co-workers<sup>11</sup> quantified the trapping efficiency of catanionic vesicles for a bromophenol blue dye, but did not study the membrane permeability or long-term stability. In short, the ability of catanionic vesicles to entrap and encapsulate solutes, especially ionic molecules, remains large untested.<sup>12</sup>

### **3.2. Materials and Methods**

Here we report preliminary results from our studies on the encapsulation and subsequent release of a model ionic solute from catanionic vesicles. We have chosen

carboxyfluorescein (CF) as our model solute. CF is a widely used probe for vesicle encapsulation due to its ability to undergo efficient self-quenching of fluorescence at millimolar concentrations. For example, when 60 mM CF is entrapped in vesicles, its fluorescence intensity is reduced by 60-80%, but as the dye is released from the vesicle, and thus diluted by the surrounding buffer, its fluorescence intensity increases.<sup>13,14</sup> We employ this self-quenching phenomenon to monitor the release of entrapped CF from cationic vesicles as well as the trapping efficiency of these vesicles. The cationic vesicles used here are from the well-known CTAT/SDBS system, which is a mixture of the single-tailed cationic surfactant, cetyltrimethylammonium tosylate (CTAT) and the single-tailed anionic surfactant, sodium dodecylbenzenesulfonate (SDBS). For comparison, we conduct similar encapsulation experiments with phospholipid vesicles formed from egg yolk phosphatidylcholine (EYPC). The key result that we report in this work is that the cationic vesicles are able to sequester CF more efficiently and for much longer periods of time than the phospholipid vesicles. We use the term sequester to refer to dye that is either captured in the inner water pool of the vesicle or adsorbed to the bilayer since both modes of sequestration are observed here. Our results, though limited in scope, demonstrate the possibility of cationic vesicles as an extremely efficient alternative for long-term sequestering of small molecules.

### **3.3. Results**

#### **3.3.1. Apparent Encapsulation Efficiency**

We studied the apparent encapsulation efficiency of CF in cationic vesicles at two different CTAT/SDBS compositions, which are pinpointed in the phase diagram (Figure 3.1).<sup>9,15</sup> The first sample falls in the CTAT-rich vesicle lobe and consists of 1 wt.% total surfactant with a 7:3 w/w of CTAT to SDBS. The vesicles in this case are denoted by  $V^+$  since they have a molar excess of the cationic surfactant. The second sample falls in the SDBS-rich vesicle lobe and it is a 3:7 w/w mixture of CTAT to SDBS at 1 wt.% total surfactant. These vesicles are denoted by  $V^-$ .

Separation of free dye from CF bearing vesicles was achieved by size exclusion chromatography (SEC), as described in Chapter 2. When encapsulation was achieved, two bands were well-resolved on the column and were visible with the naked eye or by viewing with a UV lamp. The leading band contained vesicles and the second band contained the free dye. DLS experiments were used to confirm these assignments. The DLS results from the leading band always gave values for hydrodynamic radius and total scattering intensity that were consistent with the presence of vesicles. Initial  $V^+$  samples, prior to SEC, were found to have an average radius of  $76 \pm 5$  nm, which was constant throughout the dilute surfactant range of 1.0% to 0.004% total surfactant concentration. This is consistent with the phase diagram in Figure 3.1.  $V^+$  samples were also studied after elution from the SEC column and the measured average radius was  $90 \pm 5$  nm.

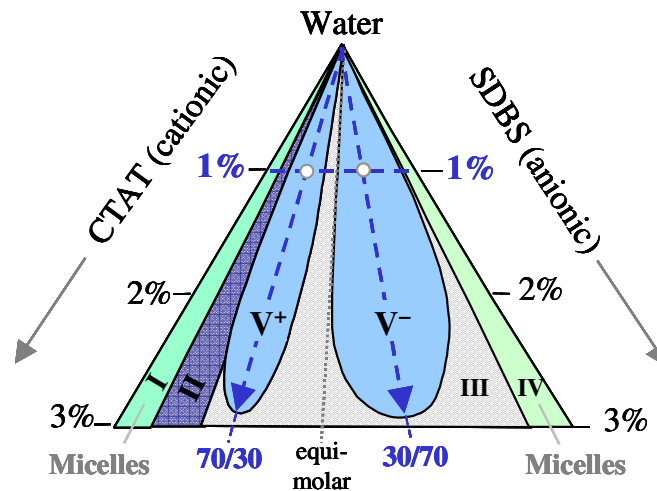


**Figure 3.1.** Phase diagram of CTAT/SDBS showing the dilute (water-rich) corner. Vesicles are present in the two lobes, denoted by V+ and V-. One composition in each lobe is used in this study and these compositions are indicated by the hollow circles. Adapted from ref. 15.

	Apparent Encapsulation Efficiency, $\varepsilon$	Adsorption
EYPC	$1.6 \pm 0.2\%$	$0.40 \pm 0.08\%$
V <sup>+</sup>	$21 \pm 2\%$	$16 \pm 4\%$

**Table 3.1.** Apparent encapsulation efficiency and dye adsorption for CF on both EYPC vesicles and V<sup>+</sup>. The apparent encapsulation efficiency reflects contributions from dyes that are adsorbed to the bilayer or captured in the inner water pool. Therefore the actual encapsulation efficiency for dye in the V<sup>+</sup> water pool is ca. 5%.

In Table 3.1, we report the apparent encapsulation efficiency,  $\varepsilon$ , for CF in V<sup>+</sup> and EYPC vesicle preparations. The apparent encapsulation efficiency is calculated using the method described in the supporting information. The value of  $\varepsilon$  gives percentage of dye that is captured by the vesicles during their preparation. In the absence of any specific

interactions between the solute and the vesicle wall,  $\varepsilon$  is a measure of the aqueous volume enclosed by the vesicles relative to the total solution volume.

For EYPC vesicles,  $\varepsilon$  is ca. 1.6%, in agreement with literature values.<sup>16</sup> In comparison, the total enclosed volume of EYPC vesicles calculated from their average DLS radius is about 6%. However, it should be noted that some leakage and rupture of the vesicles is likely to occur during the SEC process, which can explain the difference between these values. Considering next the encapsulation efficiency for the cationic  $V^+$  vesicles, we note from Table 3.1 that their  $\varepsilon$  is ca. 21%, which is extremely large compared to the EYPC lipid vesicles. Dye encapsulation was evaluated using 1 mM CF since it was found that CF concentrations above 5 mM inhibited vesicle formation. Experiments to measure  $\varepsilon$  for  $V^-$  samples were highly irreproducible, yielding ranges from 0 to 3% with no apparent dependence on any governable variables. Given that the total concentration of surfactant is the same for both  $V^+$  and  $V^-$  samples, the differences in the value and reliability of  $\varepsilon$  is unexpected from simple predictions based on enclosed volume. The large and highly reproducible value of  $\varepsilon$  for the  $V^+$  samples is likely due to strong, specific interactions between the  $V^+$  bilayer and the anionic CF dye. If this assertion is correct, one might expect a measurable value for  $\varepsilon$  even when the dye is added *after* vesicle formation due to strong interactions of CF with the outer leaflet of the  $V^+$  bilayer.

To test whether adsorption of CF to the vesicle bilayer was significant, we conducted measurements in which the dye was added to the vesicle solution *after*

vesicles were formed. These experiments were done with both EYPC and  $V^+$  vesicles, and in each case the vesicles were then separated on the SEC column and the amount of *adsorbed* dye was calculated. The results in Table 3.1 show that only 0.4% of the dye was adsorbed on the EYPC vesicles, indicating that nonspecific interactions of the dye with the lipid bilayer were weak. On the other hand, for the  $V^+$  samples, about 16% of the dye was adsorbed, which is comparable with the encapsulation efficiencies measured earlier. Thus, binding of the anionic CF to the  $V^+$  bilayer contributes significantly to the amount of sequestered dye. Since adsorption accounts for as much as 75% of the captured dye we have referred to  $\varepsilon$  as the *apparent* encapsulation efficiency. We hypothesize that adsorption occurs via direct, electrostatic interaction between the anionic dye and the excess cationic surfactant in the  $V^+$  bilayer. Electrostatic interactions between charged surfactant vesicles and polyanions in solution have been observed,<sup>17</sup> and Karukstis *et al.* have reported favorable dye-bilayer interactions in which association was observed to increase with surface charge.<sup>18</sup> Our findings are significant because they illustrate that excess charge in the bilayer effectively increases the loading capacity of the vesicles. To our knowledge this is a property of the catanionic surfactant vesicles that has not previously been reported.

### 3.3.2. Long-Term Dye Release

We now consider the question of how long the encapsulated fraction remains in the  $V^+$  vesicle interior compared to encapsulation by EYPC vesicles. As time progresses, we expect the encapsulated dye to leak through the vesicle bilayer and into the solution. As discussed earlier, the self-quenching of CF provides a convenient way to monitor its

efflux. If the dye is released into the external solution by disrupting the vesicles, there is a large increase in the CF emission intensity. This is illustrated by Figure 3.2, which shows several time traces obtained over the course of four weeks from  $V^+$  vesicles containing encapsulated CF. For these experiments, a substantial volume of the  $CF/V^+$  sample was prepared on the first day and run through the SEC column to remove free dye; therefore, each trace in Figure 3.2 is for data acquired from the same preparation at a given number of days after SEC was run. The traces show the emission intensity before and after the addition of Triton X-100, a nonionic detergent that disrupts both lipid and surfactant vesicles.<sup>19</sup> As can be seen, the resulting release of dye into the solution causes a large jump in emission intensity, and the size of this jump is proportional to the amount of dye encapsulated within the vesicles.

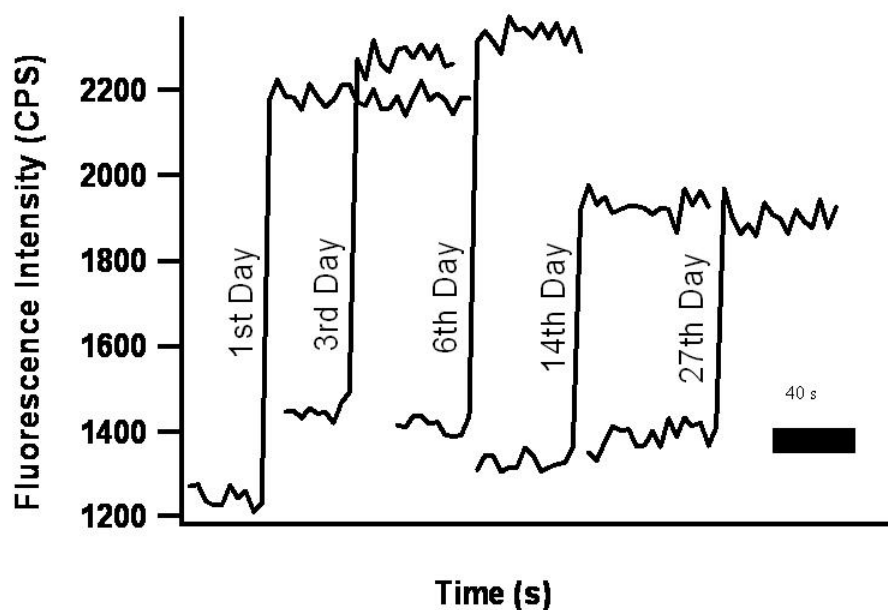


**Figure 3.2.** Denaturation of cationic vesicles and release of carboxyfluorescein. Each time trace depicts detergent-induced denaturation of a 1.5 mL aliquot of carboxyfluorescein-loaded, CTAT-rich, cationic vesicles taken from a single batch. The spike in fluorescence is due to the increase in carboxyfluorescein fluorescence efficiency as it is released upon disruption of the cationic vesicles. The scale bar shows the time scale for the individual traces and the day denotes the age of the sample.

We note that the intensity jump reports on the *encapsulated* dye and not on the adsorbed dye, since addition of Triton X-100 to vesicle samples in which the dye was added after vesicle preparation did not produce an intensity jump. As expected, the largest jump occurs for the freshly prepared vesicle solution where all the dye is encapsulated in the vesicles. As described in the Chapter 2, we compare the magnitude of the jump on *Day x* with the highest jump (*Day 0*) and thereby obtain the fraction of the dye released on day *x*,  $R(t=x)$ . It should be noted that  $R(t)$  may actually underestimate the degree of dye retention since it does not account for dequenching occurring within the

vesicles as the dye leaks out. This effect will be negligible in the cationic samples since the dye concentration remains nearly unchanged over the time course of Figure 3.3.

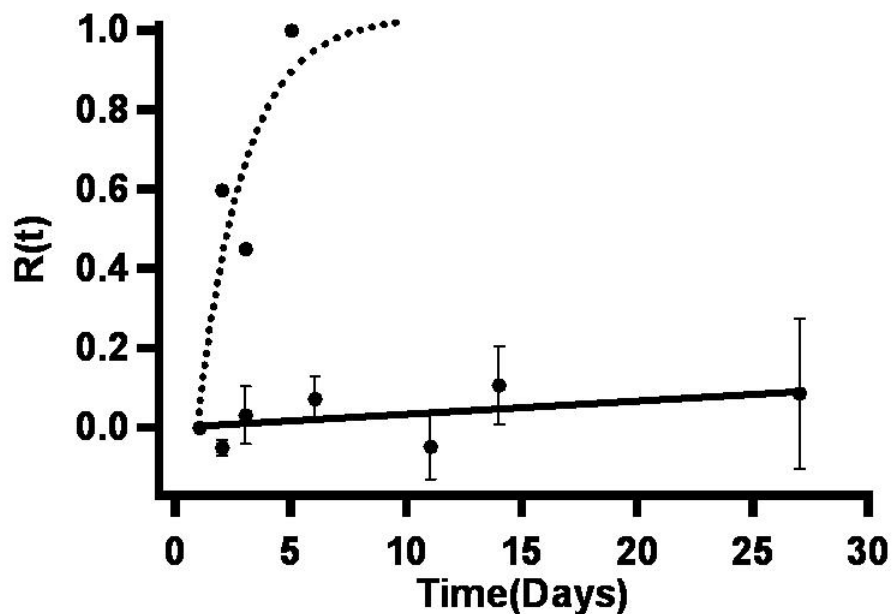


**Figure 3.3.** Comparison of dye released as a function of time,  $R(t)$ , between equilibrium vesicles (solid line) and phospholipid vesicles (dotted line). Release of carboxyfluorescein (CF) is shown as a function of time over a period of 27 days. The half-life for release in cationic vesicles is 84 days compared to 2 days in phospholipid vesicles, illustrating the enhanced stability of  $V^+$  samples.

Plots of  $R(t)$  are shown in Figure 3.3 for CF in  $V^+$  (solid line) and EYPC (dotted line) vesicles. First, consider the results for vesicles formed from EYPC. Here, the dye is released rapidly over a period of about 5 days, yielding an estimated half-life of *ca.* 2 days for the entrapped dye. When  $R(t)$  reaches 1 there is no longer an increase in fluorescence emission upon addition of detergent, i.e., the dye concentration inside the

vesicles has equilibrated with that of the bulk solution. Note that the equilibration takes place by transport across the membrane not by vesicle degradation, since the vesicles themselves are stable for up to several weeks. In contrast to EYPC vesicle samples,  $V^+$  samples are able to encapsulate CF over a much longer period of time. The release of CF is approximately 20% after 27 days giving an estimated half-life of 84 days for the entrapped dye. DLS data taken over the 27-day course of the experiments show that the cationic vesicle average radii remain unchanged and indicate that vesicle fusion or rupture is not occurring to any significant degree. This indicates a fundamental difference in the permeability of  $V^+$  membranes to anionic solutes and in the overall vesicle stability compared with lipid vesicles. We acknowledge that it is possible to obtain slower efflux rates in EYPC vesicles. For instance, the addition of cholesterol or changes in lipid composition will improve the long-term encapsulation by EYPC vesicles.<sup>1-3</sup> Xiang and Anderson<sup>1</sup> show that the addition of 0.25 volume fraction of cholesterol to EYPC decreases membrane permeability by nearly 10-fold. Here we show that cationic vesicles achieve much better encapsulation stability without additional components.

We have illustrated the ability for  $V^+$  to achieve dramatically different encapsulation of CF relative to those of EYPC vesicles. At this point we do not know how general this observation is or whether these improved characteristics will emerge for other dyes or vesicle compositions. The original motivation for investigating CF encapsulation was to provide a direct comparison with the well characterized CF/EYPC system. Recently, Fischer *et al.* have reported that CTAT-rich vesicles are less

permeable to glucose than SDBS-rich vesicles or vesicles prepared from the pure ion-pair amphiphiles.<sup>10</sup> Future work is under way to determine whether the extraordinary ability of  $V^+$  to sequester CF is more than a mere curiosity and actually the first evidence of a general trend leading to important applications.

### **3.4. Conclusions and Discussions**

In summary, spectroscopic evidence has been presented supporting the capacity and long-term encapsulation of positively charged cationic vesicles for anionic CF. The remarkable apparent encapsulation efficiency of 21% is assigned to electrostatic interaction between the anionic solute and the excess positive charge of the  $V^+$  bilayer. The long-term stability of the encapsulation is due to low membrane permeability. Previous studies have shown that fusion of cationic vesicles occurs on a relatively long time scale of months.<sup>6</sup> Here we have shown that the encapsulation of anionic solutes does not appear to radically alter this process. Cationic vesicles are promising candidates for high efficiency capture and long-term encapsulation of ionic solutes.

### **3.5. Acknowledgments**

This work was supported in part by the National Science Foundation MRSEC-DMR #0080008 and by a grant from the Center for Nano-Manufacturing & Metrology to D.S.E. The authors also wish to thank the reviewers for their helpful comments and Mr. Charles Luckett for his critical reading of the manuscript.

## References:

1. Xiang, T. X.; Chen, J.; Anderson, B. D. *J Membrane Biol* 2000, *177*, 137-148.
2. Ishida, A.; Otsuka, C.; Tani, H.; Kamidate, T. *Anal. Biochem.* 2005, *342*, 338-340.
3. Apel-Paz, M.; Doncel, G. F.; Vanderlick, T. K. *Langmuir* 2005, *21*, 9843-9849.
4. Sato, Y.; Shin-ichiro, M. N.; Yoshikawa, K. *Chem. Phys. Lett.* 2003, *380*, 279-285.
5. Kaler, E. W.; Murthy, A. K.; Rodriguez, B. E.; Zasadzinski, J. A. N. *Science* 1989, *245*, 1371-1374.
6. Almgren, M.; Rangelov, S. *Langmuir* 2004, *20*, 6611-6618.
7. Laughlin, R. G. *Colloids. Surf., A* 1997, *128*, 27-38.
8. Caillet, C.; Hebrant, M.; Tondre, C. *Langmuir* 2000, *16*, 9099-9102.
9. Kaler, E. W.; Herrington, K. L.; Murthy, A. K.; Zasadzinski, J. A. N. *J. Phys. Chem.* 1992, *96*, 6698-6707.
10. Fischer, A.; Hebrant, M.; Tondre, C. *J. Coll. Inter. Sci* 2002, *248*, 163-168.
11. Zhao, G.-X.; Yu, W.-L. *J. Coll. Inter. Sci* 1995, *173*, 159-164.
12. Tondre, C.; Caillet, C. *Adv. Coll. Inter. Sci* 2001, *93*, 115-134.
13. Schwarz, G.; Arbusova, A. *BBA-Biomembranes* 1995, *1239*, 51-57.
14. Weinstein, J. N.; Yoshikami, S.; Henkart, P.; Blumenthal, R.; Hagins, W. A. *Science* 1977, *195*, 489-492.
15. Koehler, R. D.; Raghavan, S. R.; Kaler, E. W. *J. Phys. Chem., B* 2000, *104*, 11035-11044.
16. Goldbach, P.; Brochart, H.; Wehrle, P.; Stamm, A. *Int. J. Pharm.* 1995, *117*, 225-230.
17. Antunes, F. E.; Marques, E. F.; Gomes, R.; Thuresson, K.; Lindman, B.; Miguel, M. G. *Langmuir* 2003, *20*, 4647-4656.
18. Karukstis, K.; Zieleniuk, C. A.; Fox, M. J. *Langmuir* 2003, *19*, 10054-10060.
19. Jang, H.; Pell, L. E.; Korgel, B. A.; English, D. S. *J. Photochem. Photobiol., A* 2003, *158*, 111-117.

## Chapter 4. Surfactant Vesicles for High-Efficiency Capture and Separation of Charged Organic Solutes

*Langmuir*, 23 (17), 8965 -8971, 2007.

Emily J. Danoff, Xiang Wang, Shih-Huang Tung, Nikolai A. Sinkov, Alice M. Kemme, Srinivasa R. Raghavan, and Douglas S. English

### 4.1. Introduction

Vesicles have long been of interest to the scientific community for their ability to encapsulate solute molecules such as drugs or proteins. Most studies on solute encapsulation have been carried out with vesicles made from two-tailed amphiphiles (lipids). However, *single-tailed* amphiphiles can also form vesicles<sup>1</sup> and in particular, simple mixtures of cationic and anionic surfactants, often referred to as “catanionic” systems, can spontaneously give rise to unilamellar vesicles in water.<sup>3</sup> A variety of catanionic vesicle-forming systems have been studied with respect to their phase behavior,<sup>4-11</sup> but much less is known about the ability of these vesicles to capture, encapsulate and retain organic molecules.

Recently, we published an initial report detailing some of the unique aspects of solute association with catanionic surfactant vesicles.<sup>12</sup> Specifically, we showed that catanionic vesicles with a molar excess of the cationic surfactant (CTAT) efficiently captured the anionic dye 5(6)-carboxyfluorescein (CF), and retained it for very long periods of time (half life  $t_{1/2}$  of 84 days).<sup>13</sup> In the present study, we expand on our initial

investigation to include the anionic and cationic organic solutes shown in Figure 4.1. In addition, we also study vesicle interactions with the cationic anti-cancer drug, doxorubicin. Our results show that surfactant vesicles can be highly efficient for the capture and long-term storage of organic solutes *that have a charge opposite to that of the vesicles*. Thus, there are strong, specific, charge-mediated interactions between vesicles and solutes, and we demonstrate how these interactions can be harnessed for efficient separation of oppositely-charged solutes from a solute mixture using only conventional, gravity-driven, size exclusion chromatography (SEC).

The catanionic vesicles we focus on for this study are formed by combining the cationic surfactant, cetyltrimethylammonium tosylate (CTAT) and the anionic surfactant, sodium dodecylbenzenesulfonate (SDBS).<sup>8,14</sup> The CTAT/SDBS system has been the most studied catanionic system, and the vesicles are known to be unilamellar and fairly monodisperse, with radii of 60-80 nm.<sup>8,13</sup> Catanionic surfactant vesicles have been recognized to have several advantages over conventional phospholipid vesicles: they form spontaneously without the need for additional sonication or extrusion, they have an extremely long shelf life, and the raw materials are inexpensive compared to synthetic or purified phospholipids. More importantly, this paper will demonstrate that catanionic vesicles have other advantages that have been hitherto unrecognized: they can efficiently capture and hold solutes that are of the opposite charge from the vesicles, and they retain these molecules for long periods of time.

## 4.2. Experiment and Methods

### 4.2.1. Materials

The surfactants CTAT, SDBS, and Triton X-100 were purchased from Aldrich Chemicals. The fluorescent dyes CF, sulforhodamine 101 (SR101), and Lucifer yellow (LY) were purchased from Molecular Probes, while the dye rhodamine 6G (R6G) and the chemotherapeutic drug, doxorubicin hydrochloride (Dox) were purchased from Fluka. All materials were used without further purification. The dry surfactants, CTAT and SDBS, were stored in a desiccator to prevent water absorption.

### 4.2.2 Vesicle Preparation

All samples were prepared at a total surfactant concentration of 1 wt.%. The surfactants were weighed and mixed with deionized water by gentle stirring, and then allowed to equilibrate at room temperature for at least 48 h.<sup>8</sup> Vesicle samples were prepared at two different surfactant compositions, 7:3 and 3:7 w/w CTAT to SDBS, which are denoted as  $V^+$  and  $V^-$ , respectively.  $V^+$  refers to the excess positive charge on the vesicle bilayers when there is an excess of CTAT. In these samples, the concentrations of CTAT and SDBS are 15.4 mM and 8.6 mM, respectively. This corresponds to 6.8 mM excess CTAT, or a 1.8 fold molar excess of cations. Likewise,  $V^-$  refers to vesicles with a net negative charge due to a 13.5 mM excess of SDBS (the samples contain 6.6 mM CTAT and 20.1 mM SDBS), or a 3.0 fold molar excess of anions.

### 4.2.3. Methods

#### 4.2.3.1. Evaluation of Apparent Encapsulation Efficiency ( $\varepsilon$ )

The apparent encapsulation efficiency,  $\varepsilon$ , describes the fraction of dye in a particular preparation that associates with the vesicle either through entrapment in the inner water pool or by association with the vesicle bilayer. The apparent encapsulation efficiencies of the two vesicle preparations,  $V^+$  and  $V^-$ , were evaluated for all five solute molecules. In each case, vesicles were prepared using aqueous solutions of the solute at a concentration of 1 mM. In the case of CF, a pH  $\sim$ 9 was required in order to fully dissolve the dye, and the stock solutions were adjusted accordingly. The solute/CTAT/SDBS mixtures were stirred for 30-60 min, and the resulting vesicle solutions were allowed to equilibrate in the dark at room temperature for at least 48 h. Thereafter, the samples were passed through a 25 mm syringe filter (0.45  $\mu$ m mesh) to remove any impurities or large aggregates. Dynamic light scattering (described below) was conducted to confirm vesicle formation and to measure the average vesicle size.

To measure the apparent encapsulation efficiency  $\varepsilon$ , SEC was used to separate the free solute from that which is captured by the vesicles. A 1.0 mL aliquot of the vesicle-solute sample was run through a 1.3 cm x 21 cm SEC column packed with Sephadex G50 resin (medium mesh, from Amersham Biosciences). During elution, 1.5 mL fractions were collected and analyzed, and a series of such fractions for a typical experiment is shown in Figure 4.2 (the solute here is CF). Dynamic light scattering was used to determine which of the eluted fractions contained vesicles, and the vesicles were

consistently found to elute at 5.5 mL total elution volume. The amount of solute in each fraction was determined using UV-vis spectroscopy (Hitachi U-3010 Spectrometer). The  $\varepsilon$  value is defined as the amount of vesicle-associated solute relative to the total initial amount of solute:

$$\varepsilon = \frac{V_f (A_{f1} + A_{f2} + \dots)}{V_i A_i} \quad (1)$$

where  $V$  and  $A$  are volume and absorbance and  $i$  denotes initial values taken from the original preparation and  $f$  denotes values taken from the fractions eluted from the SEC column shown by dynamic light scattering to contain vesicles. To avoid artifacts in UV-vis spectroscopy from light scattering or from solute aggregation inside the vesicles, the absorbance was determined after first disrupting the vesicles by adding Triton X-100 surfactant to each fraction. Note that  $\varepsilon$  reflects contributions from both the solute in the water pool inside the vesicle and the solute that is electrostatically adsorbed on the vesicle bilayers.

#### **4.2.3.2. Long-Term Capture and Dye Release**

To evaluate the ability of vesicles to retain solutes for long periods of time, the following procedure was adopted. First, the initial vesicle-solute mixture was purified using SEC (as described above) to remove the free solute. The sample was then checked for release of solute from the vesicles over the course of several weeks. For this purpose, quick-spin columns pre-packed with Sephadex G50 (fine) were used (column from Roche, additional beads for repacking the columns from Sigma). On a specific day, a 100  $\mu$ L aliquot was run through a quick-spin column by centrifugation (3000 rpm, 15 s),

and the eluted fraction was evaluated using UV-vis spectroscopy. Any solute that had been released from the vesicles was retained by the quick-spin column. Therefore, the amount of solute eluted by the column corresponded to the solute still associated with the vesicles. The UV-vis absorption value for the eluted sample was divided by the corresponding value obtained on day zero (immediately after SEC) to yield a fraction of solute that remains captured by the vesicles. The above procedure was repeated at various times to create a release curve (*i.e.*, released solute vs. time elapsed, as shown in Figure 4.3).

#### **4.2.3.3. Dynamic Light Scattering (DLS)**

Vesicle sizes in solution were monitored using DLS on a Photocor-FC instrument. The light source was a 5 mW laser at 633 nm and the scattering angle was 90°. A logarithmic correlator was used to obtain the autocorrelation function, which was analyzed by the method of cumulants to yield a diffusion coefficient. The apparent hydrodynamic size of the vesicles was obtained from the diffusion coefficient through the Stokes-Einstein relationship. The intensity (total counts) of the signal was also recorded for each sample.

#### **4.2.3.4. Small Angle Neutron Scattering (SANS)**

SANS experiments were conducted on the neat vesicles as well as the vesicle-solute mixtures to probe whether there were any changes in vesicle size or bilayer

integrity caused by the solutes. All samples for SANS experiments were prepared using deuterium oxide (99%D, from Cambridge Isotopes) in place of water. The measurements were made on the NG-7 (30 m) beamline at NIST in Gaithersburg, MD. Neutrons with a wavelength of 6 Å were selected. Two sample-detector distances of 1.33 m and 13.2 m were used to probe a wide range of wave vectors from 0.004 – 0.4 Å<sup>-1</sup>. Samples were studied in 2 mm quartz cells at 25°C. The scattering spectra were corrected and placed on an absolute scale using calibration standards provided by NIST. The data are shown as the radially averaged intensity  $I$  (minus the background) versus the wave vector  $q = (4\pi/\lambda) \sin(\theta/2)$ , where  $\lambda$  is the wavelength of incident neutrons and  $\theta$  is the scattering angle. Analysis was carried out as described previously.<sup>15</sup>

### 4.3. Results and Discussions

We have shown in our initial report<sup>13</sup> that the anionic dye, CF, can be efficiently sequestered in CTAT-rich vesicles ( $V^+$ ) via two mechanisms: encapsulation in the inner water pool and electrostatic adsorption to the charged bilayer. The apparent encapsulation efficiency  $\varepsilon$ , measured by the procedure described above in the Experimental Section, was found to be about 22%. Electrostatic adsorption contributed about 75% of the  $\varepsilon$  value, as shown by experiments where the CF was added to pre-formed  $V^+$  vesicles. Conversely, the  $\varepsilon$  for CF in SDBS-rich vesicles ( $V^-$ ) was only ca. 1%, which was comparable to the  $\varepsilon$  for CF encapsulation in neutral phospholipid (egg yolk-phosphatidyl choline, EYPC) vesicles. These observations confirmed that the unusually high apparent encapsulation efficiency in  $V^+$  vesicles was likely due to electrostatic interactions of the dye with the vesicles. Studies in which dye adsorption

decreases with increasing ionic strength (data not shown) also confirm that electrostatics play a principle role. In addition to apparent encapsulation efficiency, we also studied the time-dependent release of CF from the vesicles by utilizing the self-quenching of CF fluorescence. We found that the release rate from  $V^+$  surfactant vesicles was at least 40 times slower than from EYPC vesicles.

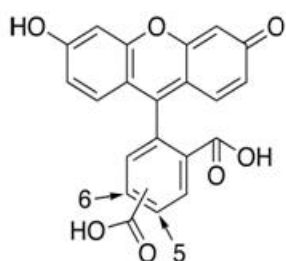
In this chapter, we have expanded our studies to include two new anionic dyes, LY and SR101, as well as two cationic solutes, the dye, R6G and the anti-cancer drug, Dox. We have measured the initial value of  $\varepsilon$  for each of these solutes in both  $V^+$  and  $V^-$  vesicles and monitored  $\varepsilon$  as a function of time for three different solute/vesicle combinations. To demonstrate the strength and specificity of vesicle capture, we have also used the vesicles to separate an oppositely charged solute from a solute mixture. These studies indicate that surfactant vesicles are promising candidates for applications such as drug delivery and molecules separation. An important requirement for realizing such applications will be to ensure the stability of vesicle-solute mixtures under a range of conditions. To investigate the issue of vesicle stability upon addition of solutes, we have conducted an initial set of studies using DLS and SANS, and these are reported in the last section of this chapter.

#### **4.3.1. Capture of Charged Solutes by Vesicles**

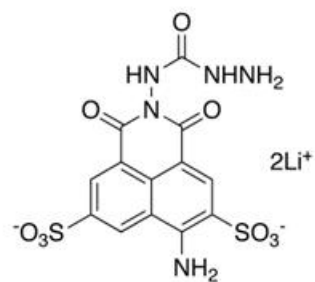
The chemical structures of the five different solutes studied here are shown in Figure 4.1. CF is a trianionic fluorescent dye at a pH above 6.9<sup>16</sup>, while LY is dianionic in water and SR101 is monanionic. R6G possesses a quaternary amine, is cationic at all

pH, and was chosen for its structural similarities with CF. Dox is a cationic drug with a pKa of  $\sim 7.6$ <sup>17</sup> that has been used to treat a variety of cancers.<sup>18-20</sup> In fact, the toxic side effects of Dox have been shown to be reduced if it is delivered using liposomes.<sup>18</sup>

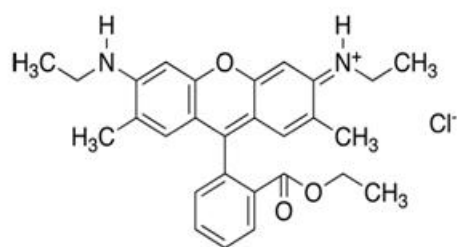
5(6)-carboxyfluorescein



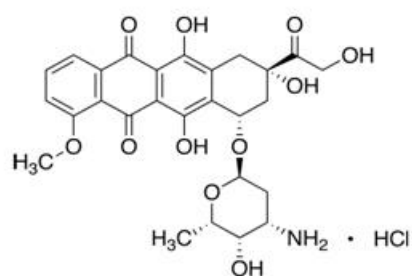
Lucifer yellow



Rhodamine 6G



Doxorubicin hydrochloride



Sulforhodamine 101

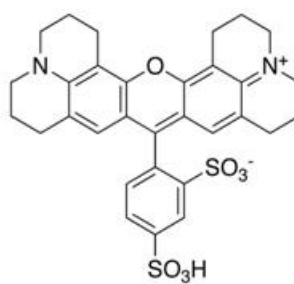


**Figure 4.1.** Structures of the five solutes used in these studies.

The apparent encapsulation efficiency,  $\varepsilon$ , for each of the above solutes was determined for both  $V^+$  and  $V^-$  vesicles using the procedure described in the Experimental Section. It is important to point out that a solute concentration of 1 mM was used in all cases. In an earlier study, Caillet *et al.* attempted to encapsulate CF in  $V^+$  cationic vesicles, but their attempt failed due to the high CF concentration (50 mM) used.<sup>21</sup> It has been well documented that addition of polyelectrolytes to oppositely charged surfactant vesicles can destabilize vesicles leading to changes in bilayer and vesicle structure as well as precipitation.<sup>22,23</sup> Consistent with these findings, we have found that high concentrations of CF (and similarly, other solutes) tend to disrupt the vesicles and lead to precipitation over time. Vesicle stability appears to be unaffected when the solute concentration is kept below 5 mM, and at these concentrations solute capture does occur. The results of experiments using 1 mM CF in  $V^+$  and  $V^-$  vesicles are shown in Figure 4.2. The photographs show successive eluted fractions (1.5 mL each) from the SEC column for  $V^+$  vesicles (Figure 4.2a) and  $V^-$  vesicles (Figure 4.2b). The vesicle-containing fractions are in vials 3-5 (fractions 4-6) in both cases, and this is evident from the high DLS intensity for these samples (plotted as a solid line in the graphs). In addition, the fraction of CF in each vial (from UV-vis) is also plotted as a yellow dotted line. Note that vials 3-5 in the case of  $V^+$  have a strong yellowish tinge, confirming that these vesicles contain an appreciable fraction of CF (23%). On the other hand, vials 3-5 in the case of  $V^-$  vesicles have a much lower dye content (1.5%). Thus, the anionic CF is efficiently incorporated into the  $V^+$  vesicles, but not the  $V^-$  ones.

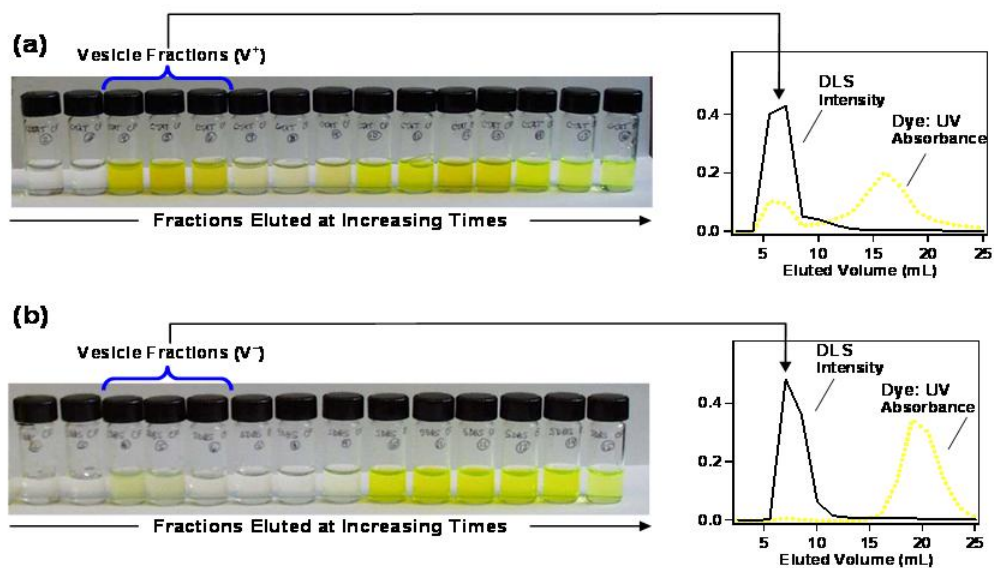


**Figure 4.2.** Results from SEC of vesicles with the anionic dye, CF: (a) V<sup>+</sup> vesicles; and (b) V<sup>-</sup> vesicles. The plots on the right show the DLS intensity, which is proportional to vesicle concentration, and the UV absorbance at 492 nm, which is proportional to CF concentration, as a function of eluted volume. The results show that a significant portion of the dye (23%) elutes with the V<sup>+</sup> vesicles, whereas only about 1.5% of the dye elutes with the V<sup>-</sup> vesicles. This can be seen visually by the more intense yellowish hue of the vesicle fractions (vials 3-5) in the V<sup>+</sup> case.

Similar results (highly efficient capture in V<sup>+</sup>, weak encapsulation in V<sup>-</sup>) were obtained for the other two anionic dyes (LY and SR101) as well. For the cationic solutes (R6G and Dox), the results were switched and these solutes are efficiently captured in V<sup>-</sup> samples and weakly in V<sup>+</sup> samples. Counterparts to Figure 4.2 with photographs, DLS intensity, and UV-vis absorbance data, for each of the solutes are provided in Appendix A. Table 4.1 shows the  $\varepsilon$  values (calculated using eq. 1) for each solute in both V<sup>+</sup> and

$V^-$  vesicles. It is clear from these data that ionic solutes are efficiently captured in cationic vesicles having an opposite net charge.

Probe Molecule	$\varepsilon$ (Apparent Encapsulation Efficiency)		Vesicle Radius after SEC by DLS (nm)	
	CTAT-Rich $V^+$	SDBS-Rich $V^-$	CTAT-Rich $V^+$ (81±13)	SDBS-Rich $V^-$ (98±6)
<b>CF</b>	24 ± 4 %	1.0 ± 0.4 %	87 ± 5	91 ± 8
<b>LY</b>	40 ± 20 %	4 %	208 ± 18	96 ± 3
<b>SR101</b>	32.8 %	8.2 %	122 ± 38	84 ± 7
<b>R6G</b>	0.07 ± 0.1 %	72 ± 3 %	156 ± 24	109 ± 16
<b>Dox</b>	0%	55 %	143 ± 32	93 ± 4

**Table 4.1.** Apparent encapsulation efficiencies and vesicle radii. The  $\varepsilon$  values were determined as described in the Experimental Section.  $\varepsilon$  includes contributions from probe molecules that are both encapsulated in the inner water pool and adsorbed at the vesicle bilayer. Vesicle radii are reported for the vesicle-containing SEC fractions only. Vesicle radii were determined by DLS and the radii for neat vesicles (no probe molecules) obtained after SEC are given in parentheses in the column headings. Radii for  $V^+$  and  $V^-$  samples before SEC are 74 nm and 70 nm, respectively.

One interesting observation from Table 4.1 is that the  $\varepsilon$  values for cationic solutes in  $V^-$  vesicles are remarkably high:  $\varepsilon$  is 72% for R6G and 55% for Dox. These values are much higher than those for the anionic solutes in  $V^+$  vesicles and may stem from the larger excess charge present in  $V^-$ , i.e. 13.5 mM vs. 6.8 mM. In addition, this difference may also result from the relative lipophilicities of the counterions for the two surfactants, these being tosylate in the case of CTAT and sodium in the case of SDBS. Tosylate (p-toluene sulfonate) is a hydrophobic counterion, and will mostly (> 90%) remain bound to the trimethylammonium headgroup in CTAT, with the aromatic ring of tosylate intercalating into the vesicle bilayer.<sup>8,14</sup> The bound tosylate counterions will reduce the cationic charge of the bilayer and, in turn, the strength of interactions between anionic

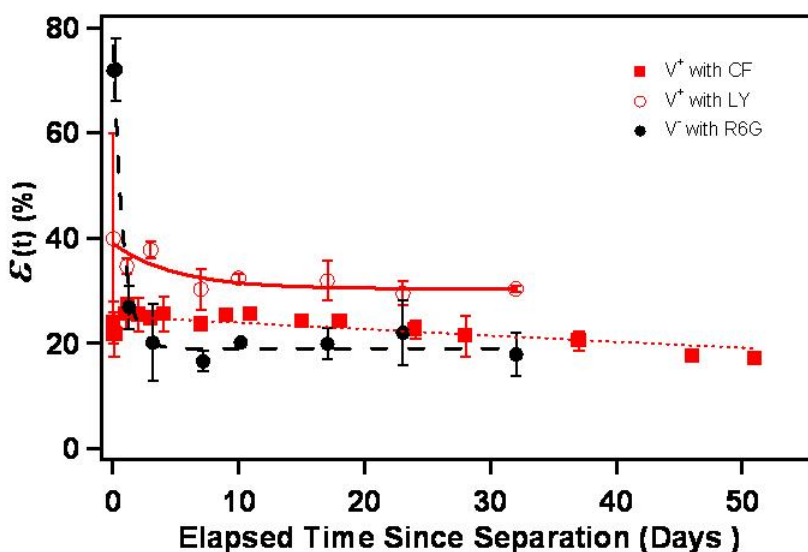
solutes and the bilayer will be reduced. In comparison, the sodium counterions in SDBS will be largely dissociated, and therefore the sulfonate headgroups will present a strongly negative bilayer surface for electrostatic binding of cationic moieties.

Next, we turn briefly to the issue of solute adsorption. In our previous chapter, we reported that electrostatic adsorption of CF to the  $V^+$  vesicle bilayer made a significant contribution to the apparent encapsulation value,  $\varepsilon$ . The contribution from electrostatics was obtained by adding the CF to pre-formed  $V^+$  vesicles, and then measuring the apparent encapsulation. This resulted in an  $\varepsilon$  value that was 75% of that measured by the conventional method. In the present study, we have conducted similar experiments with the cationic R6G dye and found that if the dye is added to pre-made  $V^-$  vesicles, we obtain an  $\varepsilon$  that is ca. 85% of the value reported in Table 4.1. Thus, the electrostatic contribution to solute binding is crucial for both  $V^+$  and  $V^-$  vesicles. Dye adsorption at the vesicle bilayer is being investigated systematically, and will be the subject of a separate chapter.<sup>24</sup>

### **4.3.2. Long-Term Solute Release from Vesicles**

In our previous paper, we used the self-quenching properties of CF fluorescence to evaluate the release rate of CF from  $V^+$  vesicles.<sup>13</sup> This is a well-established method to study solute release from vesicles,<sup>25,26</sup> but it can only be applied to fluorescent solutes that show the self-quenching phenomenon. Here, we measure release rates using a more general procedure based on SEC that can be applied to a wide range of solutes, including

non-fluorescent ones. The details of the procedure are described in the experimental section. Briefly, we start with a batch of solute-bearing vesicles, with the free dye removed using SEC. The amount of solute remaining in the vesicles is evaluated at a later time by removing an aliquot and performing a small-scale separation using a quick-spin column. Our method directly yields the apparent encapsulation,  $\varepsilon$ , as a function of time.



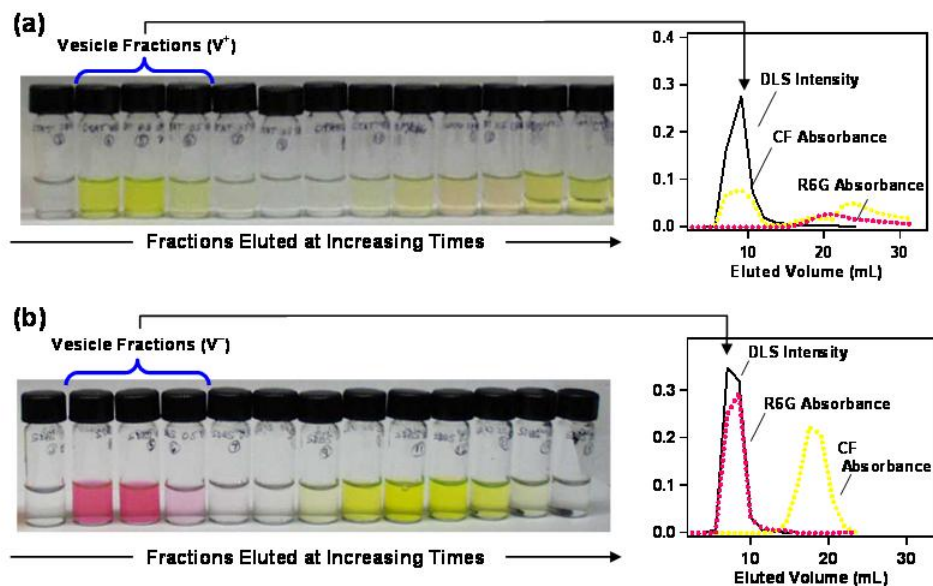
**Figure 4.3.** Dye release profiles. Long-term release as a function of time. Data was acquired for CF (red squares) and LY (empty red circles) in V+ samples, and R6G (black circles) in V- samples. The corresponding lines are fits to an exponential decay. For CF in V+, three trials were completed and the error bars on the points are the standard deviations of the averages of the three data sets. For R6G and LY, two trials were run and the error bars are the actual values for the two trials.

Figure 4.3 shows  $\varepsilon$  vs. time data for three different solute/vesicle combinations. The data for CF in  $V^+$  vesicles (red squares) are quite comparable to our previous results for the same CF/ $V^+$  system using the self-quenching of CF. The new data gives a half life for CF in the vesicles of 114 days, while previously we had estimated an 84 day half-life for the same system from a more limited data set. Also shown in Figure 4.3 are results for LY in  $V^+$  vesicles (empty red circles) and R6G in  $V^-$  vesicles (black circles). The  $\varepsilon$  values for both LY and R6G start out significantly higher than that of CF in  $V^+$ , but decay over the course of a few days to a comparable value of  $\varepsilon$  (from 0.2 to 0.3). R6G has the largest initial rate of dye leakage, which could be because it is captured to a much greater extent than the other two dyes (Table 4.1). On the whole, our new results confirm that oppositely charged solutes can be held for very long periods of time by catanionic vesicles. For comparison, the half-life for CF in EYPC liposomes is only about 2 days,<sup>12</sup> which means that the surfactant vesicles retain ionic dye for about 40-60 times as long.

#### **4.3.3. Separation of Oppositely Charged Solutes by Vesicles**

The strong electrostatic interactions between catanionic vesicles and ionic solutes may be harnessed for an interesting potential application: separation of an oppositely charged solute from a solute mixture. To test this possibility, we prepared vesicles with equimolar mixtures of two solutes, one cationic (R6G) and the other anionic (CF). The total solute concentration was maintained at either 0.5 or 1.0 mM, and the experiments were done with both  $V^+$  and  $V^-$  vesicles. Experiments with these solute mixtures were performed and analyzed in exactly the same way as the determination of  $\varepsilon$ . To account

for the overlapping of the dye spectra, we subtracted a scaled spectrum of pure R6G from the total spectrum in order to find the peak absorbance of CF.



**Figure 4.4.** Vesicle-mediated separation of mixtures of R6G and CF dyes using (a) V<sup>+</sup> vesicles; and (b) V<sup>-</sup> vesicles. The plots on the right show the DLS intensity, which is proportional to vesicle concentration, and the UV absorbances, which are proportional to the concentrations of R6G and CF, as a function of eluted volume. The results show that the V<sup>+</sup> vesicle fractions contain 31% of the CF with no detectable R6G, while the V<sup>-</sup> vesicle fractions contain 88% of the R6G with no detectable CF. This can be seen visually by the yellowish hue of the V<sup>+</sup> vesicle fractions compared to the pinkish hue of the V<sup>-</sup> vesicle fractions.

Results from an equimolar mixture of CF and R6G, at a total dye concentration of 0.5 mM, in V<sup>+</sup> vesicles are shown in Figure 4.4a. While 31% of the anionic CF is carried through the SEC column within the V<sup>+</sup> vesicle band, no detectable R6G emerges with the

vesicles. In short, the  $V^+$  vesicles are able to selectively capture the anionic dye, and thereby separate it from the dye mixture. The opposite behavior is observed for the same dye mixture in  $V^-$  vesicles (Figure 4.4b). In this case, the  $V^-$  vesicle band emerging from the SEC column contains 88% of the R6G, while the amount of CF in this band is negligible. Thus, the  $V^-$  vesicles are able to bind and separate the cationic dye from the dye mixture. To our knowledge, this is the first demonstration of the use of surfactant vesicles to separate ionic compounds. We conducted the same experiments with a total dye concentration of 1.0 mM CF and R6G, and obtained similar results. We have also conducted separation experiments using the anionic dye, LY and the cationic drug, Dox, and we again observed very efficient separation using vesicles, much like in Figure 4.4. The results for LY and Dox are given in the Appendix A. These results demonstrate that charged surfactant vesicles can be used as separation media for similarly-sized and oppositely-charged molecules. The use of surfactants in separations science is not new, micelle containing mobile phases in liquid chromatography were pioneered by Armstrong and Henry.<sup>28</sup> Since then, micellar liquid chromatography has been widely used for a variety of applications including evaluation of drug candidates.<sup>29,30</sup> Surfactant vesicles themselves have also been used as pseudostationary phases for electrokinetic chromatography with good results.<sup>31</sup>

#### **4.3.4. Effects of Solutes on Vesicle Stability**

It is clear from the above data that catanionic vesicles have the remarkable capability of binding and slowly releasing oppositely charged solutes. But for these

vesicles to be used in applications, certain questions relating to vesicle stability need to be answered. For example, what effect, if any, does the solute have on vesicle size and stability? Why is it important to use low solute concentrations (< 5 mM), i.e., what happens to the vesicles when higher concentrations of solute are added? Also, for many biological applications, the pH and ionic strength of the external solution have to be strictly controlled. How will pH and ionic strength affect vesicle stability, and more importantly, how will they influence the electrostatic binding of solutes to vesicles? Many of these aspects are being studied in detail in our labs, and will be addressed in the future. In the present study, we briefly examine the effect on vesicle stability upon addition of solute, using SANS and DLS.

As noted previously, we used a low solute concentration (1 mM) to ensure the stability of our vesicle formulations. At concentrations above 5 mM, the solutes seemed to compromise the integrity of the vesicles, as revealed by large changes in vesicle size (from DLS) and/or by the formation of a precipitate over time. Even at a concentration of 1 mM, some solutes may have a large effect on vesicle morphology. To study these aspects in some detail, we have used DLS and SANS. First, we performed DLS on the purified vesicles obtained from the SEC column (after removing all the free solute) and compared their sizes to those for the neat vesicles (no solute). DLS gave radii of 74 nm for neat  $V^+$  vesicles and 70 nm for neat  $V^-$  vesicles. Passing these neat vesicles through an SEC column changed their sizes slightly and the new radii were 81 nm for  $V^+$  and 98 nm for  $V^-$  vesicles due to the dilution. The incorporation of 1 mM solute had a negligible effect on vesicle size in some cases, but a large effect in others (Table 4.1). For

example, both  $V^+$  and  $V^-$  vesicle radii were essentially unchanged by 1 mM CF. However, while 1 mM of the anionic solute, LY had no effect on  $V^-$  vesicles, it induced a 2.5 fold increase in the radii of  $V^+$  vesicles. Interestingly, the effects on vesicle size seem to be more significant for  $V^+$  vesicles than for  $V^-$ , and this is true for both cationic and anionic solutes. The changes in hydrodynamic radii are an important indicator that structural changes are occurring in the presence of ionic solutes. Results from our lab indicate that these vesicles are stable at elevated salt concentrations. Thus, it is unlikely that the size increases are due to simple flocculation brought about by increasing ionic strength upon addition of solute. Direct imaging techniques such as cryogenic transmission electron microscopy (cryo-TEM) may be able to reveal the solute induced changes indicated by DLS. However, at this time, we do not have access to cryo-TEM and instead have turned to SANS, which is a sensitive probe of nanoscale structure.

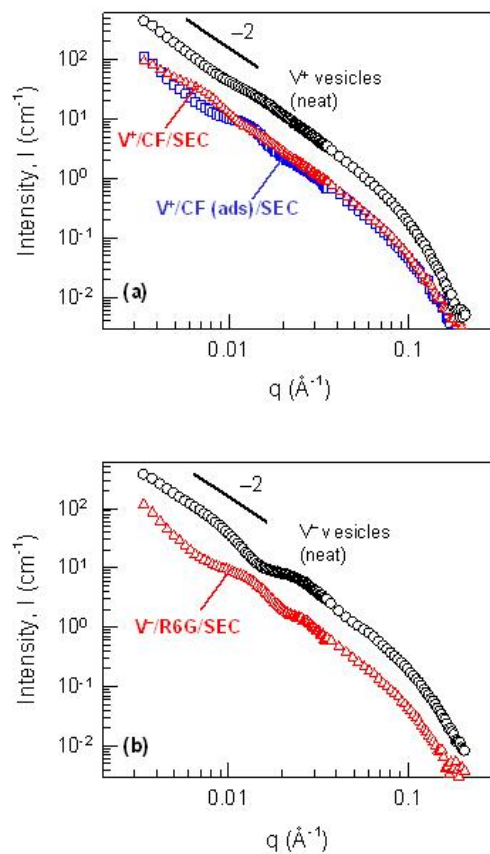


**Figure 4.5.** SANS data for neat and dye-containing V+ and V- samples. (a) Scattering data for V+ samples. A -2 slope characteristic of bilayer scattering is observed for neat vesicles (black circles) and when CF is added before (red triangles) or after (blue squares) vesicles are formed. (b) Scattering data for neat V- samples (black circles) and for V-loaded with R6G (red triangles). As in (a), the data from both samples are consistent with the presence of vesicles. The neat vesicle samples (black circles) were run as-prepared with 1% total surfactant concentration. The other samples (blue squares and red triangles) were diluted by approximately 4-fold as a result of undergoing SEC.

SANS data are reported in Figure 4.5 for two mixtures of vesicles and oppositely charged solutes:  $V^+$ /CF, and  $V^-$ /R6G. Figure 4.5a shows data for the neat  $V^+$  vesicles with no solute, and for the same vesicles prepared with 1 mM CF and purified by SEC. Additionally, data are shown for a sample of the same vesicles with 1 mM CF added after preparation (i.e., with the dye adsorbed on the bilayers), followed by purification via SEC. Passing the vesicles through SEC lowers the vesicle concentration, which is why the latter two data sets show a lower intensity. Nevertheless, all three curves have approximately the same shape and all show a limiting slope of  $-2$  at low  $q$ , which is indicative of scattering from vesicle bilayers.<sup>32,33</sup> Similar observations also hold for Figure 4.5b, which reports data for neat  $V^-$  vesicles and for the same vesicles with 1 mM R6G followed by SEC. Again, the intensity levels are lower due to the SEC purification, but the  $-2$  slope is maintained. Thus, SANS confirms that all these samples contain intact unilamellar vesicles. In all cases, there appear to be subtle differences in vesicle size and polydispersity upon incorporation of solute. Further analysis of the SANS data is beyond the scope of the present paper. However, we are putting together an expanded study of solute/vesicle interactions using SANS, accompanied by detailed modeling, and this will be communicated in the future. The combined observations from DLS, SANS and SEC experiments strongly indicate that the vesicles remain intact in the presence of dyes though precipitation has been observed when dye concentrations exceed 5 mM.

#### **4.3.5. Implications for Applications Involving Surfactant Vesicles**

As discussed in the introduction of this section, important potential applications for vesicles are in storage or controlled release applications (e.g., in drug delivery,

agrochemicals, or cosmetics). This is an area of great promise, as evidenced by the success of the liposome-based delivery of the chemotherapeutic drug, doxorubicin.<sup>34</sup> So far, most of the research in this area has focused on phospholipid vesicles (liposomes). Researchers working with liposomal encapsulation technologies have discovered many improvements in solute loading efficiency and long-term solute retention. For instance, there has been progress in enhancing the long-term retention capabilities of liposomes by varying the lipid composition of the bilayer or by adding cholesterol to the bilayer. Similarly, there have been successful attempts to reach extremely high loading efficiency of drugs like doxorubicin by employing chemical gradients.<sup>37</sup> Loading of DNA into vesicles can be greatly improved with the addition of cationic lipids<sup>38</sup> or by using micron-sized vesicles.<sup>39</sup> Such advances in liposomal preparations have led to important advances in chemotherapy. Here, we have shown that catanionic vesicles may show promise as a simple alternative to more expensive and complex liposomal-based approaches. In short, catanionic vesicles could be an attractive alternative to phospholipid vesicles (liposomes) for many controlled-release applications. For therapeutic applications, a range of toxicological studies will first need to be conducted with these catanionic vesicles. In this regard, recent studies by Kuo *et al.* are promising in that they show catanionic vesicles to be nontoxic towards mouse fibroblast and liver cells.<sup>40</sup>

#### **4.4. Conclusions**

In this study, we have measured the apparent encapsulation of five different charged solutes in catanionic CTAT/SDBS vesicles and used these vesicles to separate an oppositely charged solute from a solute mixture. We have shown that solutes can be

weakly encapsulated by like-charged vesicles but are captured much more efficiently in oppositely charged vesicles. Efficient containment in vesicles of the opposite charge is due to strong electrostatic interactions between solute and bilayer. At 1 mM solute concentrations, apparent encapsulation values range from 24% to 72%. Long-term solute release kinetics were monitored for three vesicle/solute preparations. Release profiles show that all dyes are held for long periods of time but that both R6G, and to a lesser extent LY, have an initial rapid dye release that bring them close to the initial value for CF. Highly efficient separations of mixtures of similar sized but oppositely charged probe molecules were performed by using vesicles to control the elution time of ionic probe molecules in SEC. Results from DLS and SANS experiments are also included to measure the effect of solute loading on vesicle integrity and stability. DLS results show that  $V^+$  samples appear to undergo an increase in radius when solutes are added at a concentration of 1 mM but that the effect on SDBS vesicles is negligible. SANS experiments confirm that vesicles remain intact when loaded with strongly-interacting probes.

#### **4.5. Acknowledgments**

This work was supported in part by the National Science Foundation MRSEC-DMR 0520471 and by a grant from the Center for Nano-Manufacturing & Metrology to D.S.E. A.K. thanks the MRSEC-REU program at UMCP. Partial support for this research was provided by a grant to E.J.D from the Howard Hughes Medical Institute through the Undergraduate Biological Sciences Education Program. Finally, we would

like to acknowledge NIST for facilitating the SANS experiments performed as part of this work.

## References:

1. Hargreaves, W. R.; Deamer, D. W. *Biochemistry* 1978, *17*, 3759-3768.
2. Tondre, C.; Caillet, C. *Adv. Coll. Inter. Sci* 2001, *93*, 115-134.
3. Khan, A. *Curr. Opin. Colloid. In.* 1996, *1*, 614-623.
4. Kondo, Y.; Uchiyama, H.; Yoshino, N.; Nishiyama, K.; Abe, M. *Langmuir* 1995, *11*, 2380-2384.
5. Marques, E. F.; Regev, O.; Khan, A.; Miguel, M. D.; Lindman, B. *J. Phys. Chem. B* 1998, *102*, 6746-6758.
6. Marques, E. F.; Regev, O.; Khan, A.; Miguel, M. D.; Lindman, B. *J. Phys. Chem. B* 1999, *103*, 8353-8363.
7. Herrington, K. L.; Kaler, E. W.; Miller, D. D.; Zasadzinski, J. A.; Chiruvolu, S. *J. Phys. Chem.* 1993, *97*, 13792-13802.
8. Kaler, E. W.; Herrington, K. L.; Murthy, A. K.; Zasadzinski, J. A. *N. J. Phys. Chem.* 1992, *96*, 6698-6707.
9. Berman, A.; Cohen, M.; Regev, O. *Langmuir* 2002, *18*, 5681-5686.
10. Edlund, H.; Sadaghiani, A.; Khan, A. *Langmuir* 1997, *13*, 4953-4963.
11. Yacilla, M. T.; Herrington, K. L.; Brasher, L. L.; Kaler, E. W.; Chiruvolu, S.; Zasadzinski, J. A. *J. Phys. Chem.* 1996, *100*, 5874-5879.
12. Wang, X.; Danoff, E. J.; Sinkov, N. A.; Lee, J.-H.; Raghavan, S. R.; English, D. S. *Langmuir* 2006, *22*, 6461-6464.
13. Wang, X.; Danoff, E. J.; Sinkov, N. A.; Lee, J. H.; Raghavan, S. R.; English, D. S. *Langmuir* 2006, *22*, 6461-6464.
14. Kaler, E. W.; Murthy, A. K.; Rodriguez, B. E.; Zasadzinski, J. A. *N. Science* 1989, *245*, 1371-1374.
15. Lee, J.-H.; Gustin, J. P.; Chen, T.; Payne, G. F.; Raghavan, S. R. *Langmuir* 2005, *21*, 26-33.
16. Vallotton, P.; Vogel, H. *J. Fluoresc.* 2000, *10*, 325-332.
17. Dalmark, M. *Scand. J. Clin. Lab. Invest.* 1981, *41*, 633-639.
18. Abraham, S. A.; Waterhouse, D. N.; Mayer, L. D.; Cullis, P. R.; Madden, T. D.; Bally, M. B. *Methods Enzymol.* 2005, *391*, 71-97.

19. Swain, S. M.; Whaley, F. S.; Ewer, M. S. *Cancer* 2003, 97, 2869-2879.
20. Singal, P. K.; Olweny, C. L. M.; Li, T. M. *New. Endl. J. Med.* 1999, 340, 655-655.
21. Caillet, C.; Hebrant, M.; Tondre, C. *Langmuir* 2000, 16, 9099-9102.
22. Marques, E. F.; Regev, O.; Khan, A.; Miguel, M. D.; Lindman, B. *Macromolecules* 1999, 32, 6626-6637.
23. Regev, O.; Marques, E. F.; Khan, A. *Langmuir* 1999, 15, 642-645.
24. Wang, X.; Sinkov, N.; English, D. S. *J.Phys.Chem.* 2007, *to be submitted for publication.*
25. Jang, H.; Pell, L. E.; Korgel, B. A.; English, D. S. *J. Photochem. Photobiol., A* 2003, 158, 111-117.
26. Schwarz, G.; Arbuzova, A. *BBA-Biomembranes* 1995, 1239, 51-57.
27. Rex, S. *Biophys. Chem.* 1996, 58, 75-85.
28. Armstrong, D. W.; Henry, S. J. *J. Liq. Chromatogr.* 1980, 3, 657-662.
29. Khaledi, M. G. *J. Chromatogr. A* 1997, 780, 3-40.
30. Escuder-Gilabert, L.; Molero-Monfort, A.; Villanueva-Camanas, R. M.; Sagrado, S.; Medina-Hernandez, M. J. *J. Chromatogr. B* 2004, 807, 193-201.
31. Hong, M.; Weekley, B. S.; Grieb, S. J.; Foley, J. P. *Anal. Chem.* 1998, 70, 1394-1403.
32. Glatter, O. *Small-Angle X-Ray Scattering*; Academic Press: New York, 1982.
33. *Neutron, X-Ray and Light Scattering: Introduction to an Investigative Tool for Colloidal and Polymeric Systems*; Elsevier: Amsterdam, 1991.
34. Rose, P. G.; Blessing, J. A.; Lele, S.; Abulafia, O. *Gynecol Oncol* 2006, 102, 210-213.
35. Apel-Paz, M.; Doncel, G. F.; Vanderlick, T. K. *Langmuir* 2005, 21, 9843-9849.
36. Ishida, A.; Otsuka, C.; Tani, H.; Kamidate, T. *Anal. Biochem.* 2005, 342, 338-340.
37. Haran, G.; Cohen, R.; Bar, L. K.; Barenholz, Y. *Biochim. Biophys. Acta* 1993, 1151, 201-215.
38. Semple, S. C.; Klimuk, S. K.; Harasym, T. O.; Dos Santos, N.; Ansell, S. M.; Wong, K. F.; Maurer, N.; Stark, H.; Cullis, P. R.; Hope, M. J.; Scherrer, P. *BBA-Biomembranes* 2001, 1510, 152-166.

39. Sato, Y.; Shin-ichiro, M. N.; Yoshikawa, K. *Chem. Phys. Lett.* 2003, 380, 279-285.
40. Kuo, J. H. S.; Jan, M. S.; Chang, C. H.; Chiu, H. W.; Li, C. T. *Colloids Surf., B* 2005, 41, 189-196.

## **Chapter 5. Investigation of Excess Charge, Counterion Identity, and Electrostatic Adsorption in Surfactant Vesicles: Bulk and Fluorescence Correlation Spectroscopy Studies**

*To be submitted to J. Phys. Chem.*

Xiang Wang, Nikolai A. Sinkov, Jeremy Heyman, Emily J. Danoff  
and Douglas S. English

### **5.1. Introduction**

First reported by Kaler *et al.* in 1989, surfactant vesicles are an intriguing alternative to liposomes.<sup>1</sup> These large unilamellar vesicles form spontaneously from mixtures of oppositely-charged single-tailed surfactants, and are extremely stable.<sup>1,2</sup> Surfactant vesicles are relatively unique in their ability to form spontaneously from simple two-component mixtures of surfactants. Vesicles are often observed to form spontaneously *in vivo*, but prior to Kaler *et al.* very few instances of vesicles formed spontaneously *in vitro* were known, and the few reported in the literature were formed from mixtures of surfactants.<sup>3-6</sup> According to Kaler *et al.*, the fact that the vesicles formed without the input of mechanical energy and were stable and free of aggregation for long periods of time meant that they could be classified as equilibrium structures. Whether the surfactant vesicles formed truly constitute an equilibrium state has been the subject of some debate,<sup>7,8</sup> but the fact remains that these unilamellar vesicles form easily in aqueous environments and are stable for long periods of time. An additional attraction

of surfactant vesicles is that they can be formed from relatively cheap, commercially available surfactants.

We have been investigating surfactant vesicles formed from sodium dodecylbenzenesulfonate (SDBS) and cetyltrimethylammonium tosylate (CTAT) for use as molecular vehicles in applications such as disease diagnostics or drug delivery.<sup>9-11</sup> The surfactant portion of CTAT (CTA<sup>+</sup>) is positively charged due to a trimethylammonium headgroup and each molecule is coupled with a tosylate counter ion, as seen in (Figure 5.1.). The surfactant portion of SDBS (DBS<sup>-</sup>) is negatively charged due to a sulfonate headgroup, and the salt contains sodium as the counterion. In solution, the two charged surfactants form an ion pair that resembles a phospholipid molecule with a zwitterionic headgroup and two hydrophobic tails, and achieve the geometry necessary for the formation of bilayers.

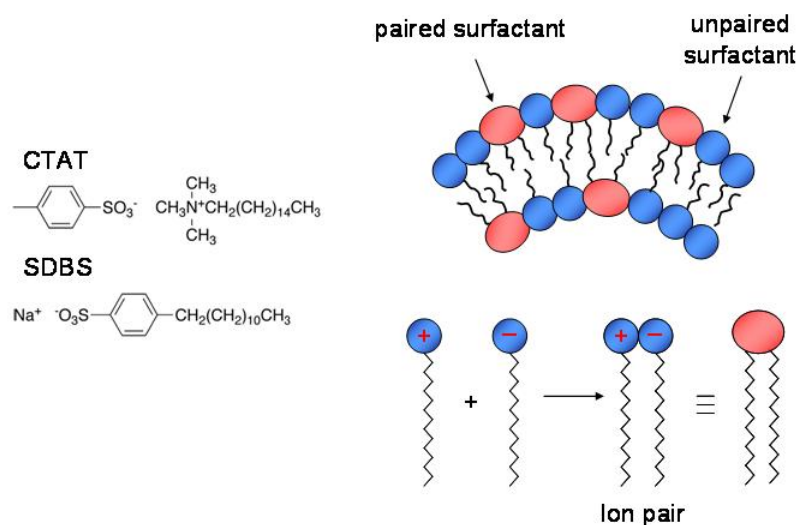


**Figure 5.1.** Structure of surfactants and illustration of bilayer formation.

Although the surfactants are thought to form 1:1 ion pairs, experiments have shown that it is necessary to have an excess of one of the surfactants in order for vesicle formation to occur. Kaler theorized that the excess surfactant helped to fluidize the vesicle bilayer.<sup>1</sup> The necessity of one surfactant being in excess can further be explained by examining the property of spontaneous curvature. The monolayers making up a bilayer each have a spontaneous curvature arising from the packing of the amphiphiles. If the packing area of the polar heads is smaller than the packing area of the hydrophobic tails due to head-head interactions being more favorable than tail-tail interactions, then the monolayer tends to bend so that the non-polar region is on the outside of the curved monolayer. If the head packing favors a larger area, then the opposite occurs and the

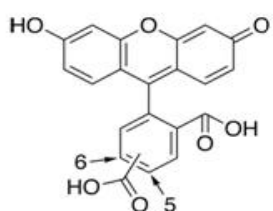
non-polar region is on the inside of the monolayer.<sup>12</sup> For single-component bilayers the spontaneous curvatures of the two monolayers exactly cancel and the net spontaneous curvature is zero, meaning any deviation from a flat bilayer costs energy.<sup>2</sup> Shortly after Kaler's report on surfactant vesicles, Safran *et al.*<sup>13</sup> presented a model to explain the unusual stability of vesicles formed from surfactant mixtures. Through various calculations he determined that it is possible to obtain spontaneous curvatures for the two monolayers that are equal and opposite (allowing a curved bilayer) if the inner and outer monolayers have differing compositions. This can be achieved through the presence of the excess, unpaired surfactant molecules. If more of the unpaired surfactants (which have a large headgroup relative to tail size) are placed in the outer monolayer and more of the zwitterionic complexes (which have a small headgroup relative to tail size) are placed in the inner monolayer, it is possible to obtain the appropriate spontaneous curvatures and achieve curved bilayers and spontaneous vesicle formation. This is shown in Figure 5.1. Ion pairing of the oppositely charged surfactants and the presence of an excess of one surfactant are both necessary for the formation of highly stable vesicles. Furthermore, each vesicle carries a net charge which is predominantly located at the external bilayer/water interface.

DNA adsorption at the external bilayer interface of surfactant vesicles has been studied with an eye toward using these systems as non-viral transfection vehicles.<sup>14-16</sup> Letizia *et al.* obtained a binding isotherm and equilibrium constant for lysozyme adsorbed to surfactant vesicles formed from sodium dodecylsulfate (SDS) and cetyltrimethylammonium bromide (CTAB).<sup>17</sup> Recently we showed that favorable

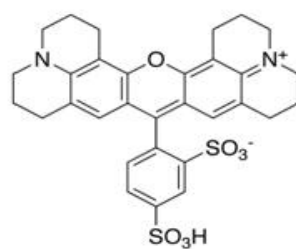
electrostatic interactions with the vesicle bilayer can lead to very efficient capture and sequestration of charged organic molecules.<sup>11</sup> In our work, we have found that as much as 75% of the sequestered molecules are bound to the exterior surface of the vesicle.<sup>10</sup> In this chapter we study the binding of dye molecules to the charged vesicle exterior and also examine the effects of surfactant stoichiometry and excess salt concentration on the adsorption isotherm. To achieve this we make use of fluorescence correlation spectroscopy (FCS).<sup>18</sup>

FCS measures the diffusion time of a fluorescing species as it passes through a laser beam and is a quick and sensitive measurement for monitoring the binding of a small particle such as a molecule or low molecular weight polymer to a much larger particle such as a vesicle or bead.<sup>19,20</sup> In our case, if the fluorescing molecule is bound to the vesicle it diffuses much more slowly than a free molecule and the fraction of bound molecules is easily determined by fitting the fluorescence fluctuation autocorrelation function. For our purposes, FCS is an ideal tool since it is suited for very low probe concentration and provides a simple and accurate way to measure binding isotherms well below the binding saturation regime. In addition, working at low probe concentration also ensures that vesicle stability is not compromised as can happen when higher concentrations, above 5 mM, are used.<sup>11</sup> Figure 5.2. shows the structures of the dye molecules that were used as FCS probes in this work.

5(6)-carboxyfluorescein



Sulforhodamine 101



Rhodamine 6G

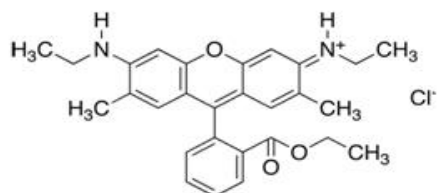


**Figure 5.2.** Structures of the fluorescent probes used for FCS studies

## **5.2. Materials and Methods**

### **5.2.1. Materials**

Surfactants CTAT, CTAB, were purchased from Aldrich. SDBS, was purchased from Tokyo Chemical Industry (in USA) and Triton X-100 was obtained from Fisher Scientific. Fluorescent dyes 5-(and 6-)carboxyfluorescein (CF), 1,1'-dioctadecyl-3,3,3',3'-tetramethylindocarbocyanine perchlorate (DiIC<sub>18</sub>), and sulforhodamine 101 (SR101) were from Invitrogen and chemotherapeutic drug doxorubicin hydrochloride (Dox) was obtained from Fluka. Materials were used without further purification. Dry surfactants CTAT, CTAB, and SDBS were stored in a desiccator. Saline solution was purchased from CVS Pharmacy.

### **5.2.2. Measuring Encapsulation Efficiency**

Dye-vesicle mixtures were run through a long Pyrex (45mm x 13mm) size exclusion chromatography column with Sephadex G-50 Medium. Fractions were collected and analyzed for vesicles with dynamic light scattering (DLS) and dye concentration with a UV-Vis spectrophotometer. Triton X-100 was added at 1% v/v to all UV-Vis samples to disrupt vesicle structure and allow for accurate measurement of dye absorbance. Encapsulation efficiency was calculated from the sum of absorbance of 1.5mL of each fraction containing vesicles divided by the stock solution (pre-SEC column) absorbance of 1mL added to column, as seen in Equation 1.

$$\varepsilon = \frac{V_f (A_{f1} + A_{f2} + \dots)}{V_i A_i} \quad (1)$$

### 5.2.3. Fluorescence Correlation Spectroscopy

FCS was performed with a previously described set-up<sup>21</sup> consisting of an air-cooled argon ion laser (532-AP-A01, Melles Griot, Carlsbad, CA), an inverted microscope (Axiovert 200, Carl Zeiss, Göttingen, Germany), and a single photon counting avalanche photodiode, or APD (SPCM-AQR-15, Perkin Elmer, Vaudreuil, QC, Canada). The collimated laser beam ( $\lambda = 488$  nm or 514 nm depending on the dye) was focused into the sample solution approximately 10  $\mu\text{m}$  from the coverslip surface using a 100X, 1.30 N.A. oil immersion objective (Fluar, Carl Zeiss). A nearly diffraction limited spot with a lateral radius of  $r = 360$  nm was achieved. Typical laser power was 5  $\mu\text{W}$ . Fluorescence was collected through the objective and filtered ( Holographic notch filter, HNF-488.0-1.0, Kaiser Optical System, Inc. Ann Arbor, MI or RazorEdge filters, LP01-514RS-25, Semrock, Rochester, NY ) to remove scattered excitation light. Collection optics consisted of a pair of achromatic doublets placed after the primary image plane and were used to match the size of the collected fluorescence spot with the 180  $\mu\text{m}$  diameter area of the APD. The output of the APD was fed to a counter timer board (PCI-6602, National Instruments, Austin, TX) operating in time-tagged photon counting mode using home written software in LabView (National Instruments, Austin, TX.).

Time-tagging mode plots time between photon counts versus the count number (e.g. 7<sup>th</sup> event is the time between photon counts 7 and 8) rather than recording the total

elapsed time from the start of a run to each photon count, saving previous time and memory and hard drive space (think dozens of gigabytes of hard drive space and weeks of time saved) in subsequent autocorrelation analysis of data. The “time-tags” are used to reconstruct the photon intensity transient or autocorrelation curve. Temporal resolution for timed tagged data is limited by the dead-time of the APD (50 ns) and the on-board clock of the counter/timer board (80 MHz). The time tagged data were autocorrelated off-line using routines home written with Igor Pro 5.0 (Wavemetrics, Portland, OR) according to the following equation:<sup>21</sup>

$$G(\tau) = \frac{\langle \delta F(t) \bullet \delta F(t + \tau) \rangle}{\langle F(t) \rangle^2} \quad (2)$$

Figure 5.3 shows fluorescence fluctuation autocorrelation decay curves acquired for CF at concentrations ranging from 1-10nM. The decays are fit with the functional form describing a single fluorescent species freely through an ellipsoidal observation volume:

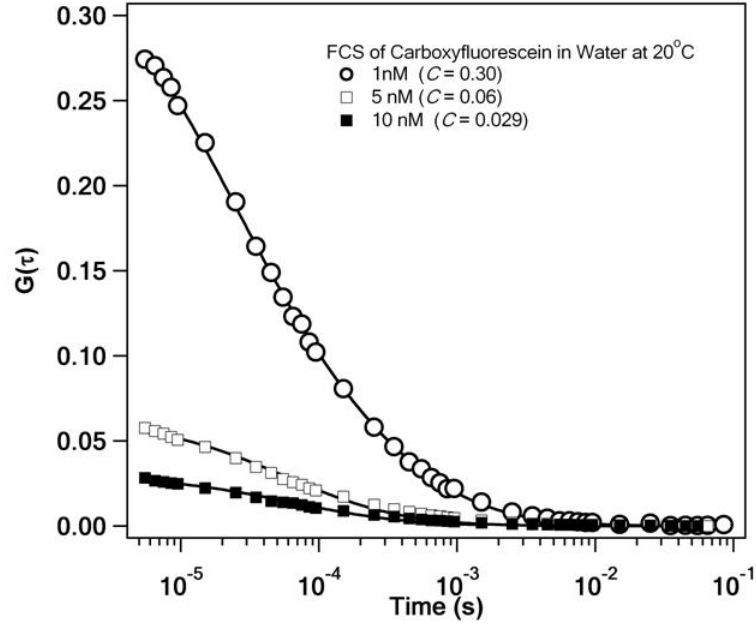


**Figure 5.3.** Autocorrelation decays for the samples containing the dye carboxyfluorescein in water at room temperature. The solid lines show the fits to Equation 2 for each set of data. Each fit gave a diffusion time of  $\sim 270 \mu\text{s}$  which corresponds to a diffusion coefficient of  $1.2 \times 10^{-6} \text{ cm}^2 \text{ s}^{-1}$ . The amplitudes vary inversely with the concentrations and are given in the legend. In all fits  $\omega$  was held at 3.0.

$$G(\tau) = C \cdot \left( \frac{1}{1 + \frac{\tau}{\tau_D}} \right) \cdot \left( \frac{1}{1 + \omega^2 \frac{\tau}{\tau_D}} \right)^{\frac{1}{2}} \quad (3)$$

where C is inversely proportional to the average number of molecules in the observation

volume,  $\tau_D$  is the characteristic diffusion time ( $\tau_D = \frac{r^2}{4D}$  where D is the diffusion

coefficient) and  $\omega^2$  is a factor proportional to the ratio of the radial and axial axes of the

three dimensional observation volume.<sup>22,23</sup> The best-fit parameters for the three curves in Figure 5.3 are consistent with expectations, yielding amplitudes that are inversely proportional to concentration and diffusion coefficients that match previously measured values ( $\approx 1.5 \times 10^{-6} \text{ cm}^2 \text{ s}^{-1}$ ).<sup>24</sup>

The adsorption of dye molecules to surfactant vesicles was studied by adding preformed vesicles to dye solutions. In all cases the dye concentration was 10 nM with varying surfactant concentrations. These samples were studied with FCS and the autocorrelation decays were fit to a two component equation:

$$G(\tau) = f \cdot \left( \frac{1}{1 + \frac{\tau}{\tau_v}} \right) \cdot \left( \frac{1}{1 + \omega^2 \frac{\tau}{\tau_v}} \right)^{\frac{1}{2}} + (1-f) \cdot \left( \frac{1}{1 + \frac{\tau}{\tau_p}} \right) \cdot \left( \frac{1}{1 + \omega^2 \frac{\tau}{\tau_p}} \right)^{\frac{1}{2}} \quad (4)$$

where  $f$  is the fraction of probe molecule (dye) that is bound to vesicles. The diffusion times for vesicles and dye molecules are  $\tau_v$  and  $\tau_p$ , respectively. Diffusion times for probe molecules are determined from the autocorrelation decay of free dye in the absence of vesicles. The vesicle diffusion time is determined from the autocorrelation decay of vesicles doped with a low concentration (1nM) of the dye DiIC<sub>18</sub>. DiIC<sub>18</sub> has a structure similar to an amphiphilic surfactant, causing it to act as a surfactant rather than an externally bound dye, integrating into the vesicle bilayer and offering a vehicle for making vesicles fluorescing species, a necessity for finding their diffusion time by FCS. When fitting autocorrelation functions from mixtures of dye and vesicles, the diffusion

times were held constant and only the value of  $f$  was varied, despite the fact that the quality of some fits are not so high as can be obtained if the diffusion times are also allowed to vary. Results from binding studies of CF on CTAT-rich vesicles along with their corresponding fits are shown in Figure 5.4. The fraction of bound dye,  $f$ , was plotted against surfactant concentration to obtain a binding isotherm for the different systems. In general, the fits were consistent for samples run on different days allowing us to construct isotherms with good reproducibility, shown in Figure 5.4. For each surfactant concentration, ranging from 1pM to 1nM, 10 2-minute decays were collected. The autocorrelations of each data were compared to check for consistency and then averaged. Each autocorrelation decay curve in Figure 5.4 is thus constructed from averaging 10 2-minute transient data files.

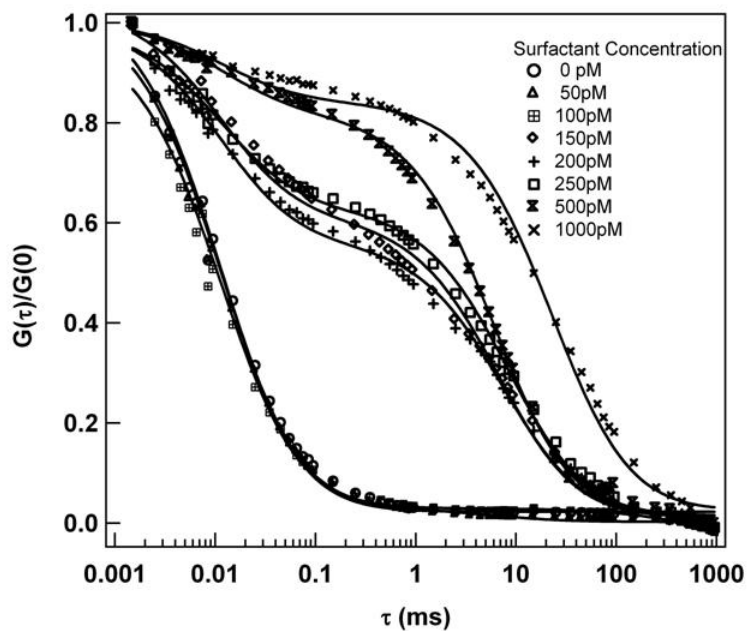


**Figure 5.4.** Normalized autocorrelation functions obtained from carboxyfluorescein (10 nM) with varying amounts of CTAT-rich vesicles.

### 5.3. Results and Discussion

We previously showed that surfactant vesicles formed from mixtures of the surfactants CTAT and SDBS are highly efficient at capturing small solute molecules of the opposite charge from the vesicle bilayer.<sup>10,11</sup> FCS was performed with a number of different vesicle/dye combinations. By varying the surfactant concentration we were able to construct binding isotherms for each combination. The binding isotherms were fit with the following equation:

$$f = \frac{K \times C}{1 + K \times C} \quad (5)$$

where K is the binding constant and C is the total surfactant concentration. The values obtained for K are shown in Table 5.1 along with the surfactant charge ratio, R:

$$R = \frac{[A]}{[B]} \quad (6)$$

where A is the surfactant in excess and B is the oppositely charged surfactant. Hence R is always greater than one and is a quantitative expression of the amplitude of excess negative or positive charge associated with a bilayer. A related quantity reported in Table 5.1 is  $\Delta C$ , which expresses the absolute excess charge concentration as the difference in concentration between [A] and [B] in Equation 6. Table 5.1 also includes entries for the apparent encapsulation efficiencies,  $\varepsilon$ , which were reported previously<sup>11</sup> but have been remeasured using a longer column to give more precise results (longer SEC column allows for greater separation of vesicle and free dye bands). The  $\varepsilon$  values were calculated by measuring the fraction of dye in a 1 mM solution that eluted with the vesicle band during SEC. It is referred to as the apparent encapsulation efficiency because it contains contributions from both encapsulated and adsorbed dyes. K values, however, only represent dye adsorption to the vesicle *exterior*. The good correspondence between  $\varepsilon$  and K confirms that bilayer adsorption is responsible for the efficient capture and sequestration of dye molecules by oppositely-charged vesicles. The K values are also related to the binding free energy  $\Delta G^\circ$ :

$$K = e^{\frac{-\Delta G^\circ}{RT}} \quad (7)$$

where  $R$  is the ideal gas constant ( $8.3145 \text{ J mol}^{-1} \text{ K}^{-1}$ ) and  $T$  is the sample temperature.

Sample <sup>a</sup> (Cationic:Anionic Surfactant, w/w)	$R^b$	$\Delta C$ (mM)	Dye	$K$ ( $M^{-1}$ )	$\varepsilon$ (%) <sup>c</sup>	Outside $\varepsilon$ (%)	Saline $\varepsilon$ (%)
<b>SDBS-rich (<math>V^-</math>)</b>							
4:6	2	8.4	<b>R6G</b>	$13 \times 10^4$	$53 \pm 3$	n/a	n/a
3:7	3.1	13.5	<b>R6G</b>	$11 \times 10^4$	$56 \pm 3$	n/a	n/a
2:8	5.2	18.6	<b>R6G</b>	$15 \times 10^4$	n/a	n/a	n/a
3:7	3.1	13.5	<b>Dox</b>	n/a	23	n/a	44
<b>CTAT-rich (<math>V^+</math>)</b>							
7:3	1.8	6.8	<b>CF</b>	$3.5 \times 10^4$	$16 \pm 3$	21	Negligible
8:2	3	11.8	<b>CF</b>	$7.5 \times 10^4$	$62 \pm 7$	n/a	n/a
<b>CTAB-rich (<math>V^+</math>)</b>							
6.5:3.5	1.8	7.8	<b>CF</b>	$7.5 \times 10^4$	$41 \pm 2$	41	Negligible

**Table 5.1.** Association constants and encapsulation efficiencies for different vesicle/dye combinations. a. Surfactant mixtures were characterized by their CTAT-to-SDBS weight ratios (w/w). b. The charge ratio is determined from Equation 5.5. c. The  $\varepsilon$  values are the percentage of a 1 mM dye solution that elutes with vesicles during SEC.<sup>11</sup> "n/a" refers to a value that cannot be obtained or is superfluous to the current study. Saline and "dye outside" vesicle measurements are also shown here.

For consistency with our previous studies, vesicle samples were initially prepared at two different surfactant compositions, 7:3 and 3:7 w/w CTAT to SDBS. Vesicles with excess CTAT or SDBS are denoted as  $V^+$  and  $V^-$ , respectively.  $V^+$  refers to the excess positive charge on the vesicle bilayers when there is an excess of CTAT. In 7:3 w/w samples, the concentrations of CTAT and SDBS are 15.4 mM and 8.6 mM, respectively. This corresponds to 6.8 mM excess CTAT, which yields a 1.8 fold molar excess of cations,  $R = 1.8$ . Likewise,  $V^-$  refers to vesicles with a net negative charge. In 3:7 w/w

samples there is a 13.5 mM excess of SDBS (the samples contain 6.6 mM CTAT and 20.1 mM SDBS), or a 3.1 fold molar excess of anions.

To study electrostatic adsorption using FCS, oppositely charged probe molecules were used (see Figure 5.5). For  $V^-$  samples R6G was used and for  $V^+$  samples either SR101 or CF were used. In Table 5.1 it can be seen that adsorption of R6G to  $V^-$  samples is significantly stronger than for CF to CTAT-rich  $V^+$  samples and, to a lesser extent, for CF bound to CTAB-rich  $V^+$  vesicles.

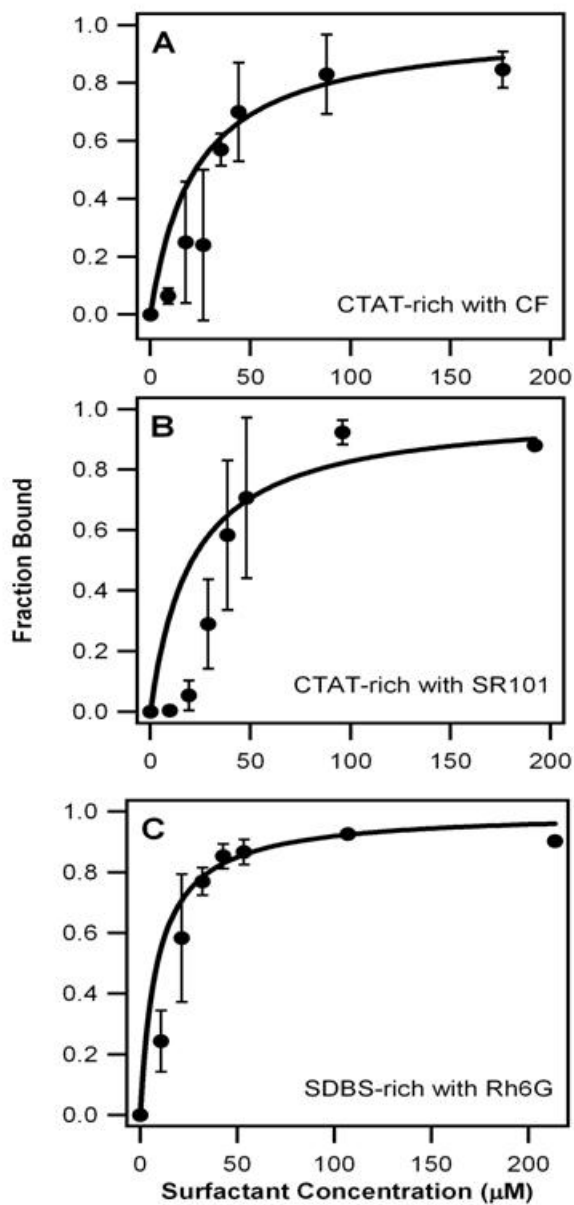


**Figure 5.5.** Adsorption isotherms obtained from FCS. Each isotherm was fit to equation 5 and the binding constant is given in Table 5.1. For CTAT-rich vesicles (A) and (B) the points corresponding to 10, 20 and 30  $\mu\text{M}$  were excluded in the fitting process as discussed in the text.

This may be attributed to the greater bilayer charge associated with  $V^-$  samples; however, the increasing R values measured for R6G in  $V^-$  samples does not induce a marked increase in K. In comparing K values from the 4:6 and 7:3 samples, which have similar R values but opposite bilayer charges, there is a great difference in K that can not be accounted for by charge alone. Previous work shows that in the case of  $V^+$  samples, there is very little difference between binding of SR101, net charge of -1, and CF, net charge of -3. These observations suggest that charge stoichiometry is unimportant in determining bilayer adsorption. Figure 5. shows binding curves collected from  $V^-$  samples with different charge ratios. The isotherms for the three samples are essentially indistinguishable. Interestingly, preliminary results of apparent encapsulation efficiency *do* suggest a dependence on charge stoichiometry, with an increase in R from 1.8 to 3.0 for CTAT-rich vesicles leading to nearly a fourfold increase in  $\epsilon$  for the R=3.0 sample. Then again, CTAT-rich vesicles also showed unique behavior in FCS studies as the only vesicles to show a marked (twofold) increase in K when moving to higher charge stoichiometry.

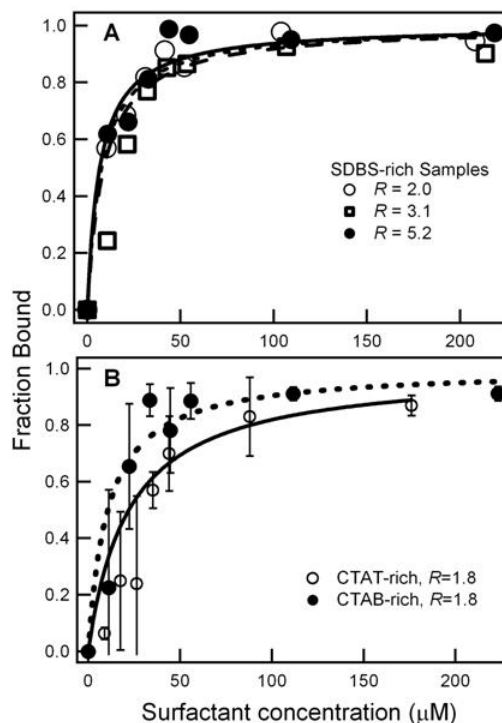


**Figure 5.6.** Adsorption isotherms illustrating the effects of (A) bilayer charge stoichiometry and (B) excess counter ion identity.

A plausible explanation to account for the relatively weaker adsorption of CTAT-rich samples could be the lipophilicities of the counter ions. In CTAT-rich samples the unpaired cetyltrimethylammonium ( $\text{CTA}^+$ ) is available to interact with tosylate ions ( $\text{TOS}^-$ ). Bulky organic ions such as tosylate readily form ion pairs in water and this increases their hydrophobicity. Adsorption to the bilayer interface of the CTAT-rich vesicles is extremely favorable for tosylate since the hydrophobic toluene moiety can intercalate into the bilayer leaflet while the sulfonate group forms an ion pair with  $\text{CTA}^+$ . This arrangement is energetically favorable and hence is unlikely to be disrupted by the addition of other organic anions (i.e. binding large tosylates will block the vesicle surface from binding to probe molecules). In SDBS-rich samples the excess  $\text{DBS}^-$  only weakly

pairs with sodium residing in the Stern layer which is a much weaker interaction. To test this we have substituted CTAT with CTAB and prepared CTAB-rich vesicles with a charge ratio of  $R = 1.8$  for comparison with our 7:3 CTAT-to-SDBS samples. For comparison with CTAT-rich samples, both  $K$  and  $\epsilon$  were determined for CF binding to the CTAB-rich vesicle samples. These values are reported in Table 5.1 and the binding isotherms for CF on both CTAT-rich and CTAB-rich vesicles are compared in Figure 5.6B. From the two curves, the average bound fraction of CF on CTAB-rich vesicle for each concentration is larger than CF on CTAT-rich vesicle. Although the errors of bound fraction for several vesicle concentrations are overlapped, which can be introduced by the error from the vesicle preparation, the overall trend of the two curves confirms that the binding of CF on  $R=1.8$  CTAB-rich vesicle is stronger than CF on  $R=1.8$  CTAT-rich vesicle. There are no reports of CTAB/SDBS vesicles in the literature, but from dynamic light scattering and SEC measurements vesicle do appear present for 6.5:3.5 w/w CTAB to SDBS ( $R=1.8$ ) at 1% total surfactant.

The results from the above study revealed that electrostatic forces play an important role in determining the encapsulation efficiency of surfactant vesicles. A common method for confirming and evaluating the role of electrostatic interactions in a binding process is to monitor the effect of salt concentration on binding. When additional salt is added, electrostatic interactions between an ionic probe molecule and a charged surfactant bilayer is expected to be reduced due to the change in ionic strength of the solution. The loading ability of the surfactant vesicles is expected to be diminished as

well. Therefore understanding electrostatic interactions is critical to understanding the result of these experiments and the basic theory<sup>25</sup> is introduced below.

The distribution of ionic molecules as counterions near a charged surface which could be a surfactant vesicle surface is described by the Boltzmann equation

$$n_i(x) = n_{i0} \exp\left(\frac{-z_i e \Phi(x)}{k_B T}\right) \quad (8)$$

where  $n_i$  is the concentration of ion  $i$  at a certain position  $x$ ,  $n_{i0}$  is the concentration of ion  $i$  in the bulk,  $z_i$  is the valency of ion  $i$ ,  $e$  is the charge of an electron and  $\Phi(x)$  is the electrostatic potential at position  $x$ . what is kb and T.

The electrostatic potential  $\Phi$  of a charged surface in a liquid medium is described by the Poisson equation,

$$\nabla^2 \Phi = -\frac{\rho^*}{\epsilon_0 \epsilon} \quad (9)$$

where  $\rho^*$  is the charge density, equal to  $-\sum z_i e n_i$ .

When considering a Boltzmann distribution of molecules near a charged surface, one can use the Poisson-Boltzmann distribution equation to describe the charge density of ionic molecules at distance  $x$  from the charged surface,

$$\nabla^2 \Phi = -\frac{\sum z_i e n_i}{\epsilon_0 \epsilon} \quad (10)$$

Solving this equation gives an electrostatic potential:  $\Phi = \Phi_0 \exp(-\kappa x)$ , where  $\kappa$  is the Debye-Huckel parameter with units of inverse length. Another parameter is defined as  $\lambda_D = \kappa^{-1}$ , which is called Debye length (See Figure 5.7.).  $\lambda_D$  in turn is related to another important parameter, ionic strength  $I$  and is found to be proportional to  $I^{-1/2}$ . Ionic strength is defined as

$$I = \frac{1}{2} \sum z_i^2 n_{i0} = \frac{1}{2} \sum z_i^2 1000 N_{AV} C \quad (11)$$

where  $C$  is the bulk concentration of ionic molecule in mole/L.

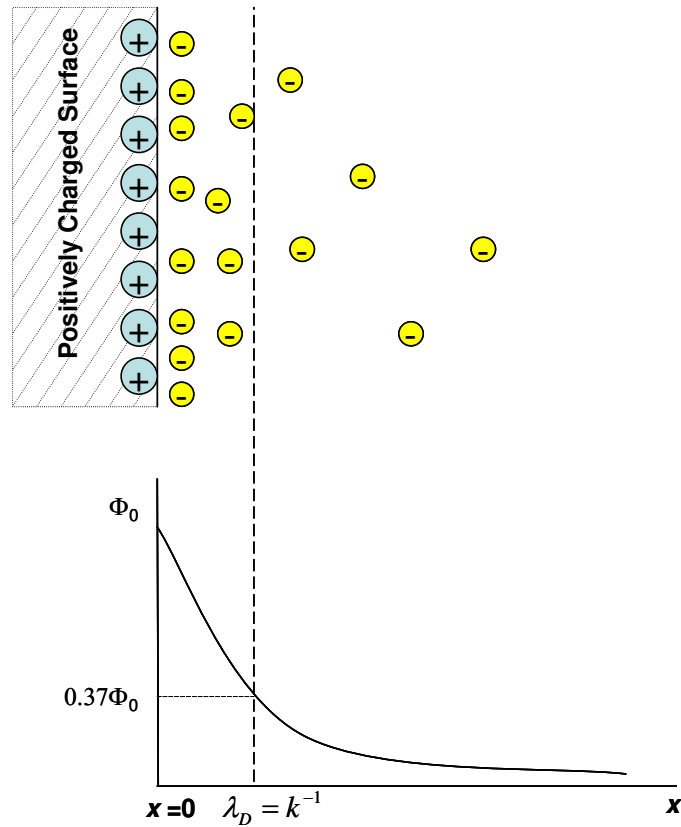


**Figure 5.7.** Illustration of Debye length.

The Debye length for 1:1 electrolyte (e.g. NaCl ) in solution at a concentration C (mol/L) is:

$$\lambda_D = \frac{0.304}{\sqrt{C}} \text{ nm} \quad (12)$$

When C is 0.001, 0.01 and 0.1 M respectively, the corresponding Debye length  $\lambda_D$  is 9.6, 3.04, 0.96 nm respectively.

From above deduction, most counterions are held within the Debye length of the charged surface due to the electrostatic interaction. Electrolyte valency and concentration determines the of the Debye length. The binding of ionic molecules to a charged surface is reduced by addition of an electrolyte, sodium chloride in this study.

Sodium chloride, a critical component making up the physiological environment, was utilized to explore this effect. These studies were undertaken as an important first step toward investigating the potential of surfactant vesicles as a drug delivery system.

Bulk SEC measurements were made for CF encapsulated in CTAT-rich vesicles and for R6G in SDBS-rich vesicles. Both vesicles were made with normal saline solution instead of aqueous solution. The overlap of resulting DLS and UV-vis absorption are shown in the Figure 5.8. CF encapsulation was seriously impacted (the encapsulation efficiency was dropped from 24% to 0%). On the contrary, encapsulation of R6G in SDBS-rich vesicles had an undistinguishable change.

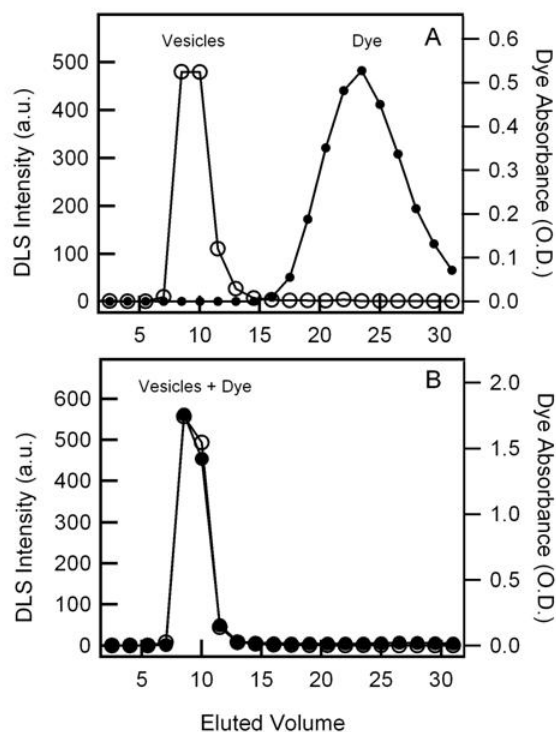


**Figure 5.8.** SEC results from studies of dye binding and encapsulation in normal saline. (A) Apparent encapsulation of carboxyfluorescein drops from 24% to 0% under physiological salt concentrations. (B) Conversely, the apparent encapsulation of Rhodamine 6G is unchanged in normal saline.

FCS measurements of the binding efficiency of above systems also were conducted (see Figure 5.9.). The fraction of R6G bound to the SDBS-rich vesicles was not impacted at the salt concentration range from 10 $\mu$ M to 200mM. CTAT sample lost nearly all ability to sequester when 100mM sodium chloride was present in the solution. FCS results were consistent with bulk measurement since sodium chloride concentration in normal saline is 150mM.

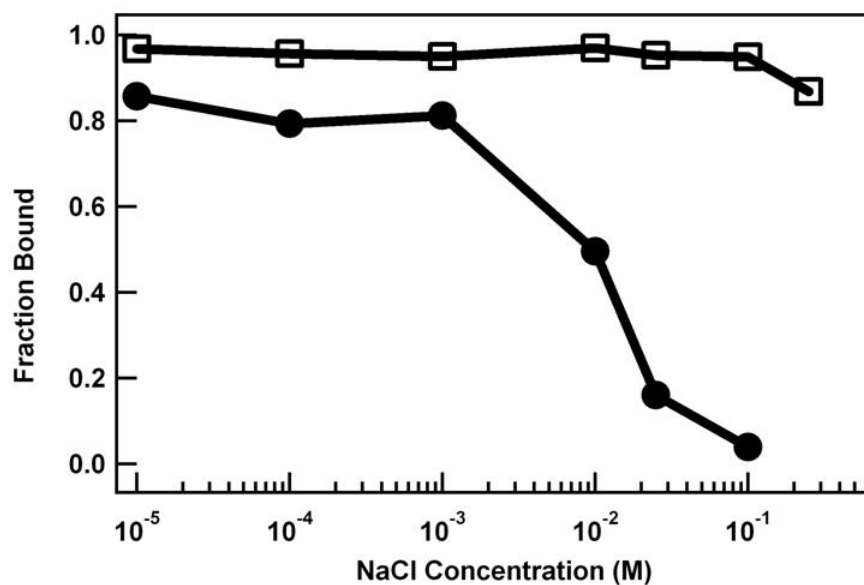


**Figure 5.9.** FCS results from studies of dye adsorption as a function of salt concentration. The dots and squares are the fraction of CF bound to the CTAT-rich vesicles and R6G bound to SDBS-rich vesicles as the changes of concentration of sodium chloride, respectively.

Salt studies in both bulk and FCS measurements revealed that electrostatic interactions were impacted by addition of sodium chloride. However, the effect of salt on different systems varies. The encapsulation depends on the nature of surfactant vesicles. In our study, SDBS-rich vesicles are less susceptible than CTAT-rich vesicles. Extra salts can displace CF from the bilayer easily due to the decreased interaction of CF with tosylate rich external layer of  $V^+$ . By contrast, the interaction of R6G with the sodium rich external layer is very strong. The impact of salt is diminished in  $V^-$ . Those results are consistent with the previous counterion study.

## 5.4. Conclusions

Our studies demonstrate the utility of fluorescence correlation spectroscopy as a means of studying binding of probe molecules to surfactant vesicles. Electrostatic adsorption on the outside surface of the vesicle bilayer seems to predominate over dye that is truly “encapsulated” within the inner core of the vesicles, as observed by using size exclusion chromatography to compare dye sequestration and capture for vesicle mixtures with dye added before and after vesicle formation. This adsorption phenomenon may be explained by models of charge segregation between the inner and outer leaflets of the vesicle bilayer, which suggest that excess charge resides mostly on the outer bilayer surface. After all, excess charge at the outside vesicle surface makes electrostatic binding of oppositely charged dye to the outside surface very favorable. Binding isotherms constructed from FCS measurements yield a picture of free energy, and larger binding coefficients for the default 3:7  $V^-$  system (charge ratio  $R=3.0$ ) than for the benchmark 7:3  $V^+$  system ( $R=1.8$ ) support the charge segregation concept. While the higher binding coefficients and encapsulation efficiencies initially observed for  $V^-$  systems appear to be due to counterion identity and excess charge, these systems do appear much more stable in saline (a necessity for drug delivery and *any* other biological application) than  $V^-$  vesicles rich in either CTAT or CTAB, as indicated by measurements of  $\varepsilon$  in saline solutions for  $V^+$  and  $V^-$  solutions. Before prematurely declaring  $V^-$  vesicles as innately superior encapsulation/adsorption vesicles, however, it would be wise to await further results of  $\varepsilon$  (not yet shown in Table 5.1) and to conduct FCS and SEC experiments with a cationic fluorescent dye other than R6G. Such results,

taken into consideration with cell targeting and toxicity studies currently underway in collaborating labs at the University of Maryland.

## References:

1. Kaler, E. W.; Murthy, A. K.; Rodriguez, B. E.; Zasadzinski, J. A. N. *Science* 1989, *245*, 1371-1374.
2. Kaler, E. W.; Herrington, K. L.; Murthy, A. K.; Zasadzinski, J. A. N. *J. Phys. Chem.* 1992, *96*, 6698-6707.
3. Talmon, Y.; Evans, D. F.; Ninham, B. W. *Science* 1983, *221*, 1047-1048.
4. Gebicki, J. M.; Hicks, M. *Nature* 1973, *243*, 232-234.
5. Hargreaves, W. R.; Deamer, D. W. *Biochemistry* 1978, *17*, 3759-3768.
6. Jain, M. K.; Vanechteld, C. J. A.; Ramirez, F.; Degier, J.; Dehaas, G. H.; Vandeenen, L. L. M. *Nature* 1980, *284*, 486-487.
7. Laughlin, R. G. *Colloids Surf., A* 1997, *128*, 27-38.
8. Almgren, M.; Rangelov, S. *Langmuir* 2004, *20*, 6611-6618.
9. Park, J.; Danoff, E. J.; Stein, D. C.; English, D. S.; DeShong, P. *In Preparation for JACS* 2007.
10. Wang, X.; Danoff, E. J.; Sinkov, N. A.; Lee, J.-H.; Raghavan, S. R.; English, D. S. *Langmuir* 2006, *22*, 6461-6464.
11. Danoff, E. J.; Wang, X.; Tung, S.-H.; Sinkov, N. A.; Kemme, A. M.; Raghavan, S. R.; English, D. S. *Langmuir* 2007, *23*, 8965 - 8971.
12. Israelachvili, J. N. *Intermolecular and Surface Forces*; Academic Press: London, 1985.
13. Safran, S. A.; Pincus, P.; Andelman, D. *Science* 1990, *248*, 354-356.
14. Bonincontro, A.; La Mesa, C.; Proietti, C.; Risuleo, G. *Biomacromolecules* 2007, *8*, 1824-1829.
15. Dias, R. S.; Lindman, B.; Miguel, M. G. *J. Phys. Chem. B* 2002, *106*, 12600-12607.

16. Mel'nikov, S. M.; Dias, R.; Mel'nikova, Y. S.; Marques, E. F.; Miguel, M. G.; Lindman, B. *FEBS Lett.* 1999, *453*, 113-118.
17. Letizia, C.; Andreozzi, P.; Scipioni, A.; La Mesa, C.; Bonincontro, A.; Spigone, E. *J. Phys. Chem. B* 2007, *111*, 898-908.
18. Rigler, R.; Elson, E. S. *Fluorescence Correlation Spectroscopy Theory and Applications*; Springer: Berlin, 2001.
19. Rusu, L.; Gambhir, A.; McLaughlin, S.; Radler, J. *Biophys. J.* 2004, *87*, 1044-1053.
20. Allen, N. W.; Thompson, N. L. *Cytom. Part A* 2006, *69A*, 524-532.
21. Elson, E. L.; Magde, D. *Biopolymers* 1974, *13*, 1-27.
22. Thompson, N. L. In *Topics in Fluorescence Spectroscopy*; Lakowicz, J. R., Ed.; Plenum Press: New York, 1991, pp 337-378.
23. Hess, S. T.; Webb, W. W. *Biophys. J.* 2002, *83*, 2300-2317.
24. Magde, D.; Webb, W. W.; Elson, E. *Phys. Rev. Lett.* 1972, *29*, 705-&.
25. Israelachvili, J. N. *Intermolecular and Surface Forces*; Academic Press: London, 1991.

## Chapter 6. Conclusions and Future Work

### 6.1. Conclusions

Initial experiments conducted in this work revealed that charged surfactant vesicles, formed in mixtures of CTAT/SDBS/water, are extraordinarily efficient for sequestering charged organic molecules. Vesicles only form when one surfactant is in excess and therefore the vesicle bilayer always possesses a charge, either negative or positive depending on the surfactant that is in excess. High efficiency capture is observed when the cargo molecule has the opposite charge from the vesicle bilayer. Because these systems are equilibrium structures and are extremely stable, the release rate of captured solutes is very slow; hence preparations of surfactant vesicles with cargo molecules possess extremely long shelf-lives. Among the probe molecules investigated, a drug molecule, Doxorubicin HCL (Dox), could be encapsulated with 55% efficiency in SDBS-rich (V-) vesicles. This is in contrast with previous studies for the application of liposomes in drug delivery that showed lower capture and higher leakage rates.<sup>1</sup> Given the extremely high capture efficiency and long-term stability, surfactant vesicles are promising candidates for use as drug delivery “vessels”.

In addition to being possible candidates for drug delivery, surfactant vesicles may also be promising new media for charge-based separations. It was shown in previous chapters that electrostatic interactions play an important role in the high “apparent”

encapsulation efficiencies of surfactant vesicles. By taking advantage of such strong interactions between charged surfactant bilayers and ionic molecules, we were able to show that surfactant vesicles can be used to separate oppositely charged molecules. This was achieved by using a simple sephadex column to separate vesicles containing oppositely charged molecules (e.g. SDBS-rich vesicles containing the Rhodamine 6G cation) from free dye possessing the same charge sign as the vesicles (e.g. the carboxyfluorescein anion with SDBS-rich vesicles). This separations method is efficient, easy and cheap relative to methods such as gel electrophoresis.

The high encapsulation efficiency for surfactant vesicles is dependent on many factors and several have been investigated here. The first one is the excess charge on the surfactant vesicle bilayer due to the different compositions of CTAT and SDBS. In Chapter 5, Table 5.1, different excess charge concentrations ( $\Delta C$  (mM)) lead to different “apparent” encapsulation efficiencies of dyes at various CTAT/SDBS ratios. As  $\Delta C$  increases so does the encapsulation for ionic dye molecules in CTAT/SDBS system. This is simply due to the increasing number of available binding sites for electrostatic adsorption.

The second important factor investigated is the counter ion identity which was found to impact encapsulation efficiency. In CTAT-rich vesicles the tosylate ion occupies the potential electrostatic binding sites represented by the excess CTAT molecules and in SDBS-rich vesicles the excess counterion is the sodium ion. CTAT-rich vesicles have a lower encapsulation efficiency than SDBS-rich ( $V^-$ ) vesicles. Even

when one considers excess charge,  $V^-$  still encapsulates more oppositely-charged molecules. It is hypothesized that this is due to the amphiphilic tosylate counterion being more stable and less likely to be replaced at the bilayer binding sites represented by the  $CTA^+$  surfactant. The counterion of  $DBS^-$ , is the water soluble sodium ion and interacts weakly with the bilayers and therefore is easily replaced by a positively charged amphiphilic probe molecule such as Rhodamine 6G or doxorubicin. A similar trend was observed for vesicles formed from CTAB, in which improved efficiency was observed relative to CTAT-rich vesicles.

A final important issue that impacts all electrostatic interactions is that of ionic strength. Additional salts in solution can reduce the Debye screening length between charges in aqueous solution, and therefore between unpaired surfactants in the vesicle bilayer and oppositely charged molecules in solution. This effect leads to less binding or encapsulation when surfactant vesicles are exposed to high salt concentration. The consequence for adding salt to  $V^+$  or  $V^-$  systems varies. Unlike  $V^+$  samples, encapsulation by  $V^-$  samples remains high at salt concentrations above physiological conditions up to tens of millimolar sodium chloride. This finding suggests that  $V^-$  samples are promising for drug delivery or cellular diagnostics in buffers with high ionic strength.

Under conditions where high apparent encapsulation efficiency is observed most ionic molecules are believed to be adsorbed on the exterior of the surfactant vesicle bilayer. This has been investigated and quantified by comparing SEC results of vesicles

formed in the presence of dye solution with SEC results when dye molecules are added after the vesicles formed. As discussed in Chapters 1 and 5, the asymmetric distribution of unpaired charged surfactant between the outer and inner bilayer accounts for the fact that vesicle loading does not depend very much on whether dye is added before or after vesicle formation. The observation that dye molecules bind strongly to the outer membrane is consistent with more unpaired charges on the outer layer compared to the inner layer of the bilayer and this agrees with theoretical models suggesting that nonideal mixing in the bilayer is crucial for spontaneous bilayer curvature.

FCS has been successfully introduced to quantitatively explore the strong electrostatic interaction between charged dye molecules and oppositely charged surfactant bilayers. FCS allows one to conduct binding measurements at very low sample concentration ( $10^{-9}$ - $10^{-8}$  M). This technique was successfully used to obtain binding isotherms for vesicles interacting with low concentrations of probe molecules. Results from FCS studies were consistent with bulk SEC measurements in that higher binding constants correlated with higher encapsulation. It was found that both bilayer composition and counter ion identity can strongly affect the apparent encapsulation efficiency; hence FCS can provide quantitative data about electrostatic interactions between surfactant vesicles and charged solutes.

## **6.2. Future Work**

The use of surfactant vesicles as drug carriers should be investigated by studying the vesicles under physiological conditions and determining the effects of the vesicles on

biological systems and vice versa. For example, it is important to determine the stability and encapsulation efficiency of these vesicles when exposed to differing environments, such as high or low pH and varying salt concentrations.

In order for surfactant vesicles to be of therapeutic use, the cytotoxicity of the vesicles must be investigated. Kuo *et al.* have shown that cationic vesicles composed of the surfactants HTMAB and SDS are nontoxic towards mouse fibroblast and liver cells.<sup>2</sup> Work is currently being done on the CTAT/SDBS system in conjunction with Dr. John Fisher's lab in the Department of Bioengineering to measure the cytotoxicity of the vesicles. Initial results show that V<sup>-</sup> vesicles are nontoxic toward chondrocytes at concentrations up to 0.1 µg/ml total surfactant.

To date, many surfactant vesicle systems have been discovered. This can lead to finding other intriguing systems with high encapsulation and slow release rates is an important goal. For example, CTAB/SDBS system has been initially explored in Dr. English's lab for the encapsulation ability and long term stability and the work will continue in the future.

Recently, a study showed that surfactant vesicle was encapsulated by chitosan and co-electrodeposited on a charged surface such as a microfabricated wafer in solution.<sup>3</sup> By control localized electrical stimulations, the solubility of chitosan film was impacted. Hence, surfactant vesicle entrapped within chitosan was mobilized. This approach can be

potentially used in controllable means, such as varying electronic signal, pH, to store and release vesicle-based reagents/therapeutics for microfluidic/medical applications.

There is still a great deal of work to be done concerning surfactant vesicles and their potential use as drug delivery agents, but the present research has shown that they are remarkably efficient at entrapping solutes—a fact that could be of great importance for developing drug carrier technology. One shouldn't forget that there are other possible applications of these vesicles as well, in such areas as cosmetics and agrochemicals. Overall surfactant vesicles hold exciting implications for future use.

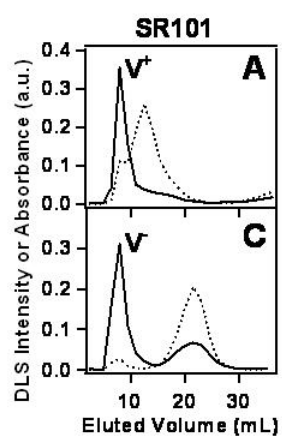
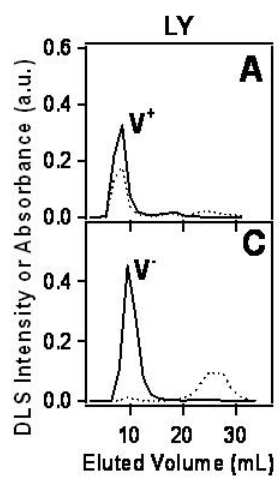
## References:

1. Nii, T.; Ishii, F. *Int. J. Pharm.* 2005, 298, 198-205.
2. Kuo, J. H. S.; Jan, M. S.; Chang, C. H.; Chiu, H. W.; Li, C. T. *Colloids Surf., B* 2005, 41, 189-196.
3. Zhu, C.; Wu, L. Q.; Wang, X.; Lee, J. H.; English, D. S.; Ghodssi, R.; Raghavan, S. R.; Payne, G. F. *Langmuir* 2007, 23, 286-291.

## Appendix A

### **A.1. Data and Images from SEC Experiments for Evaluation of Apparent Encapsulation Efficiency ( $\epsilon$ )**

The four figures below are counterparts to Figure 4.2. of the Chapter 4 with photographs, DLS intensity (solid line), and UV-vis absorbance data (dotted line), for each of the solutes studied. The encapsulation values for each solute are reported in Table 4.1 of Chapter 4.



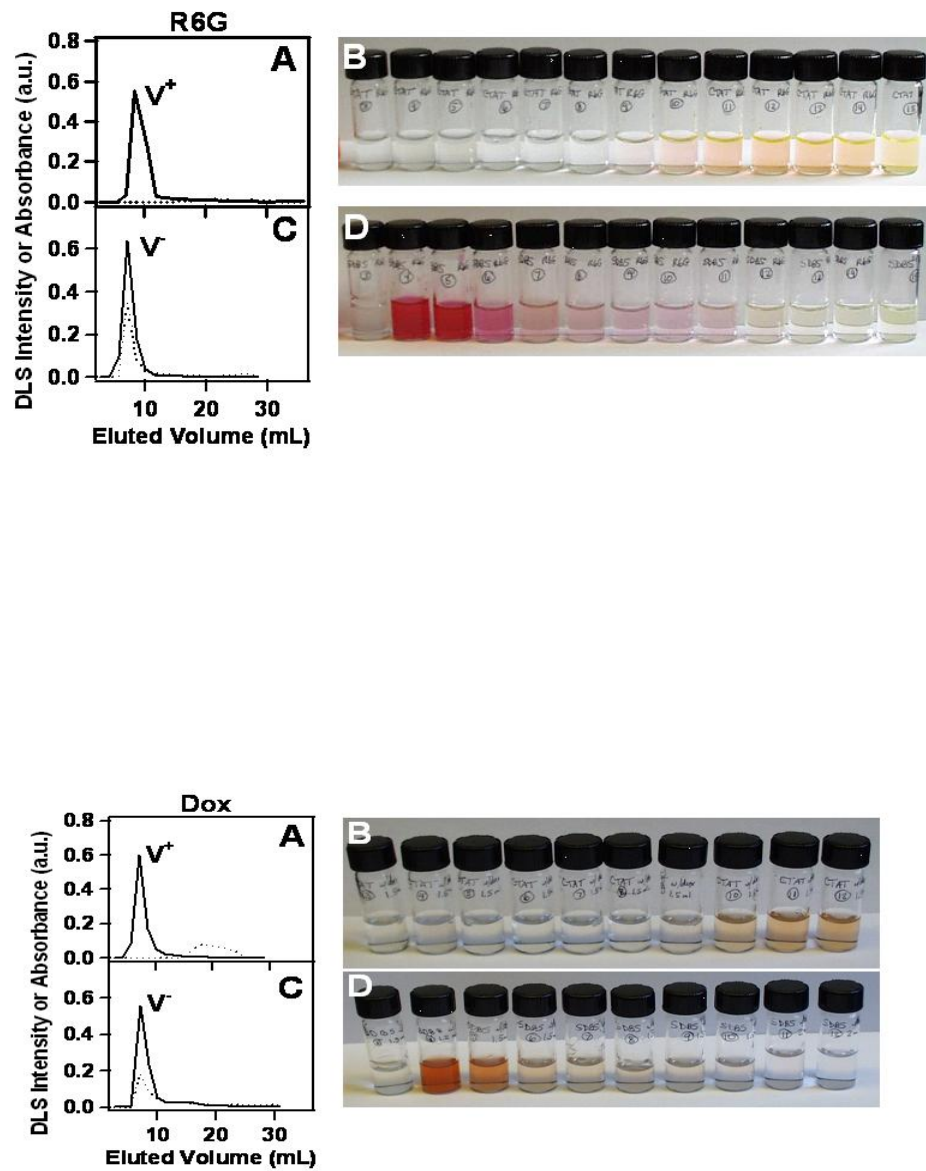


**Figure A.1.** DLS and encapsulation efficiency study through SEC for dye molecules of LY, SR101, R6G and Dox.

## A.2. Separations Performed on a Mixture of LY and Dox

In addition to using cationic vesicles to separate the dyes CF and R6G, we also conducted separation experiments using the anionic dye, LY and the cationic drug, Dox. The separation illustrated below was performed on an equimolar solution of the two dyes. The total dye concentration was 1 mM. We again observed very efficient separation using vesicles, much like in Figure 4 of the main paper. The figure below shows the DLS intensity (solid line) and UV-vis absorbance of LY (dashed line) and Dox (dotted line) for each eluted fraction. The vesicle band for the  $V^+$  sample contained 30% of the LY with no detectable Dox, while the vesicle band for the  $V^-$  sample contained 63% of the Dox with no detectable LY. (See in Figure A..)

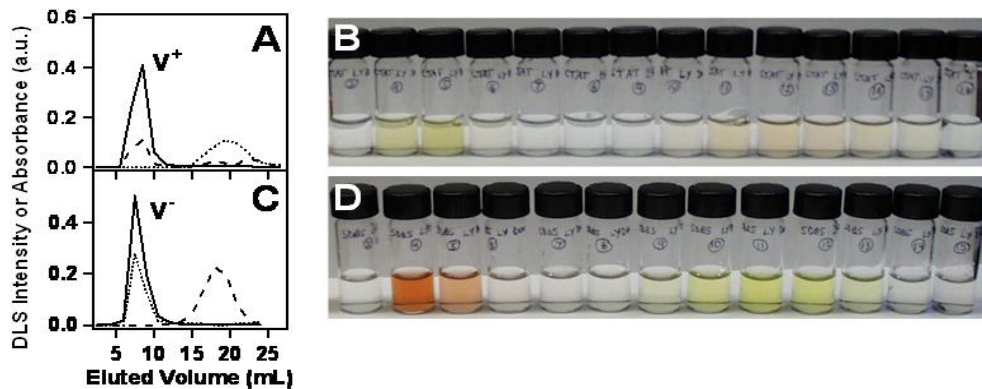


**Figure A.2.** Separation of LY and Dox.

## Appendix B

**B.1.** Diffusion coefficient for micelles is lower than for free dye and higher than for vesicles. In fact, it happens to be right in-between. That also follows our prediction since micelles are larger than individual molecules but much smaller than the vesicles. No very slow component was seen, so there are either no huge SDBS aggregates or if there are any dye does not bind to them. Therefore, the data looks like it allows us to conclude that the slow component we see in the SDBS-rich samples is due to SDBS-CTAT structures, presumably vesicles. (See Figure B.)

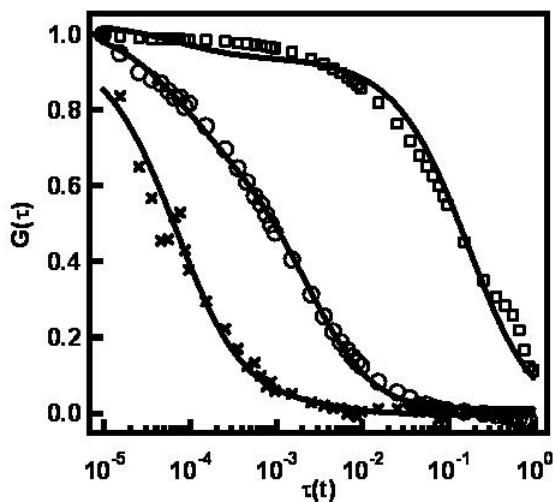


**Figure B.3.** Square, circle, and cross represents autocorrelation curve of vesicle, SDBS micelle, and free dye, respectively. Corresponding diffusion coefficient ( $\text{cm}^2 \cdot \text{s}^{-1}$ ) is  $1.08 \times 10^{-9}$ ,  $7.9 \times 10^{-8}$  and  $2.6 \times 10^{-6}$ , respectively.

## References:

### Chapter 1:

1. Bangham, A. D.; Horne, R. W. *J. Mol. Biol.* 1964, 8, 660-668.
2. Bangham, A. D.; Standish, M. M.; Watkins, J. C. *J. Mol. Biol.* 1965, 13, 238-252.
3. Bangham, A. D. *Liposome Letters*; Academic Press, 1983.
4. Lasic D. D., T. N. S. *Gene therapy: therapeutic mechanisms and strategies*,; Marcel Dekker,: New York, 2000.
5. Xu, Y. H.; Szoka, F. C. *Biochemistry* 1996, 35, 5616-5623.
6. Wu, G. Y.; Wu, C. H. *J. Biol. Chem.* 1987, 262, 4429-4432.
7. Felgner, P. L.; Gadek, T. R.; Holm, M.; Roman, R.; Chan, H. W.; Wenz, M.; Northrop, J. P.; Ringold, G. M.; Danielsen, M. *P. Natl. Acad. Sci. USA* 1987, 84, 7413-7417.
8. Sheff, D. *Adv. Drug. Deliver. Rev.* 2004, 56, 927-930.
9. Langer, R. *Nature* 1998, 392, 5-10.
10. Esfand, R.; Tomalia, D. A. *Drug. Discov. Today* 2001, 6, 427-436.
11. Peppas, N. A.; Bures, P.; Leobandung, W.; Ichikawa, H. *Eur. J. Pharm. Biopharm.* 2000, 50, 27-46.
12. Baillie, A. J.; Florence, A. T.; Hume, L. R.; Muirhead, G. T.; Rogerson, A. J. *Pharm. Pharmacol.* 1985, 37, 863-868.
13. Schreier, H.; Bouwstra, J. *J. Controlled Release* 1994, 30, 1-15.
14. Gebicki, J. M.; Hicks, M. *Nature* 1973, 243, 232-234.
15. Hargreaves, W. R.; Deamer, D. W. *Biochemistry* 1978, 17, 3759-3768.
16. Fendler, J. H. *Accounts Chem Res* 1980, 13, 7-13.
17. Helfrich, W. *Z. Naturforsch., C: Biosci.* 1973, C 28, 693-703.
18. Safran, S. A.; Pincus, P.; Andelman, D. *Science* 1990, 248, 354-356.
19. Lasic, D. D. *Trends Biotechnol.* 1998, 16, 307-321.
20. Tondre, C.; Caillet, C. *Adv. Coll. Inter. Sci* 2001, 93, 115-134.

21. Laughlin, R. G. *Colloids Surf., A* 1997, *128*, 27-38.
22. Almgren, M.; Rangelov, S. *Langmuir* 2004, *20*, 6611-6618.
23. Kaler, E. W.; Murthy, A. K.; Rodriguez, B. E.; Zasadzinski, J. A. N. *Science* 1989, *245*, 1371-1374.
24. Israelachvili, J. N.; Mitchell, D. J.; Ninham, B. W. *J. Chem. Soc., Faraday Trans. II* 1976, *72*, 1525-1568.
25. Israelachvili, J. N. *Intermolecular and Surface Forces*; Academic Press: London, 1985.
26. Zana, R., Ed. *Dynamics of Surfactant Self-Assemblies*; CRC Press: Boca Raton, 2005.
27. Koehler, R. D.; Raghavan, S. R.; Kaler, E. W. *J. Phys. Chem. B* 2000, *104*, 11035-11044.
28. Safran, S. A.; Pincus, P. A.; Andelman, D.; Mackintosh, F. C. *Phys. Rev. A* 1991, *43*, 1071-1078.
29. Caillet, C.; Hebrant, M.; Tondre, C. *Langmuir* 2000, *16*, 9099-9102.

## Chapter 2:

1. Kaler, E. W.; Murthy, A. K.; Rodriguez, B. E.; Zasadzinski, J. A. N. *Science* 1989, *245*, 1371-1374.
2. Berne, B. J.; Pecora, R. *Dynamic Light Scattering: With Applications to Chemistry, Biology, and Physics*; Dover Publications, 2000.
3. Brown, W. *Dynamic Light Scattering: The Method and Some Applications*; Oxford University Press, USA, 1993.
4. Koppel, D. E. *J. Chem. Phys.* 1972, *57*, 4814-4820.
5. Jang, H.; Pell, L. E.; Korgel, B. A.; English, D. S. *J. Photoch. Photobio. A* 2003, *158*, 111-117.
6. Magde, D.; Webb, W. W.; Elson, E. *Phys. Rev. Lett.* 1972, *29*, 705-708.
7. Magde, D.; Elson, E. L.; Webb, W. W. *Biopolymers* 1974, *13*, 29-61.
8. Elson, E. L.; Magde, D. *Biopolymers* 1974, *13*, 1-27.

9. Rigler, R.; Mets, U.; Widengren, J.; Kask, P. *Eur. Biophys. J. Biophys* 1993, 22, 169-175.
10. Schwille, P.; Haupts, U.; Maiti, S.; Webb, W. W. *Biophys. J.* 1999, 77, 2251-2265.
11. Rusu, L.; Gambhir, A.; McLaughlin, S.; Radler, J. *Biophys. J.* 2004, 87, 1044-1053.
12. O'Connor, D. V.; Philips, D. *Time-Correlated Single Photon Counting*; Academic: London, 1984.
13. Lakowicz, J. R. *Principles of Fluorescence Spectroscopy*; Plenum: New York, 1991.
14. Lamb, D. C.; Schenk, A.; Rocker, C.; Scalfi-Happ, C.; Nienhaus, G. U. *Biophys. J.* 2000, 79, 1129-1138.
15. Eggeling, C.; Berger, S.; Brand, L.; Fries, J. R.; Schaffer, J.; Volkmer, A.; Seidel, C. A. M. *J. Biotechnol.* 2001, 86, 163-180.

### Chapter 3:

1. Xiang, T. X.; Chen, J.; Anderson, B. D. *J Membrane Biol* 2000, 177, 137-148.
2. Ishida, A.; Otsuka, C.; Tani, H.; Kamidate, T. *Anal. Biochem.* 2005, 342, 338-340.
3. Apel-Paz, M.; Doncel, G. F.; Vanderlick, T. K. *Langmuir* 2005, 21, 9843-9849.
4. Sato, Y.; Shin-ichiro, M. N.; Yoshikawa, K. *Chem. Phys. Lett.* 2003, 380, 279-285.
5. Kaler, E. W.; Murthy, A. K.; Rodriguez, B. E.; Zasadzinski, J. A. N. *Science* 1989, 245, 1371-1374.
6. Almgren, M.; Rangelov, S. *Langmuir* 2004, 20, 6611-6618.
7. Laughlin, R. G. *Colloids. Surf., A* 1997, 128, 27-38.
8. Caillet, C.; Hebrant, M.; Tondre, C. *Langmuir* 2000, 16, 9099-9102.
9. Kaler, E. W.; Herrington, K. L.; Murthy, A. K.; Zasadzinski, J. A. N. *J. Phys. Chem.* 1992, 96, 6698-6707.
10. Fischer, A.; Hebrant, M.; Tondre, C. *J. Coll. Inter. Sci* 2002, 248, 163-168.
11. Zhao, G.-X.; Yu, W.-L. *J. Coll. Inter. Sci* 1995, 173, 159-164.

12. Tondre, C.; Caillet, C. *Adv. Coll. Inter. Sci* 2001, 93, 115-134.
13. Schwarz, G.; Arbuzova, A. *BBA-Biomembranes* 1995, 1239, 51-57.
14. Weinstein, J. N.; Yoshikami, S.; Henkart, P.; Blumenthal, R.; Hagins, W. A. *Science* 1977, 195, 489-492.
15. Koehler, R. D.; Raghavan, S. R.; Kaler, E. W. *J. Phys. Chem., B* 2000, 104, 11035-11044.
16. Goldbach, P.; Brochart, H.; Wehrle, P.; Stamm, A. *Int. J. Pharm.* 1995, 117, 225-230.
17. Antunes, F. E.; Marques, E. F.; Gomes, R.; Thuresson, K.; Lindman, B.; Miguel, M. G. *Langmuir* 2003, 20, 4647-4656.
18. Karukstis, K.; Zieleniuk, C. A.; Fox, M. J. *Langmuir* 2003, 19, 10054-10060.
19. Jang, H.; Pell, L. E.; Korgel, B. A.; English, D. S. *J. Photochem. Photobiol., A* 2003, 158, 111-117.

#### Chapter 4:

1. Hargreaves, W. R.; Deamer, D. W. *Biochemistry* 1978, 17, 3759-3768.
2. Tondre, C.; Caillet, C. *Adv. Coll. Inter. Sci* 2001, 93, 115-134.
3. Khan, A. *Curr. Opin. Colloid. In.* 1996, 1, 614-623.
4. Kondo, Y.; Uchiyama, H.; Yoshino, N.; Nishiyama, K.; Abe, M. *Langmuir* 1995, 11, 2380-2384.
5. Marques, E. F.; Regev, O.; Khan, A.; Miguel, M. D.; Lindman, B. *J. Phys. Chem. B* 1998, 102, 6746-6758.
6. Marques, E. F.; Regev, O.; Khan, A.; Miguel, M. D.; Lindman, B. *J. Phys. Chem. B* 1999, 103, 8353-8363.
7. Herrington, K. L.; Kaler, E. W.; Miller, D. D.; Zasadzinski, J. A.; Chiruvolu, S. *J. Phys. Chem.* 1993, 97, 13792-13802.
8. Kaler, E. W.; Herrington, K. L.; Murthy, A. K.; Zasadzinski, J. A. *N. J. Phys. Chem.* 1992, 96, 6698-6707.
9. Berman, A.; Cohen, M.; Regev, O. *Langmuir* 2002, 18, 5681-5686.
10. Edlund, H.; Sadaghiani, A.; Khan, A. *Langmuir* 1997, 13, 4953-4963.

11. Yacilla, M. T.; Herrington, K. L.; Brasher, L. L.; Kaler, E. W.; Chiruvolu, S.; Zasadzinski, J. A. *J. Phys. Chem.* 1996, *100*, 5874-5879.
12. Wang, X.; Danoff, E. J.; Sinkov, N. A.; Lee, J.-H.; Raghavan, S. R.; English, D. S. *Langmuir* 2006, *22*, 6461-6464.
13. Wang, X.; Danoff, E. J.; Sinkov, N. A.; Lee, J. H.; Raghavan, S. R.; English, D. S. *Langmuir* 2006, *22*, 6461-6464.
14. Kaler, E. W.; Murthy, A. K.; Rodriguez, B. E.; Zasadzinski, J. A. *N. Science* 1989, *245*, 1371-1374.
15. Lee, J.-H.; Gustin, J. P.; Chen, T.; Payne, G. F.; Raghavan, S. R. *Langmuir* 2005, *21*, 26-33.
16. Vallotton, P.; Vogel, H. *J. Fluoresc.* 2000, *10*, 325-332.
17. Dalmark, M. *Scand. J. Clin. Lab. Invest.* 1981, *41*, 633-639.
18. Abraham, S. A.; Waterhouse, D. N.; Mayer, L. D.; Cullis, P. R.; Madden, T. D.; Bally, M. B. *Methods Enzymol.* 2005, *391*, 71-97.
19. Swain, S. M.; Whaley, F. S.; Ewer, M. S. *Cancer* 2003, *97*, 2869-2879.
20. Singal, P. K.; Olweny, C. L. M.; Li, T. M. *New. Endl. J. Med.* 1999, *340*, 655-655.
21. Caillet, C.; Hebrant, M.; Tondre, C. *Langmuir* 2000, *16*, 9099-9102.
22. Marques, E. F.; Regev, O.; Khan, A.; Miguel, M. D.; Lindman, B. *Macromolecules* 1999, *32*, 6626-6637.
23. Regev, O.; Marques, E. F.; Khan, A. *Langmuir* 1999, *15*, 642-645.
24. Wang, X.; Sinkov, N.; English, D. S. *J. Phys. Chem.* 2007, *to be submitted for publication.*
25. Jang, H.; Pell, L. E.; Korgel, B. A.; English, D. S. *J. Photochem. Photobiol., A* 2003, *158*, 111-117.
26. Schwarz, G.; Arbuzova, A. *BBA-Biomembranes* 1995, *1239*, 51-57.
27. Rex, S. *Biophys. Chem.* 1996, *58*, 75-85.
28. Armstrong, D. W.; Henry, S. J. *J. Liq. Chromatogr.* 1980, *3*, 657-662.
29. Khaledi, M. G. *J. Chromatogr. A* 1997, *780*, 3-40.
30. Escuder-Gilabert, L.; Molero-Monfort, A.; Villanueva-Camanas, R. M.; Sagrado, S.; Medina-Hernandez, M. J. *J. Chromatogr. B* 2004, *807*, 193-201.

31. Hong, M.; Weekley, B. S.; Grieb, S. J.; Foley, J. P. *Anal. Chem.* 1998, 70, 1394-1403.
32. Glatter, O. *Small-Angle X-Ray Scattering*; Academic Press: New York, 1982.
33. *Neutron, X-Ray and Light Scattering: Introduction to an Investigative Tool for Colloidal and Polymeric Systems*; Elsevier: Amsterdam, 1991.
34. Rose, P. G.; Blessing, J. A.; Lele, S.; Abulafia, O. *Gynecol Oncol* 2006, 102, 210-213.
35. Apel-Paz, M.; Doncel, G. F.; Vanderlick, T. K. *Langmuir* 2005, 21, 9843-9849.
36. Ishida, A.; Otsuka, C.; Tani, H.; Kamidate, T. *Anal. Biochem.* 2005, 342, 338-340.
37. Haran, G.; Cohen, R.; Bar, L. K.; Barenholz, Y. *Biochim. Biophys. Acta* 1993, 1151, 201-215.
38. Semple, S. C.; Klimuk, S. K.; Harasym, T. O.; Dos Santos, N.; Ansell, S. M.; Wong, K. F.; Maurer, N.; Stark, H.; Cullis, P. R.; Hope, M. J.; Scherrer, P. *BBA-Biomembranes* 2001, 1510, 152-166.
39. Sato, Y.; Shin-ichiro, M. N.; Yoshikawa, K. *Chem. Phys. Lett.* 2003, 380, 279-285.
40. Kuo, J. H. S.; Jan, M. S.; Chang, C. H.; Chiu, H. W.; Li, C. T. *Colloids Surf., B* 2005, 41, 189-196.

## Chapter 5:

1. Kaler, E. W.; Murthy, A. K.; Rodriguez, B. E.; Zasadzinski, J. A. N. *Science* 1989, 245, 1371-1374.
2. Kaler, E. W.; Herrington, K. L.; Murthy, A. K.; Zasadzinski, J. A. N. *J. Phys. Chem.* 1992, 96, 6698-6707.
3. Talmon, Y.; Evans, D. F.; Ninham, B. W. *Science* 1983, 221, 1047-1048.
4. Gebicki, J. M.; Hicks, M. *Nature* 1973, 243, 232-234.
5. Hargreaves, W. R.; Deamer, D. W. *Biochemistry* 1978, 17, 3759-3768.
6. Jain, M. K.; Vanechteld, C. J. A.; Ramirez, F.; Degier, J.; Dehaas, G. H.; Vandeenen, L. L. M. *Nature* 1980, 284, 486-487.

7. Laughlin, R. G. *Colloids Surf., A* 1997, 128, 27-38.
8. Almgren, M.; Rangelov, S. *Langmuir* 2004, 20, 6611-6618.
9. Park, J.; Danoff, E. J.; Stein, D. C.; English, D. S.; DeShong, P. *In Preparation for JACS* 2007.
10. Wang, X.; Danoff, E. J.; Sinkov, N. A.; Lee, J.-H.; Raghavan, S. R.; English, D. S. *Langmuir* 2006, 22, 6461-6464.
11. Danoff, E. J.; Wang, X.; Tung, S.-H.; Sinkov, N. A.; Kemme, A. M.; Raghavan, S. R.; English, D. S. *Langmuir* 2007, 23, 8965 - 8971.
12. Israelachvili, J. N. *Intermolecular and Surface Forces*; Academic Press: London, 1985.
13. Safran, S. A.; Pincus, P.; Andelman, D. *Science* 1990, 248, 354-356.
14. Bonincontro, A.; La Mesa, C.; Proietti, C.; Risuleo, G. *Biomacromolecules* 2007, 8, 1824-1829.
15. Dias, R. S.; Lindman, B.; Miguel, M. G. *J. Phys. Chem. B* 2002, 106, 12600-12607.
16. Mel'nikov, S. M.; Dias, R.; Mel'nikova, Y. S.; Marques, E. F.; Miguel, M. G.; Lindman, B. *FEBS Lett.* 1999, 453, 113-118.
17. Letizia, C.; Andreozzi, P.; Scipioni, A.; La Mesa, C.; Bonincontro, A.; Spigone, E. *J. Phys. Chem. B* 2007, 111, 898-908.
18. Rigler, R.; Elson, E. S. *Fluorescence Correlation Spectroscopy Theory and Applications*; Springer: Berlin, 2001.
19. Rusu, L.; Gambhir, A.; McLaughlin, S.; Radler, J. *Biophys. J.* 2004, 87, 1044-1053.
20. Allen, N. W.; Thompson, N. L. *Cytom. Part A* 2006, 69A, 524-532.
21. Elson, E. L.; Magde, D. *Biopolymers* 1974, 13, 1-27.
22. Thompson, N. L. In *Topics in Fluorescence Spectroscopy*; Lakowicz, J. R., Ed.; Plenum Press: New York, 1991, pp 337-378.

23. Hess, S. T.; Webb, W. W. *Biophys. J.* 2002, 83, 2300-2317.
24. Magde, D.; Webb, W. W.; Elson, E. *Phys. Rev. Lett.* 1972, 29, 705-&.
25. Israelachvili, J. N. *Intermolecular and Surface Forces*; Academic Press: London, 1991.

## **Chapter 6:**

1. Nii, T.; Ishii, F. *Int. J. Pharm.* 2005, 298, 198-205.
2. Kuo, J. H. S.; Jan, M. S.; Chang, C. H.; Chiu, H. W.; Li, C. T. *Colloids Surf., B* 2005, 41, 189-196.
3. Zhu, C.; Wu, L. Q.; Wang, X.; Lee, J. H.; English, D. S.; Ghodssi, R.; Raghavan, S. R.; Payne, G. F. *Langmuir* 2007, 23, 286-291.